Imperial College London

Department of Mechanical Engineering

A STUDY ON THE INTEGRATION OF A HIGH-SPEED FLYWHEEL AS AN ENERGY STORAGE DEVICE IN HYBRID VEHICLES

Pablo Martinez-Gonzalez

June 2010

Thesis submitted for the Diploma of the Imperial College (DIC),

PhD degree of Imperial College London

I declare that the research presented in this thesis is my own work and that the work of others is properly acknowledged and referenced.

Pablo Martinez-Gonzalez

ABSTRACT

The last couple of decades have seen the rise of the hybrid electric vehicle as a compromise between the outstanding specific energy of petrol fuels and its low-cost technology, and the zero tail-gate emissions of the electric vehicle. Despite this, considerable reductions in cost and further increases in fuel economy are needed for their widespread adoption.

An alternative low-cost energy storage technology for vehicles is the high-speed flywheel. The flywheel has important limitations that exclude it from being used as a primary energy source for vehicles, but its power characteristics and low-cost materials make it a powerful complement to a vehicle's primary propulsion system. This thesis presents an analysis on the integration of a high-speed flywheel for use as a secondary energy storage device in hybrid vehicles.

Unlike other energy storage technologies, the energy content of the flywheel has a direct impact on the velocity of transmission. This presents an important challenge, as it means that the flywheel must be able to rotate at a speed independent of the vehicle's velocity and therefore it must be coupled via a variable speed transmission. This thesis presents some practical ways in which to accomplish this in conventional road vehicles, namely with the use of a variator, a planetary gear set or with the use of a power-split continuously variable transmission. Fundamental analyses on the kinematic behaviour of these transmissions particularly as they pertain to flywheel powertrains are presented. Computer simulations were carried out to compare the performance of various transmissions, and the models developed are presented as well.

Finally the thesis also contains an investigation on the driving and road conditions that have the most beneficial effect on hybrid vehicle performance, with a particular emphasis on the effect that the road topography has on fuel economy and the significance of this.

a los ingenieros Martínez: Juan y a los dos Claudios (¡bueno hasta los tres Claudios!), quienes cada uno a su manera han sido mis mejores maestros de ingeniería

ACKNOWLEDGMENTS

Foremost, I would like to thank my supervisor Dr. Keith Pullen for his academic and personal mentorship throughout the course of my degree. Dr. Pullen's command of the subject and unwavering enthusiasm provided continuous support even after he moved to City University London.

I am very grateful as well to Dr. Andrew Olver who kindly agreed to take on some of the supervisory duties after Dr. Pullen changed institutions. Dr. Olver's pragmatic approach ensured that this thesis was not only completed on time but also that it was properly structured.

The research presented in this thesis builds upon previous work by Dr. Ulises Diego-Ayala, whose mentorship during collaborative experimental research is much appreciated. I am indebted as well to Matthew Read who simultaneously to my own research, carried out research on the integration of flywheels in trains. Many insights and answers on this thesis came from stimulating conversations where we candidly discussed our own research findings and challenges encountered.

Many friends and family supported my throughout these years. My father Claudio lent his engineering knowledge and personal experience in building an electric car to answer many of my questions and to leave me with many more. My brother Claudio also lent his scientific skills to probe the fallibility of my assumptions. My friends Jaime and Matthew provided substantial assistance in reviewing this manuscript. I am very grateful as well to my dear friend Marielle who provided emotional support during personal difficult times.

I especially want to thank Daniela for her love and partnership throughout these years and for helping me to enjoy a world beyond engineering.

Finally, I would like to thank Mexico's CONACyT (Consejo Nacional de Ciencia y Tecnología) and Imperial College for their financial support of this project.

NOMENCLATURE

ENGLISH

Symbol	Units	Meaning
A_{rim}	m^2	Surface area of the sides of the flywheel
A_s	m^2	Surface area of the rim of the flywheel
C_{rim}	-	Drag coefficient for the rim for the flywheel
C_r	-	Normalised transmission ratio coverage
C_s	-	Drag coefficient for the size for the flywheel
D_R	m	Pitch diameter of the ring gear of the PGS
D_S	m	Pitch diameter of the sun gear of the PGS
E	J	Energy
f	$1 / kW$	Fuel economy factor
F	N	Force
FD	-	Vehicle's Final drive
G	m/s^2	gravity
G_V	-	Gear ratio variator branch
G_M	-	Gear ratio fixed-ratio branch
GR	-	Fixed Gear ratio
H	$kg\ m^2 / s^2$	Angular momentum
I	$kg{\cdot}m^2$	Mass moment of inertia
m	kg	mass
M_w	Nm	Windage torque
$\%ON_{ICE}$	-	Percentage of time the ICE is on for a cycle
P	W	Power
r	m	Radius
r	-	Overall transmission ratio
$r_{(V_{\max})}$	-	Transmission ratio at Vmax
$r_{(V_{\min})}$	-	Transmission ratio at Vmin
R_{fw}	-	Ratio of radius to length of flywheel
R_p	-	PGS ratio
r_t		Transmission ratio coverage
t	s	Time
V	-	Variator instantaneous speed ratio
V_{max}	-	Maximum variator ratio
V_{min}	-	Minimum variator ratio
V_t	-	Ratio coverage of the variator

GREEK

Symbol	Units	Meaning
α	rad / s^2	Angular acceleration
η	-	Efficiency
$\theta_{H\Omega}$	*radians*	Angle between the direction of the angular momentum and precession vectors
ρ	kg / m^3	Density
σ	N / m^2	Stress
τ	$N \cdot m$	Torque
ω	rad / s	Angular velocity
Ω	rad / s	Precession rate

SUBSCRIPTS

Text	**Meaning**
1,2,3,etc	Branches of the transmission
acc	Acceleration
aero	aerodynamic
anc	Vehicle's Ancillaries
avg	Average
axle	Vehicle's driveshaft
c	carrier gear of the planetary gear set
D_S	Diameter of the planetary gear set sun gear
D_R	Diameter of the planetary gear set ring gear
eng	Engine
fw	Flywheel
g	Gravity
gyro	Gyroscopic
i	Input branch
n	Current time step
o	Output branch
PGS	Planetary Gear Set
r	ring gear of the planetary gear set
ratio	Gear ratio
resist	Related to vehicle resistance forces (aerodynamic, rolling, gravity)
roll	Rolling (vehicle friction)
s	Sun gear of the planetary gear set
shaft	Shaft of the carrier of the planetary gear-set
tract	Related to the tractive force of the vehicle
Var	Variator
Veh	Vehicle
Wh	Wheel
wheel	Vehicle's wheel

ABBREVIATIONS

Abbreviation	Meaning
ADVISOR	Advanced Vehicle Simulator (program developed by NREL)
ARTEMIS	Assessment and Reliability of Transport Emission Models and Inventory Systems
CAPTAIN	Car Advanced PowerTrain Analysis (Program)
CVT	Continuously Variable Transmission
EPA	US Environmental Protection Agency
EPRI	Electric Power Research Institute
ESD	Energy Storage Device
EUDC	Extra urban section of the New European Driving Cycle
EV	Electric Vehicle
FA	Flywheel assisted acceleration mode
FE	Fuel economy
HEV	Hybrid Electric Vehicle
HV	Hybrid Vehicle
HYZEM	European Hybrid Technology Development approaching Zero Emission Mobility
ICE	Internal Combustion Engine
IPCC	Intergovernmental Panel on Climate Change
Li-ion	Lithium-Ion
mpg	miles per UK gallon
N	Neutral mode
NEDC	New European Driving Cycle
NiMH	Nickel/metal-hydride
ORNL	Oak Ridge National Laboratory
PGS	Planetary Gear-set
PHEV	Plug-in Hybrid Electric Vehicle
PS-CVT	Power-Split Continuously Variable Transmission
PSOC	Partial State of Charge
RB	Regenerative braking mode
SOC	State of Charge
UDC	Urban section of the New European Driving Cycle
UDDS	Urban Dynamometer Driving Schedule cycle
UN	United Nations
UNFCCC	United Nations Framework Convention on Climate Change
VAR	Variator
VRLA	Valve-Regulated Lead-Acid (Battery)
rpm	Revolutions per minute

TABLE OF CONTENTS

LIST OF FIGURES

LIST OF TABLES

1. INTRODUCTION

The last couple of decades have seen the rise of the hybrid electric vehicle as a solution which bridges the gap between conventional end electric vehicles. Conventional vehicles offer low cost and high range, but have low efficiency in urban driving conditions resulting in high emissions and the concentration of pollution in urban areas. Electric vehicles are expensive and have limited range, but their zero tailgate emissions and potentially low well-to-wheel emissions offer a very attractive answer in the quest to reduce greenhouse gas emissions and pollution.

Despite this, considerable reductions in cost and further increases in fuel economy are needed for the widespread adoption of hybrid vehicles. An alternative low-cost energy storage technology for vehicles is the high-speed flywheel. The flywheel has important limitations that exclude it from being used as a primary energy source for vehicles. Its energy density is much lower than that of petrol fuels and although it is comparable to that of most battery technologies, its time dependent losses means that it must be replenished often. However, its outstanding power characteristics and low-cost materials make it a powerful complement to a vehicle's primary propulsion system. This thesis presents an analysis of the integration of high-speed flywheels for use as secondary energy storage devices in hybrid vehicles.

This first part of this introductory chapter gives an overview of the environmental issues and resulting policies that motivate the research presented in this work. Next, some of the technologies that have been proposed to tackle these issues are briefly reviewed, and the use of flywheels in hybrid vehicles is presented as an alternative. Finally the main objectives and structure of the thesis are presented in the last two sections.

1.1. Motivation

1.1.1. Environmental Concerns: Climate Change

During recent years, there has been a growing concern about the effect of greenhouse gas emissions from human activities on the environment. There is consensus among the scientific community that observed increases in global average temperatures over the past decades were caused mostly by greenhouse emissions from human related-activities (see Figure 1.1) [1,2].

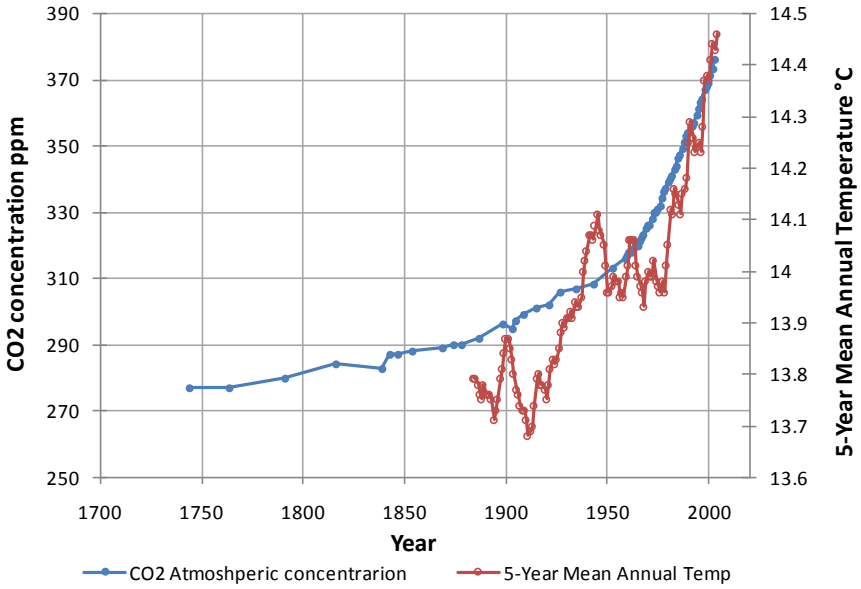

Figure 1.1. Relationship between average surface temperature and CO_2 concentration. Prepared with data from the World Resources Institute [3],

Predicting the effects of this phenomenon is one of the most pressing tasks facing scientists today. Estimating climate changes and the response of natural systems is complex and highly sensitive to assumptions. However, in recent years, more robust models have been developed that have allowed scientists to quantify with considerable confidence the future effects of global warming as well as to explain some of the current and past climate changes.

Recognising the danger that climate change poses on human society and the need to act quickly and multilaterally, governments have established international organisations through the UN framework, as well as national organisations to help them understand the science of climate change and to establish common ground for the enactment of international and national policy. Among the most influential organisations is the Intergovernmental Panel on Climate Change (IPCC), which was established in 1988 “to assess…the scientific, technical and socio-economic information relevant to understanding the… risk of human-induced climate change, its potential impacts and options for adaptation and mitigation.” As a result

of the IPCC's first report in 1990, a treaty was signed under the United Nations Framework Convention on Climate Change (UNFCCC) to set an agenda for governments to discuss and reach a consensus on strategies to tackle climate change.

The key mechanism of the UNFCCC for global action, and probably the most famous international mechanism to tackle climate change, is the Kyoto Protocol, adopted in Japan in 1997, and ratified as of June 2007 by 174 countries and the EEC. The United States, that accounted for 22% of the world's CO_2 emissions in 2004 (see Figure 1.2) adopted the protocol, but has indicated its intention to not ratify the treaty [4]. However, in recent years the United States has seen serious efforts to address climate change, for instance the Environmental Protection Agency (EPA) recently issued an endangerment finding on greenhouse gas emissions, which may open the way for the EPA to regulate greenhouse gases directly as a pollutant [5].

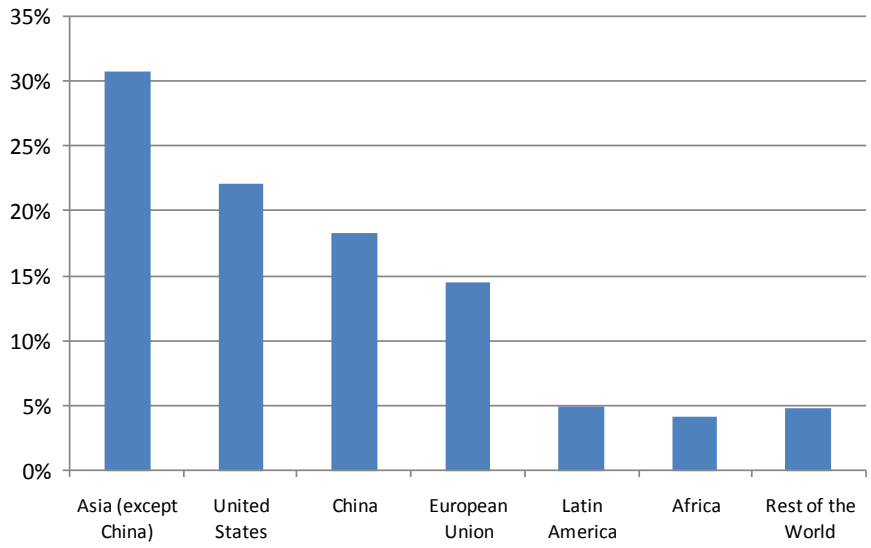

Figure 1.2. Distribution of the world's CO_2 emissions (2004) Prepared with data from: The Carbon Dioxide Information Analysis Center [6].

The Kyoto Protocol provides a specific structure for the estimation of greenhouse emissions and establishes legally-binding targets on reducing the greenhouse emissions of its signatories. Its importance cannot be underestimated, as probably the most widely recognised piece on legislation pertaining climate change, it has shaped international and national policy, and it has provided a framework for regional and national treaties on emissions. Specifically the European Union has established the European Trading Scheme as a means to ensure that its members comply with the Kyoto protocols by allocating different targets to member nations based on economic and technology factors.

The influence of the Kyoto Protocol in shaping European Union regulations is evident in the Transport White Paper European transport policy for 2010: time to decide (2001), which lays down the general policy by which several directives curtailing vehicle emissions have been enacted. Greenhouse gas emissions from the transport sector account for 26% of total emissions from energy related activities in the European Union (see Figure 1.3 (a)), of which 84% are caused by road transport (see Figure 1.3 (b)) [7]. With the number of motorised vehicle ownership to further increase worldwide [8] (see Figure 1.4), this poses a considerable challenge for transport policymakers and automotive manufacturers.

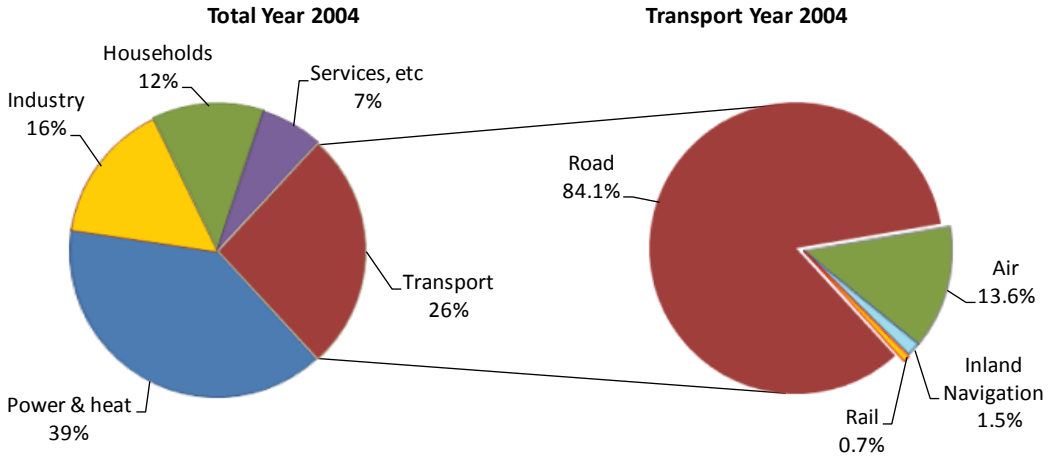

(a) (b)

Figure 1.3 (a). Share of EU25 emissions by sector or year 2006 and (b) EU25 Transport's sector CO_2 emissions by type of transport for 2004 [4]

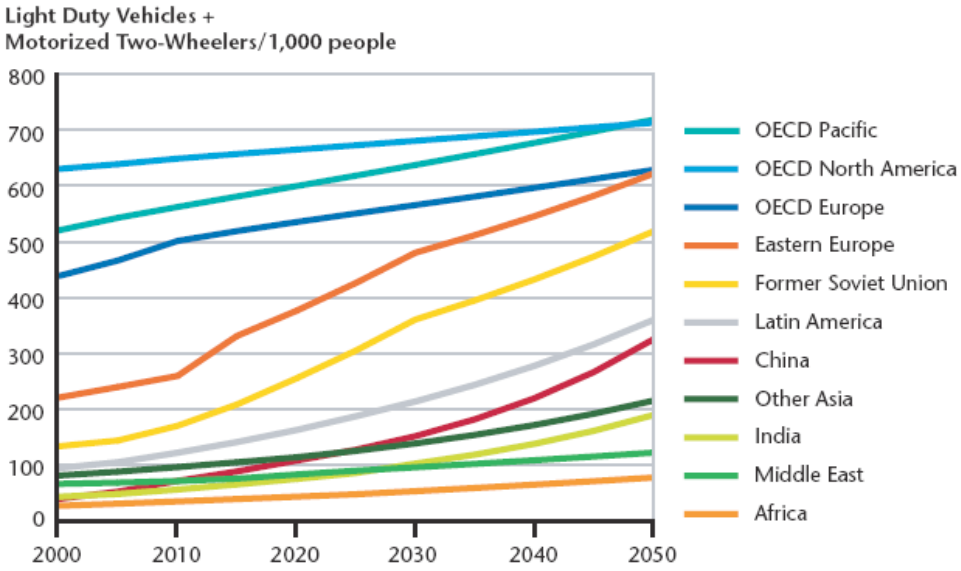

Figure 1.4. Projected growth in personal motorised vehicle ownership [5].

1.1.2. Emissions level regulations

In order to tackle emissions from the transport sector, the European Commission has introduced standards to limit pollutant emissions of new vehicles, including NO_X, HC, CO, and particulate matter emissions. The standards have been regularly updated to more restrictive limits, with Euro 5 [9] being the latest standard to affect the vehicle fleet introduced in 2009. Although these standards do not cover CO_2, the European Parliament promised to introduce binding legislation to limit CO_2 emissions for the average new car fleet to 120 g CO_2/km by 2012[10]. Under the proposed legislation, vehicle propulsion technology is expected to achieve a target of 130 g CO_2/km on its own and the remaining 10 g CO_2/km to come from other technologies (new fuels and tyres, improved efficiency of air-conditioning systems and changes in driving behaviour).

This has been met with scepticism by the European Automobile Manufacturers Association, which claims that relying heavily on vehicle technology to meet these demands would not be cost-effective and the targets would not be met within the proposed time frame [11].

Furthermore, cities have started to play a more active role in regulating transport with its boundaries with the aim of reducing the concentration of airborne pollutants. London for example implemented a low emissions zone in 2008 and exempts some low pollutant vehicles from the congestion zone tax. Other cities have ambitious plans to transform a substantial portion of their vehicle fleet to electric vehicles including San Francisco and Copenhagen.

It is evident that if these targets are to be met, and that to significantly reduce the impact that road transportation has on the environment, novel powertrains with low energy consumption must be introduced. Furthermore, this must be done at a marginal cost increase to assure a large market penetration.

1.1.3. Urban driving

As part of the study of the HYZEM project (European Hybrid Technology Development approaching Zero Emission Mobility) [12], 77 vehicles were monitored over a period of one month, in which several parameters were recorded in order to gather information that would allow for the development of realistic driving cycles that more accurately describe driving behaviours and emissions estimations.

The collected data, revealed some interesting insights about car usage rate and vehicle's daily energy requirements. A large portion of short trips was observed, with 13% of them shorter than 500 meters, 35% shorter than 2 km, and 60% shorter than 5 km. Significantly only about 13% of trips surpassed 20 km. This is shown statistically in plot (a) of Figure 1.5.

Thus an important segment of travel takes place in urban-like driving conditions of short and slower trips. Considering that the typical engine has lower efficiency under these conditions makes it particularly attractive to target an improvement in energy efficiency use of city vehicles.

The study also revealed the number of days that vehicles were used and the total distance travelled for that day, which is shown in plot (b) of Figure 1.5. Discounting the days when the vehicles were not used at all, in about 75 % of days the total distance travelled was less than 60 km, and in about 60% it was less than 40 km. This could be an important consideration when sizing an energy storage unit for a vehicle.

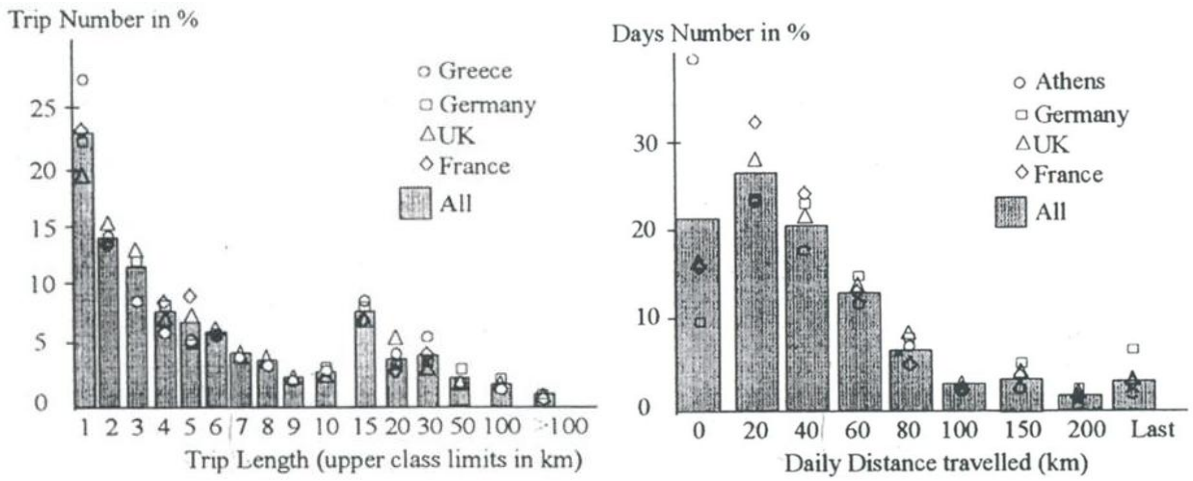

(a) (b)

Figure 1.5. (a) Percentage of trips by their length and (b) percentage of days according to total distance travelled as measured by the HYZEM study [12].

1.2. Current state of some proposed low-emitting technologies for the automotive sector: Biofuels, hydrogen, turbochargers, electric and hybrid vehicles

In order to meet the demand for low-polluting automotive transport, several technologies have been proposed and implemented over the years with mixed results. This section presents an overview of the current state of these technologies and an appraisal on their potential to address environmental concerns.

1.2.1. Biofuels

Biofuels have become increasingly popular in recent years for their potential in reducing greenhouse gas emissions and the increased energy security gained from diversifying fuel sources. In addition, soaring oil prices during the latter half of the 2000s decade made biofuels competitive at a global scale with an accompanying surge in supply. There is however soaring controversy on the benefits of biofuels and their suitability as a long-term alternative to fossil fuels.

Firstly, the role of biofuels in reducing greenhouse gas emissions has been questioned by Crutzen et al. [13] who found that reductions in CO_2 from the use of biofuels were offset by increasing concentrations of nitrous oxide (N_2O), a more powerful greenhouse gas than CO_2, that result from the use of nitrogen in fertilizers in the production of crops. This is heightened for crops that require intensive use of nitrogen, such as rapeseed and maize, whose increased N_2O emissions were found to contribute more to global warming than the displaced CO_2 equivalent. Crops with less nitrogen demands, such as sugar cane, produce less N_2O emissions and have the potential of reducing the impact on global warming, provided that energy intensity in farming and the production of fertilizers is kept at a minimum.

Secondly, there are serious concerns on the social impacts arising from competition of biofuels with food demands. This was evidenced early in 2007, when massive protests were held in Mexico due to an increase in the price of tortilla (an important element of the Mexican diet) linked to competition by biofuel producers for US grown maize [14]. These along with environmental concerns led the United Nations Special Rapporteur on the Right to Food, Jean Ziegler, to call for a five-year moratorium on biofuels produced by current methods until more research on its impact has been carried out [15].

1.2.2. Hydrogen

The use of hydrogen as a fuel for vehicles has been met with enthusiasm for its non-polluting emissions (water vapour) and was the technology of choice for a road map for future vehicles at least during most of the 90s and 2000s decades in the United States. However, these policies have suffered from criticism as hydrogen suffers from some fundamental problems that have greatly hindered its widespread use in the transport sector beyond some prototypes.

Firstly, hydrogen is a gas at ambient temperatures and it thus has a low energy volume density. Automobile fuel cell prototypes must hence store hydrogen at a high pressure, which requires an expensive technology to safely handle and contain these high pressures.

Another important criticism concerns with the production of hydrogen. The most common hydrogen production methods are electrolysis and hydrocarbon disassociations. The former requires the input of more energy in the form of electricity that is obtained in the form of hydrogen, begging the use directly of electricity in EVs. The latter method produces some emissions, but they can be easily managed in a properly fitted plant, however it relies on the use of fossil fuels which is an important obstacle for sustainable transport.

Perhaps the most promising hydrogen production method is through metabolic reactions in algae. This method uses the sun input as fuel for production, and reaction emissions are easily treatable. However, a large area may be required to obtain the necessary sun incidence for large-scale hydrogen production.

Regardless of the method of production, hydrogen must still be transported and compressed for it to be useable in mobile applications. These are important challenges that must still be overcome for the widespread adoption of this fuel.

1.2.1. Electric vehicles

The zero-tailgate-emissions of electric vehicles (EVs) make them a very attractive option for the transport sector. Even though the generation of electricity to power the vehicles does produce greenhouse emissions (unless renewable sources are used), the transfer of emissions into a power plant might be the easiest way to control them, as carbon sequestration is setting out to prove. EVs are increasingly becoming attractive as advances in battery technology and power electronics keep on extending the range and power capabilities of these vehicles as well as reducing required charging times. Government funding and tax breaks have also helped consumers to burden some of the extra costs associated with owning an EV and have encouraged the development and subsequent introduction of EVs by main vehicle manufacturers.

However batteries remain the Achilles heel of EVs. Their cost remains a major obstacle in the massive adoption of EVs, and there are serious concerns on their subsequent disposal and on the availability of raw materials. Battery technology is covered in more detail in section 2.3.1.

1.2.2. Technologies Improving Conventional Powertrains

Several technologies have the potential to improve the efficiency at which conventional powertrains operate [16-18]. A summary of their projected fuel economy benefits and their projected cost to consumers is shown in Table 1.1 these include:

- Better fuel mixture technologies – Which optimises the fuel-air mixture such as in direct fuel injection or the combustion in the cylinder as in homogeneous charge compression ignition.

- Variable valve timing and cylinder deactivation which optimise engine timing according to operating conditions and shuts off cylinders at low power requirements.

- Turbochargers and superchargers – These technologies increase the pressure of the combustion engine's air intake by using a compressor run either by a turbine using the engine's exhaust or directly from the engine's crankshaft.

- Better transmission systems – Higher numbers of gears, continuously variable transmissions, aggressive shift logic.

- Hybrid vehicles – Covered in great detail in section 1.3 and throughout the rest of this thesis.

The first three technologies in the previous list also have the potential of providing the same power by using a downsized engine saving fuel and weight.

Table 1.1 Projected fuel economy gains and cost to consumers for some powertrain improvement technologies. Source: US National Highway Traffic Safety Administration [19].

Technology	Fuel economy gains over conventional vehicle (%)	Estimated cost to consumer (in 2006 USD)
Low friction lubricants	0.5	3
Engine friction reduction	1 - 3	0 - 168
Variable valve timing	1 - 4	169 - 508
Cylinder deactivation	4.5 - 6	203 - 229
5 speed automatic (relative to 4-speed)	2.5	76 - 167
Continuously variable transmission (relative to a 4-speed)	6	100 - 139
Turbocharging & downsizing	5 - 7.5	120 - 690
Stop-start system (42 V electric)	5 - 10	563 - 600
Motor assist hybrid	25 - 40	1636 - 2274
2-mode hybrid electric	20 - 28.5	4655
Power-split hybrid electric vehicle (P-S HEV)	25 - 35	3700 - 3850

1.3. Hybrid Vehicles

1.3.1. The role of Hybrid Vehicles in addressing environmental concerns

Whether the primary source of energy in vehicles is fossil fuels, hydrogen or electricity, hybrid vehicles have the potential of greatly increasing the efficiency of the vehicle. Indeed, one of the main advantages of hybrid powertrains is that the integration of two power sources allows (in varying degrees and depending on the topology) for some optimisation on the operation of its power sources.

Some automobile manufacturers have concentrated their research efforts in more immediate goals, relying on existing technologies to develop novel powertrains that provide better fuel economy and lower emissions. This has led to extensive research and the market introduction of hybrid vehicles (HVs), which deliver higher fuel economy and lower emissions than conventional vehicles by regenerative braking and a more efficient use of the Internal Combustion Engine (ICE). Regenerative braking is the process by which the kinetic energy of the vehicle is transferred during braking to an energy reservoir for later use (usually accomplished by using a generator and storing the energy in batteries).

HVs rely on the use of two or more power sources to power the vehicle and deliver better performance. Most HVs are designed to deliver better fuel economy, however for some sport utility vehicles and military vehicles the hybrid capability is used to boost tractive power. Usually the two power sources used are an ICE and an electrical motor. These are termed Hybrid Electric Vehicles (HEVs).

1.3.2. History of the Hybrid Vehicle

Throughout the 19th century, the steam-powered, the internal combustion and the electric vehicles engaged in a competitive race to develop the automobile with the longest range and highest speed. Landmark designs of internal combustion engines by Nikolaus August Otto, Gottlieb Daimler and Karl Benz, as well as the developments of very efficient motors and improved batteries allowed the internal-combustion-engine vehicle and the electrical vehicle to surpass the hegemony of steam engines that had prevailed throughout the first part of the 19th century. By the end of the 19th century and beginning of the 20th century, it was a two horse race between the electric vehicle and the combustion engine. It was during this era, that the young Ferdinand Porsche used an internal combustion engine to spin a generator to power

electric motors at the wheels of the vehicle, producing the world's first hybrid vehicle and probably the first four-wheel drive as well [20].

However, further developments of the internal combustion engine compounded with a relative abundance of mineral oil meant the internal combustion gained a competitive advantage which translated in the virtual disappearance of the electric vehicle for decades to come. It was not until the 1970s oil crisis that interest in alternative modes of propulsion arose again, and automakers started to fund considerable research in this area.

It was however, the 1990s that proved the pivotal point. Amid growing awareness on the effect of tail pipe emissions and the resultant environmental policies, automakers started to invest heavily on developing the next generation of cleaner vehicles [21]. In 1993, the United States government established a partnership with the major US auto corporations to carry research into developing super fuel efficient vehicles while maintaining their affordability. Ford, General Motors and Chrysler all produced concept cars with impressive fuel economy based on hybrid electric vehicles. The program was then discontinued in 2001, with efforts redirected into The FreedomCAR and Vehicle Technologies Program, which carries an integrated approach into providing long-term environmentally friendly solutions for the transport sector [20].

Commercially speaking though, Japanese carmakers have led the way in the development of cleaner automotive technologies, with the market introduction of hybrid electric vehicles (HEVs). These vehicles have received a very warm response by consumers and governments, as they have shown some of the most promising advances on fuel economy and emissions mitigation.

Toyota has emerged as the leading developer and seller of HEVs, amounting for more than ¾ of all hybrid car sales in Europe and the US in 2006 (see Figure 1.6) [22,23]. Notably, Toyota's flagship vehicle, the Prius outsold by a threefold the second most sold hybrid vehicle in Europe and the US (also a Toyota).

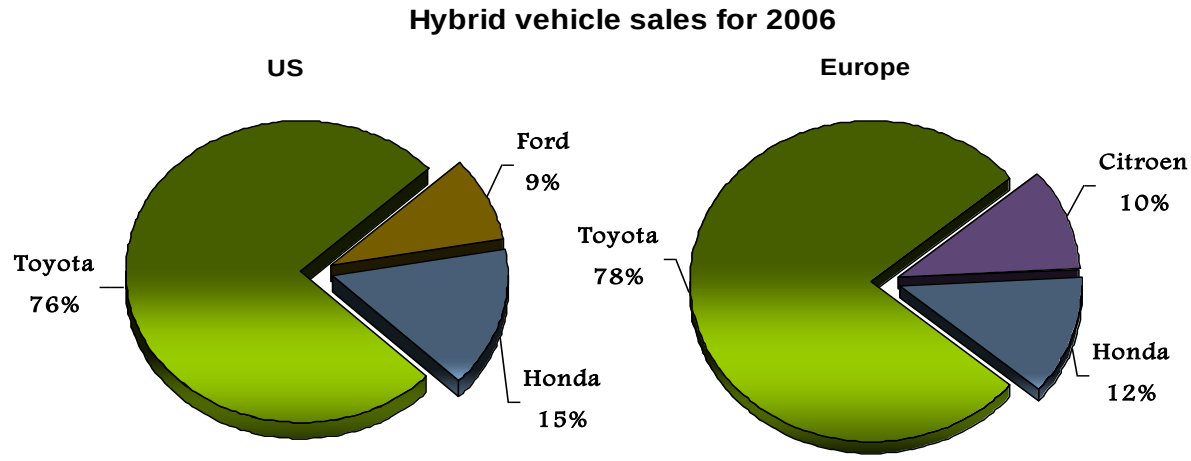

Figure 1.6 US and Europe Hybrid car sales for year 2006 [22,23].

Automakers from all over the world recognise now the importance of the hybrid market, with most introducing their own hybrid version in the near future. However, most of the vehicles on the UK market with the highest fuel economy and lowest CO_2 emissions are diesel powered, as shown in Table 1.2. Although diesel engines have had better fuel economy than petrol engines for some time, recent developments in this technology have further improved their performance. However, diesel engines still suffer from high NOx and particulate matter emissions, which is a source of environmental concern as it is responsible for serious respiratory illnesses as well as being a major contributor to the formation of acid rain.

Table 1.2 Vehicles with the top fuel economies and lower CO_2 emissions for sale in the UK (May 2007) Prepared with data from the Vehicle Certification Agency [24].

Manufacturer	Model	Urban Cycle [km/l]	Extra-Urban Cycle [km/l]	Combined Cycle [km/l]	CO_2 [g/km]	Fuel Type
Volkswagen	Polo Blue Motion	20.4	31.3	26.3	99	Diesel
Citroen / Toyota	C1 / Aygo	18.9	29.4	24.4	109	Diesel
Toyota	Prius	20.0	23.8	23.3	104	Petrol Hybrid
Citroen	C2	18.9	27.0	23.3	113	Diesel
Fiat	Panda	18.5	27.0	23.3	114	Diesel
Renault	Clio Campus	18.5	27.0	23.3	115	Diesel
Peugeot	206	18.5	27.0	23.2	112	Diesel
Vauxhall	Corsa	18.2	27.8	23.2	115	Diesel

1.4. Introduction to energy storage technologies

In order to have an effective hybrid vehicle, an appropriate choice of energy storage device for both primary and secondary propulsion must be made. This section will briefly introduce some of the energy storage devices must commonly used and proposed in hybrid vehicles.

The energy storage type chosen must complement each other operationally, so that at least one is able to power the vehicle when necessary and so that each is used to obtain a desired performance (typically the maximisation of fuel economy). This symbiosis may be achieved for example with the choice of a high specific energy density energy storage device for primary propulsion (to guarantee a minimum range and provide base energy) and a high specific power density as a secondary propulsion system (to provide a power boost and possibly regenerative braking). Figure 1.7 shows a Ragone plot of different energy storage technologies where the specific power and energy densities of the technologies can be compared.

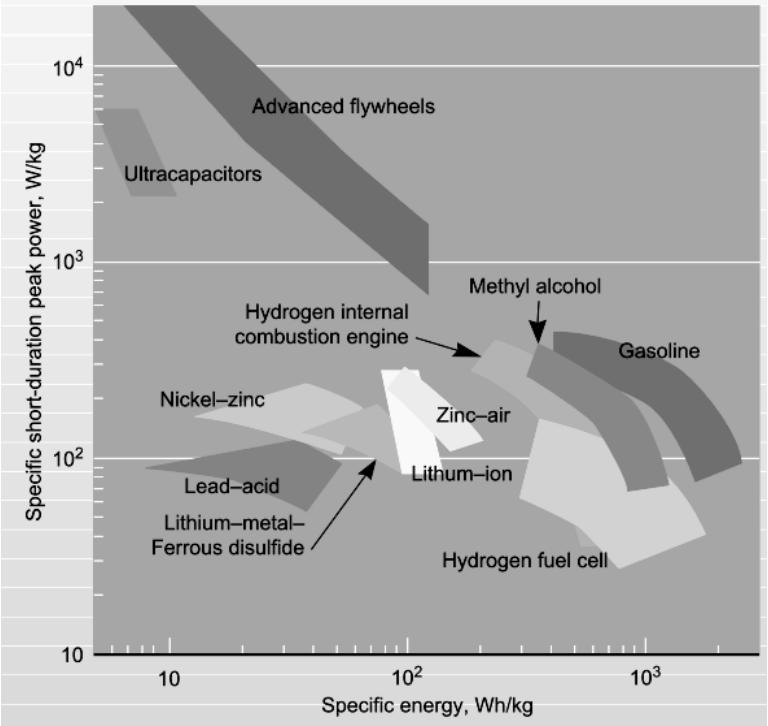

Figure 1.7. Ragone plot of energy storage technologies, showing their power and energy densities. Source: Science & Technology Review [25]

In all, these characteristics make the flywheel particularly suited for applications where power surges are common. This suggests their applicability in HVs, particularly for regenerative braking and assisted acceleration, where a high speed flywheel has the potential

to offer improved energy efficiency over batteries alternatives and potentially at a fraction of the cost.

Indeed the suitability for flywheels as secondary energy storage devices is increasingly being recognised. In particular, flywheels have made an appearance in Formula 1 racing, as teams incorporate 'kinetic energy recovery systems' into their racing cars. A major objective of this strategy is to encourage research by F1 teams that could translate into better fuel economy for road vehicles. Regulations for the 2009 season sets limits on the amount of energy that can be recuperated by regenerative braking and delivered at any one time, otherwise it purposefully leaves any specifications on what the 'Kinetic Energy Recovery System' should be, leaving which leaves the door open for innovative developments [26].

1.5. Objectives of thesis

This thesis presents an analysis on the integration of a high-speed flywheel on road vehicles. Although inexpensive in nature, the integration of the flywheel presents an important kinematic challenge for the transmission. The research presented in this thesis attempts to create an understanding of the complex kinematics involved in these transmissions and to provide engineers with tools to enable them to make an informed judgement in the specification of transmission and flywheel.

Three main objectives are identified:

1. The identification of the characteristics that are most desirable in hybrid vehicles, and of the conditions where they are most effective in reducing emissions and fuel consumption. This is discussed throughout the first two chapters and analysed in more detail in Chapter 5.

2. The carrying out of fundamental analyses on the performance of continuously variable transmissions in flywheel-hybrid powertrains, which can be extrapolated by designers to more complex transmissions involving multiple regimes of operation. Methodologies and analyses for this purpose are presented in Chapters 3 and 6.

3. The building of an understanding of the possible benefits from using a flywheel as a secondary storage device in hybrid vehicles. This is discussed throughout the thesis and simulations are presented in Chapter 6.

1.6. Structure of thesis

The topics covered on each chapter are the following:

Chapter 1 presents the main objectives of this thesis. It starts by presenting the motivation behind the research and then gives a snapshot of the state of current low-emissions vehicle technologies.

Chapters 2 and 3 together present a literature survey on the research carried out on flywheels and continuously variable transmissions respectively. Chapter 2 also presents a background on hybrid vehicles and energy storage technologies with an extended section covering flywheels.

Chapter 3 is devoted to analysing the kinematics of mechanical continuously variable transmissions. Among different options, these can be accomplished with variators, planetary gear sets or power split transmissions combining these components. Literature covering these transmissions is reviewed and further analyses are carried out to present the complex kinematics and power flow relations of these transmissions as they are integrated in vehicles with flywheels.

Chapter 4 presents the computer model developed to assess the performance of alternative powertrains. The main assumptions of the model are discussed as well as its limitations. This model is used in the simulations presented in Chapters 5 and 6.

Chapter 5 presents results from a study carried out to assess the potential fuel economy of hybrid vehicles under the influence of road gradients. It then dissects these results to identify the factors affecting the fuel economy of hybrid vehicles leading to some insights into possible control strategies.

Chapter 6 uses the model presented in Chapter 4 to assess the behaviour of various powertrains incorporating flywheels, and their potential in improving the fuel economy of hybrid vehicles. The powertrains analysed are based in the studies presented in Chapter 3.

Chapter 7 summarises the research presented in this thesis and presents conclusions for this study as well as recommendations for future research.

2. LITERATURE SURVEY AND TECHNOLOGY BACKGROUND

This chapter is divided into two main parts. A literature survey is presented in Section 2.1 where some of the most important research of the past half century on the integration of flywheels on board road vehicles is reviewed.

A technology background on hybrid vehicles is then presented in section 2.2, followed by a review of energy storage technologies for vehicles in section 2.3. Flywheels are reviewed in more detail in section 2.4.

Finally section 2.5 introduces the concept of continuously variable transmissions and discusses some of the fundamental components that can be used to construct such a transmission.

2.1. Flywheel Literature Survey

2.1.1. History and uses

For a comprehensive review on the historical uses of the flywheel as an energy storage device, the reader is referred to an article by Robert Clerk [27]. This article covers ancient uses of inertia flywheels from its first recorded use in potter's wheel, through its short-lived industrial era use as a silent propeller for torpedoes and its first uses as an energy storage device onboard road vehicles. It culminates with the author's own research for its use in the *Gyreacta* bus which is covered in more detail in the next section.

Aside from its uses on board road-vehicles which are covered in detail in section 2.1.2, it is worth reviewing other applications that have found use for flywheels. These devices have been proposed as energy storage devices for aerospace applications and are currently being researched by the US space agency NASA [28]. The vacuum of outer space provides an ideal environment for the long term storage of energy as aerodynamic losses are avoided. On earthly applications the long term storage of energy in flywheels is challenging and their use tends to be limited to applications requiring only short term storage of energy or power buffering [29].

2.1.2. Flywheels in transport

2.1.2.1. Gyreacta

In the early part of the 60s decade a group led by Robert Clerk carried out research into the recovery and reutilisation of braking energy [27]. The group developed the *Gyreacta* transmission which consisted of a series of planetary gear sets with its three branches free to rotate, creating a two degree of freedom device, which can be used to match the speeds of the vehicle and a disk-like steel flywheel. In the *Gyreacta* transmission the vehicle's engine, the flywheel and the vehicle's driveshaft connect to each of the branches of the planetary gear set, with different modes of operation possible selectable depending on the actuation of different planetary gears via a clutch. This type of transmission which relies solely on the use of a planetary gear set is discussed in more detail in section 3.5. Figure 2.1 (a) shows a *Gyreacta* transmission developed for a bus application and Figure 2.1 (b) shows the connections at the planetary gear set for acceleration operation.

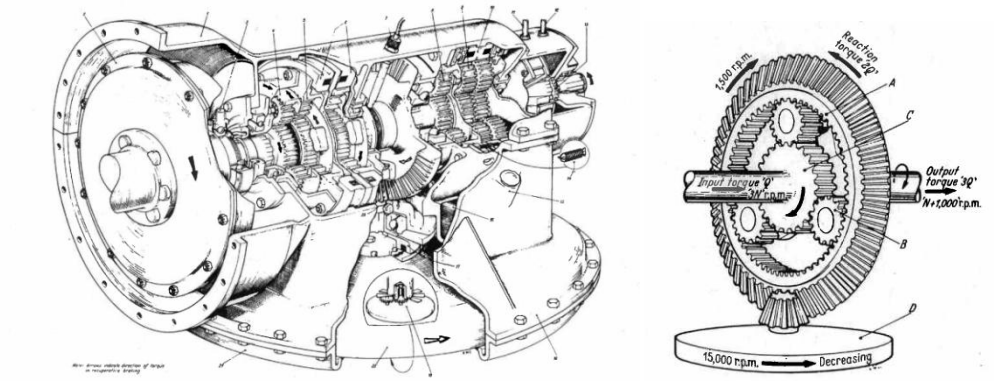

(a) (b)

Figure 2.1 (a) The *Gyreacta* transmission developed for a bus application. (b) An example on the operation of the planetary gear set during an acceleration event.

2.1.2.2. The University of Wisconsin Group

Between the latter part of the 70s and early 80s, Andrew Frank and Norman Benchley from the University of Wisconsin-Madison performed research on the integration of flywheels in vehicles [30-32]. Their research centred primarily in the development of an efficient continuously variable transmission suitable for an application with a flywheel.

The Wisconsin group identified four significant operation objectives with the potential for significant fuel savings: eliminating the use of the engine during idling and braking periods, operating the engine as close as possible to its most efficient operation, recuperation and reutilisation of braking energy and improved efficiency of the transmission system. The group proposed and analysed three transmission concepts capable of providing continuously variable speed: one with a multi-speed gearbox and a slipping clutch; and the other two involving power-split arrangements incorporating either a hydrostatic or a V-belt variator.

The multi-speed gearbox system proposed used a gearbox with 12 fixed speed ratios and a multi plate wet clutch that was allowed to slip to provide the required variable speed ratios. It was found that even though losses were expected from slipping the clutch, the overall efficiency of the system would remain relatively high as the other components of the transmission had high efficiencies. A main downside of this system is that it requires excessive shifting to match the speed of the flywheel which may be impractical.

Given the current technology at the time, the transmission with the hydrostatic variator was favoured and a prototype vehicle was built. It used the hydrostatic variator and a planetary gear set to form a power-split arrangement that they complemented with an in series 4-speed manual transmission as shown in Figure 2.2.

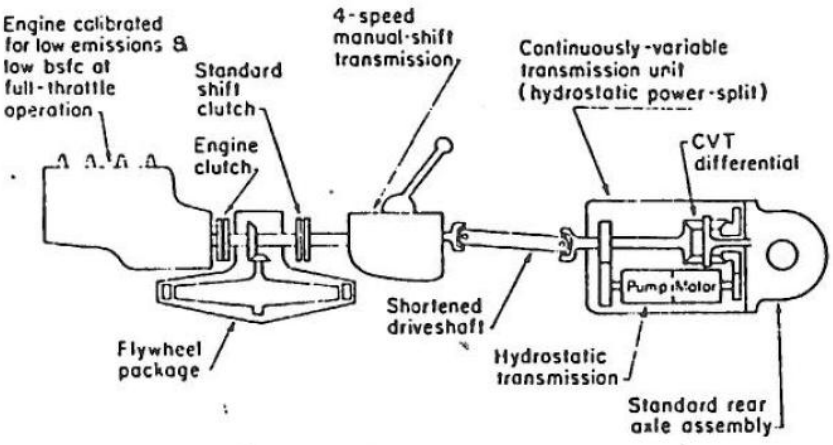

Figure 2.2. Schematic diagram of the series hybrid powertrain proposed by the Wisconsin group.

Only data for the numerical simulations was found, and it is unclear if the empirical results were similar. It was found that the single most important factor in determining fuel economy of the vehicle was the transmission, which sustained considerable losses. Nevertheless, their analysis found that an improvement of 59% in fuel economy was possible for city driving, as energy recovered from braking and turning off the engine during idle more than compensated transmission losses. The potential for 117% fuel economy improvement for city driving was identified with the use of a more efficient transmission.

It is worth noting that at the time, fuel economy levels averaged 15.8 mpg (US gal) in the US, and that engine development over the next years led to improvements on the scale expected by this hybrid for an average in 2007 of 37 mpg (US gal) [19]. This may account partially for the limited research into hybrid alternatives during that era. Also, although it is not specified it can be inferred from data reported that the material used for the flywheel's rotor was metallic, which presents a much lower specific power over current carbon-fibre alternatives.

2.1.2.3. The General Motors study

One of the most insightful studies on the use of flywheels on vehicles was performed at General Motors Research Laboratories during the early part of the 80s [33]. The research included a detailed study (including laboratory analyses) of all the elements in the powertrain, notably the flywheel and the transmission. In the proposed powertrain, the hybrid was installed in parallel to the engine, and transmission to the wheels was accomplished with the use of a V-belt variator. It was found that the hybrid powertrain transmission could yield fuel saving of 36% on an urban cycle, but losses of 13% for a highway cycle, resulting from losses associated with a more complex transmission, and presumably also because of the limited use of the hybrid system on these conditions. Research was abandoned as fuel economy savings were not deemed high enough to justify the costs.

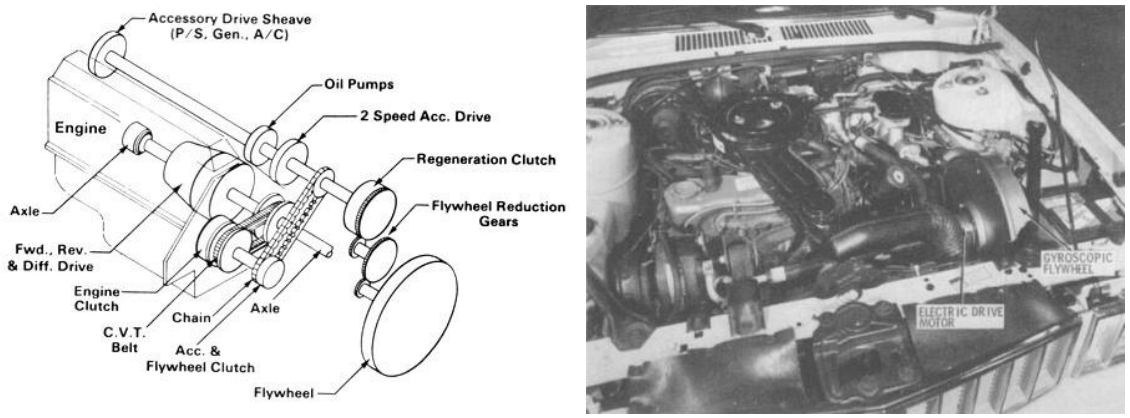

Figure 2.3 Transmission and installation of the flywheel used by the General Motors group.

2.1.2.4. Swiss Federal Institute of Technology and Eindhoven University of Technology

The Swiss Federal Institute of Technology [34] has also developed a powertrain incorporating a flywheel which uses a V-belt variator and a power split transmission. The use of the flywheel is limited to supplementing engine power output used and its regenerative braking capabilities are limited. Similarly in the hybrid transmission developed at the University of Eindhoven [35] the flywheel is used to boost power and protect engine from low efficiency operation, with limited regenerative braking attempted.

2.1.2.5. University of Texas at Austin Group

When the University of Texas at Austin developed, integrated and tested a flywheel energy storage system for a hybrid electric transit bus [36-38]. The original hybrid electric bus did not include batteries, but converted mechanical energy from a natural gas combustion engine to electrical energy that would drive two wheel motors, and did not include regenerative braking. The Austin group designed the flywheel to boost the power capabilities of the bus and to increase the efficiency of the system by adding regenerative braking capabilities. Although the system was designed and tested for a transit bus, it is scalable to other transport systems including passenger vehicles.

The flywheel transmission and containment package is an interesting design in that energy transfer to and from the flywheel is electrical, and since the motor is integrated into the containment system of the flywheel, there is no through shaft coming out the package. As such, a vacuum environment is more easily maintained, which greatly reduces aerodynamic losses of the flywheel.

The flywheel is mounted on magnetic bearings which eliminates friction losses of the flywheel, although it does induce magnetic and electric losses. A second set of backup bearings are also integrated on the package. The whole flywheel package is mounted in a couple of gimbals that reduces impact on the backup bearings that arise from movements of the flywheel in response to rolling and pitching motions of the vehicle. Power is spent in controlling the stator of the bearings. An important limitation of this design is the limited heat removal capacity of the system. Since the flywheel (including the motor) is levitated in magnetic bearings and it is spinning in a vacuum environment, all the heat is dissipated through radiation. Indeed a lot of the design effort of the group was devoted to reducing motor induced losses, bearing induced losses and windage losses. The use of magnetic bearings and gimbals capable of sustaining high momentums in the event of a flywheel failure involve a higher cost than using rolling bearings.

An acceleration test was performed by the Austin group and it was found that by incorporating the flywheel, the bus was capable of doubling its acceleration rate. This was also accomplished with a further reduction of power demanded of the bus's engine. Fuel economy measurements were not performed, and it may be difficult to predict what they might be considering that the operating conditions of the engine change with the flywheel and it is likely to have different specific fuel consumption. Nevertheless the reduction in power

demanded of the engine is significant and those suggest that significant improvements in fuel economy can be accomplished with an appropriate control strategy.

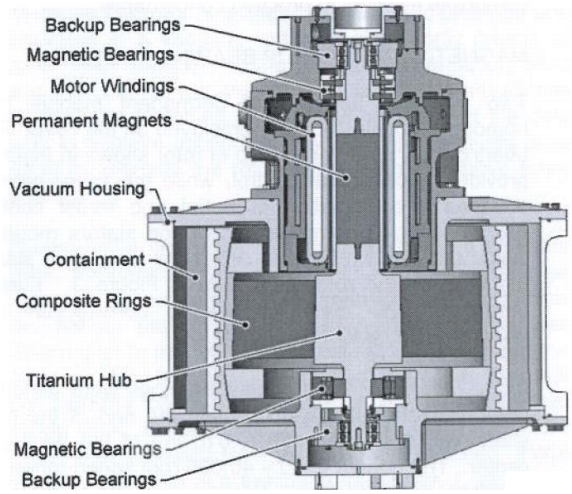

Figure 2.4. Cross section of the flywheel used by the University of Texas in hybrid bus.

Some of the current main applications for this technology are as uninterruptible power supplies, power quality supply, with interest also arising in its use with intermittent energy technologies such as renewable energy generation [16,39,40]. There is also interest in flywheels for their potential use in space technologies as substitutes for batteries, which impose a heavy weight penalty on current systems [41].

2.1.2.6. Flywheel powertrains in Formula 1

Recent changes in motorsport Formula 1 regulations allowing for the recovery and reutilisation of braking power has seen the development of some systems based on flywheels. One group led by Williams racing team has developed an electromechanical flywheel in which power is transferred to and from the flywheel electrically [42]. This type of transmission is briefly discussed in section 2.5.1.

Another group has been formed between a purposely formed company *Flybrid* and toroidal variator specialists *Torotrak*. This system uses a carbon fibre filament wound rim wrapped around a steel rotor and uses a toroidal variator [43]. The system designed for F1 goes in parallel to the engine and uses only a toroidal variator and a clutch as the transmission between the vehicle's driveshaft and the flywheel. In general this approach greatly limits the usability of the system as it can only be used within the ratio coverage of the variator which is relatively limited. However the regulations of Formula 1 only allow a limited amount of

energy to be stored per lap which is easily recovered and used within the limited range of operation. The system is shown in Figure 2.5

Figure 2.5 Flybrid Formula One Kinetic Energy Recovery System. Source: www.flybridsystems.com

The Flybrid-Torotrak group have also promoted the use of the system for low carbon vehicle applications [44,45]. The system proposed for road vehicles uses a power split transmission that increases the ratio coverage of the transmission at the expense of increased power through the variator and increase losses. This type of transmission is covered extensively in section 3.4.

2.1.2.7. Research at Imperial College and City University London

Research carried out at Imperial College and City University London have led to the proposal of powertrains incorporating flywheels with purely mechanical transmissions [46-50].

In [50] two different powertrain designs are presented. The first one uses a planetary gear set and a friction brake to control power flow between the flywheel and the vehicle. The second one uses a power split transmission with a variator and a friction brake as control devices.

The author of this thesis collaborated with Diego-Ayala in carrying out experimental analyses on the first powertrain and in carrying out simulations on the performance of both powertrains. The experimental work and simulations are presented in [47,48,50].

Fuel economy improvements of 4-11% and 10-25% were identified for the drive cycles presented in [50] for the two powertrains mentioned before. However, it has also been identified that a substantial portion of the fuel economy benefits stem from turning off the engine rather than from the reutilisation energy recuperated during braking. These will be further discussed in section 3.5.

2.2. Classification of Hybrid Vehicles

Depending on how they use the secondary power source, HVs can be divided into the following classes [51,52][1]:

Micro hybrid: The electric motor in this vehicle does not provide driving torque. The main feature of this type of hybrid is that it allows the ICE to shut off when the vehicle is stopped (mainly) or when it is coasting or braking. The ancillaries of the vehicle are powered by the electric motor during these periods, and the hybrid system may also support regenerative braking.

Power requirements are 1–2.5 kW for a period of 20–200 s [53]. Fuel economy gains in the region of 5 to 15% are possible.

The GM Silverado hybrid is an example of this configuration, and the Zero inertia powertrain proposed by Shen and Veldapus [35] is an example of a micro hybrid that uses a mechanical flywheel instead of an electric motor.

Mild hybrid (also called power-assist hybrid): The electric motor is capable of assisting the ICE in driving the vehicle, which also allows for some downsizing of the ICE. The electric motor is also used as a generator to charge the batteries when regenerative braking.

Power levels are around 6-10 kW for 3-10 s [53]. Fuel savings are in the range of 15 to 25%.

Examples of these vehicles are the Honda Civic Hybrid and the Honda Accord Hybrid.

Full hybrid: These hybrids have more powerful electric motors and battery capacity and are capable of driving the vehicle solely on electrical power, the ICE or a combination of both. It maximises the ICE efficiency by operating it at near optimal load conditions and using the extra available energy to charge the batteries via an alternator. Batteries are also charged by regenerative braking.

Power values of 60 kW for up to 20 s may be required [53]. This configuration allows for impressive fuel savings in excess of 50%.

[1] For simplicity, it will be assumed that the hybrid is a hybrid electric vehicle when explaining these classes, but it is important to note that the power sources can be different, as it will be later explored.

The most famous example for this type of HEV and also the most commercially successful hybrid in the market is the Toyota Prius.

Plug-in hybrid: These vehicles are also known as electric vehicles with range extenders. The batteries are recharged primarily through the electricity grid and the vehicle is driven almost exclusively by the electric motor(s). The ICE starts when the state of charge of the batteries is low and it is used either to drive the vehicle directly or to charge the batteries.

Power requirements are in excess of 70 kW for compact cars and twice that amount for sport utility vehicles [53]. These vehicles are capable of fuel economy in excess of 100 mpg and very low emissions when accounting for the onboard fuel only, but their true fuel economy and emissions depend on the sources used to generate the grid's electricity.

Series hybrid: These vehicles are driven exclusively through electrical motors and the ICE is used only to generate electrical power. Many plug-in hybrids are series hybrids, but other examples include fuel cells–batteries configurations or even batteries–batteries configurations where one bank of batteries is optimised for range and another one for power delivery [54].

Figure 2.6 shows a diagram depicting the classes according to their use of batteries and electric motor.

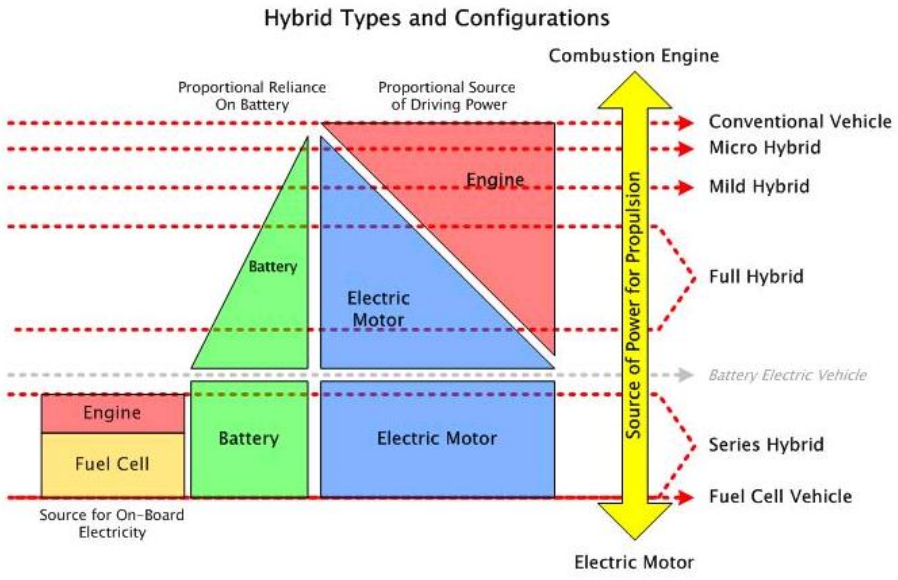

Figure 2.6. Hybrid types according to their use of batteries and their source of driving power. Source: Green Energy Congress [51]

2.3. Energy storage technologies (Batteries and supercapacitors)

2.3.1. Batteries

As mentioned in the last chapter, HEVs have dominated the hybrid market for a number of years. In particular, developments in battery technology during the past few decades, driven in part by portable consumer products, has made it possible for the development of vehicles that substantially decrease fuel usage by regenerative braking and an intermittent use of the ICE.

HEV technology is undoubtedly the most mature hybrid powertrain technology. However it suffers from fundamental technical drawbacks that may hinder its standard introduction in new vehicles on a massive scale, and ultimately their long term success.

One of the main problems with HEVs is associated with the electrochemical batteries sensitivity to internal and external conditions that affect their performance. The amount of power a battery can deliver and the rate at which they accept charge depends mainly on their state of charge (SOC) and temperature conditions. This is particularly a problem under regenerative braking, since high surges of power must be accepted by the batteries in a short period. Since charge acceptance is best at partial SOC (PSOC), batteries must be able to withstand prolonged PSOC [55]. Furthermore, current automotive batteries do not deliver the reliability required in the industry (i.e. six-sigma), and must be replaced several times during the vehicle's life [56].

The three most promising batteries for HEVs are: the Ni-MH batteries currently used in the Toyota Prius, Honda Insight and Ford Escape; the valve-regulated-lead-acid (VRLA) used in the Citröen C3 [57]; and the Li-ion that is set to make its debut in 2010-2011 with the Mercedes S300 [58]. The characteristics of these batteries and the common Lead-acid battery are examined next:

Lead-acid batteries are the most mature battery technology and have been the choice of auxiliary battery of the industry for a long time. However, they have low power acceptance and have low specific power (200-400 W/kg) [53], making them unsuitable for most hybrid applications.

Valve-regulated lead-acid (VRLA) batteries have better charge acceptance (300-600 W/kg @ 60-80% SOC), although their power is deeply dependent on SOC. Cycle life is affected by its depth of discharge, operating temperature, and average SOC [53]. Most developments on these types of batteries are aimed at mild hybrids [56].

Nickel/metal-hydride (NiMH) batteries are the current preferred battery for full-hybrids. Power levels of 1000 W/kg are achievable over a relatively wide SOC. Its main problem is that its power levels drop sharply at low temperatures (see Figure 2.7), and its charge acceptance is low at high temperatures [53]. Its life is currently guaranteed for 8 years and it must be further increased. Its cost is also a main challenge, as the cost of replacing a bank of batteries for a full-hybrid is $2,000 to $3,000 USD [59].

Lithium-Ion (Li-ion) batteries may be the most promising battery technology, at least in the mid-term. Power at the cell level is very high (2000 W/kg), it has a high energy efficiency, good charge acceptance, and good power at low temperatures. The main challenges for this technology are to significantly reduce the cost of the batteries and to improve their operating life (from current 3-5 to 10 years) [53].

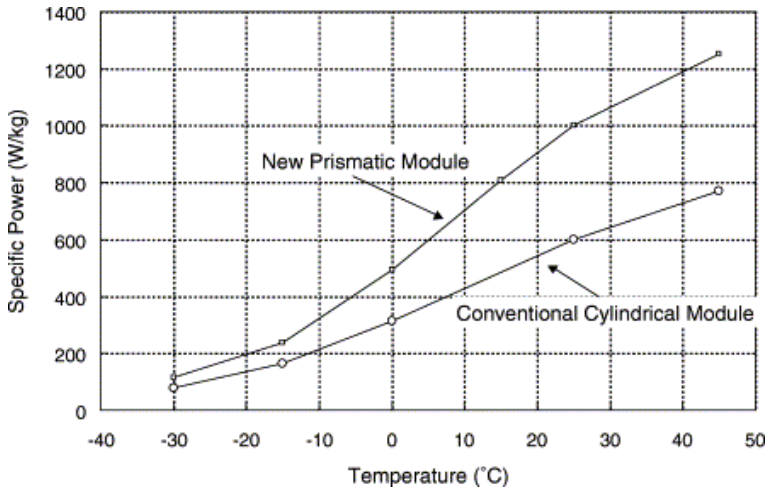

Figure 2.7 Power dependence of a Panasonic NiMH batteries on temperature at 60% SOC [53].

Regenerative braking also poses a considerable challenge when using batteries, as the vehicle's kinetic energy must undergo several transformations within its full cycle wheels-storage-wheels as follows:

1. First the vehicle's kinetic energy is transformed to electrical energy in the motor/generator (regenerative braking).
2. The electrical energy is then converted to chemical energy at the batteries as they are charged (energy storage).
3. Afterwards, chemical energy is transformed back to electrical energy as the battery powers the motor/generator (first step for acceleration).
4. Finally as the motor/generator drives the vehicle, energy is transformed from electrical to kinetic again (vehicle acceleration).

These constant energy transformations carry associated losses that can amount to a considerable amount of the energy available for regeneration. This is particularly a problem for the round-trip energy efficiency, which depends heavily on SOC and temperature.

Since the hybrid powertrain provides additional power to the vehicle, HEVs can benefit from engine downsizing and offer important savings on manufacturing costs. However, the cost of the batteries and power inverter substantially increase the cost of hybridisation. The US Environmental Protection Agency (EPA), produced an interim report on the projected costs of new powertrains technologies. The report, which compiles research done by the Oak Ridge National Laboratory (ORNL) and the Electric Power Research Institute (EPRI), found that despite the incremental cost of manufacturing, consumers would benefit from savings over the life of the vehicle, assumed to be 14 years. The payback period is quite long however, and even though there are substantial savings in fuel costs, the additional retail price might deter prospective buyers. Table 2.1 shows the incremental retail price over an equivalent conventional vehicle and the payback period for petrol and diesel HEVs, over the next decade. Diesel/HEVs have a larger cost premium mainly since practical engine downsizing is limited due to lower torque response capabilities [60].

Table 2.1 Incremental retail price ($US) and payback period for Petrol/HEV and Diesel/HEV. Prepared with data from [60].

	Midsize Car				Large SUV			
	Incremental Price		Payback Period		Incremental Price		Payback Period	
Source	Petrol HEV	Diesel HEV	Petrol HEV	Diesel HEV	Petrol HEV	Diesel HEV	Petrol HEV	Diesel HEV
ORNL	$2,683	$4,123	9.5 years	11.4 years	$3,039	$5,912	4.1 years	5.8 years
EPRI	$2,500		7.4 years		$4,464		5.0 years	

Currently the incremental cost of HEVs is higher than the figures presented above. The Honda Civic Hybrid for example carries a premium of about US$ 6,800 for a similarly equipped Civic Sedan [61]. Sport utility vehicles carry a similar premium, with the Toyota Highlander Hybrid and the Lexus RX 400h, costing an extra US$ 5,600 and US$ 6,590 respectively [62,63].

HEVs have benefited from considerable public and governmental acceptance due to their considerable lower fuel consumption and emissions. How much of this is attributable to the hybrid powertrain is debatable though. Commercially released HEVs also integrate other technologies such as lower resistance tires and improved aerodynamics while being built with low-weight materials that substantially reduce the amount of energy needed to power the vehicle thus accounting for a considerable amount of the fuel savings.

In the case of the Plug-in Hybrid Electric Vehicle (PHEV), its requirements, unlike those of the HEV, causes the batteries to sustain deep discharges, which requires batteries capable of sustaining acceptable levels of performance over a wide SOC. Cycle life may be the most important challenge that batteries for this application will need to overcome. It is estimated that with a life span of 1000 cycles, the battery will have to be replaced every three years [59]. Weight is an important issue, as the PHEV requires considerably more batteries than the HEV in order to achieve similar range capabilities [60].

2.3.2. Supercapacitors

Some of the shortcomings of HEVs may be overcome with the inclusion of supercapacitors (also called ultracapacitors). Supercapacitors are devices capable of achieving very high levels of capacitance by using carbon electrodes with very large surface areas and an organic electrolyte. Its main attractive feature is its very high power density, which is in the range of 5,000 W/kg, and that is well maintained over a wide temperature range. They also have very long shelf life and high cycle efficiency [16]. However, supercapacitors suffer from low energy density, which can be as little as <5 Wh/kg [16].

Nevertheless, their excellent power capabilities make supercapacitors a very attractive option for their integration in HEVs, particularly to boost regenerative braking capabilities and acceleration. Buses using supercapacitors have already been developed and tested in Germany and China [64,65]. The city of Shanghai is unveiling its second generation of buses with supercapacitors that will also rely on lithium cells that will extend the buses range; previously the capacitors had to be charged at every bus stop [65].

Their high cost is one of the main problems hampering their introduction in most HEV applications, and the potential for cost reduction is controversial [53]. Furthermore, as their voltage varies with SOC, electronic control and switching equipment is needed [56], adding to its price tag. As the system is electrical, hybrid vehicles with supercapacitors still carry a penalty for transforming energy.

2.4. Flywheels

As discussed in section 1.4, one of the most promising energy storage technologies for automotive applications are high-speed flywheels. Advanced flywheels exhibit energy storage densities comparable to that of batteries, but with much higher power densities. In fact the power density of flywheels is determined essentially by the torque rating of the transmission and not by the flywheel itself.

This extensive section will present some of the most relevant characteristics of flywheels which understanding is critical for their successful integration in automotive applications and for a correct assessment on their effectiveness as energy storage devices for hybrid vehicles.

2.4.1. Key Characteristics

In contrast with batteries, the power capabilities of flywheels are independent on the amount of energy stored and on temperature, and its service lifetime is quoted in ranges of 10^5 to 10^7 full-cycles [16]. In fact, flywheels structural characteristics and its longevity are unaffected by deep cycling, which on a battery is highly detrimental [39]. Another useful characteristic is the ease by which the state of charge of the flywheel can be readily determined, as a simple measurement of its rotating velocity can establish this. The round-trip energy efficiency is typically quoted above 90%, but it is time dependant. For short-term storage, it can reach levels close to 100%, but aerodynamic and bearing losses causes it to decrease for medium and long term storage.

It is essential thus that the flywheel operates in a vacuum environment and that high efficiency bearings are used [66].

2.4.2. Flywheel dimensioning

The kinetic energy content of a body rotating with speed ω is given by

$$E = \frac{1}{2} I \omega^2 \tag{2.1}$$

Where I is the inertia of the body around its spin axis and is defined as

$$I = \int r \, dm \tag{2.2}$$

For a hypothetical wheel with its mass concentrated at the rim, its moment of inertia around its spin axis is simply $I = mr^2$. Substitution into equation (2.1) and subtracting by mass gives an expression for the energy density:

$$\frac{E}{m} = \frac{1}{2} r^2 \omega^2 \tag{2.3}$$

Clearly, increasing mass, shape and rotational speed increase the energy content of the flywheel. However, the amount of energy that can be stored is limited by the rotor's capacity to withstand the centrifugal forces, which are highest at the rim and that for the hypothetical flywheel are determined by:

$$\sigma = \rho r^2 \omega^2 \tag{2.4}$$

where σ is the stress at the rim of the rotor. With this, a ω_{max} for the tensile strength of the material σ_{max} can be found, which can then be used to find the maximum energy that can be stored by in the flywheel by substitution into equation (2.3):

$$\frac{E_{max}}{m} = \frac{1}{2}\left(\frac{\sigma_{max}}{\rho}\right) \tag{2.5}$$

It can be seen from the above equation that light materials with high strength wild yield the highest energy densities. Indeed one of the reasons for the renewed interest in flywheels has been the development of composite materials that substantially increase the energy densities achievable with this technology. For example, steel has a σ/ρ value of 0.23 X 10^6 m^2/s^2, while for polymer with reinforced glass fibre it is 0.8 X 10^6 m^2/s^2 and with reinforced carbon fibre it is an even higher 1.6 X 10^6 m^2/s^2 [66].

It is also worth remembering that the angular acceleration α of a rotating body with inertia *I* is directly proportional to the torque applied to it as given by

$$\tau = I\alpha \tag{2.6}$$

2.4.3. Sizing of the flywheel

The energy capacity of the flywheel is a measure of the maximum energy that the flywheel can hold, which can be easily found by substituting a maximum speed ω_{max} in equation (2.1) for a given flywheel design. Determining the energy capacity required goes hand in hand with the integration of the flywheel in the powertrain and depends heavily on the autonomy desired while powering the vehicle using the flywheel. If the flywheel is to be used mainly for regenerative purposes, then a reasonable estimate for the energy capacity might be the kinetic energy of the vehicle at cruising speed, say 60 mph. This energy may be provided by a single or multiple flywheels.

Ultimately the choice of energy capacity and dimensions of the flywheel must de decided by considering the energy requirements of the vehicle, the ratio requirements of the transmission as well as its losses, the aerodynamic and bearing losses on the flywheel, and of course the packaging of the whole system. The effect that changing the size of the flywheel can have on its speed and torque ratings can be briefly examined with a simple analysis:

Equation (2.1) can be rewritten as

$$\frac{dE}{dt} = \frac{1}{2} I_{fw} \alpha_{fw}^2 \tag{2.7}$$

Thus, using the expression above, for a given constant power it can be shown that for two flywheels with inertias I_{fw_1} and I_{fw_2}, the ratio of their angular accelerations can be written as

$$\frac{\alpha_{fw\_2}}{\alpha_{fw\_1}} = \sqrt{\frac{I_{fw\_1}}{I_{fw\_2}}} \tag{2.8}$$

and its torque ratio as

$$\frac{\tau_{fw\_2}}{\tau_{fw\_1}} = \sqrt{\frac{I_{fw\_2}}{I_{fw\_1}}} \tag{2.9}$$

Thus to store the same amount of energy increasing the inertia of the flywheel by a factor of four will decrease the speed of the flywheel and increase the required torque by twofold.

Increasing the inertia has therefore two important effects, it increases the torque rating required of the transmission but at the same time it reduces the angular speeds. Also, to have the same kinematic operability of the system, changing the inertia requires a change in the transmission ratio. This will be demonstrated in Chapter 6.

2.4.4. Bearings

The choice of bearings is one of the most important design challenges of flywheel systems. Bearings must be able to provide excellent stability at high-speeds, have high load capacity, resist shock and gyroscopic loads, run at very low friction and be able to do this under a reduced environment. They must also have an acceptable service life at a reasonable cost. The choice of flywheel geometry and its orientation will be determinant on the loads experimented by the bearings and ultimately in the choice of bearings.

Some flywheel designs incorporate magnetic bearings that significantly reduce friction losses. For instance, the group at University of Texas at Austin [38] chose magnetic bearings for their electric flywheel which they complemented with angular contact rolling bearings as backup. These types of bearings significantly reduce bearing friction which is necessary in applications requiring the long term storage of energy in the flywheel, but their non-contact nature further limits the dissipation of heat from the flywheel.

However, most designs use either angular contact bearings or a combination of rolling bearings providing protection for axial and radial loads. At reduced atmospheres bearing losses can be expected to be in the order of 20-35% of total losses at operating speeds. For instance, the General Motors group [33] which used a design combining ball and needle bearings, reported losses of 75 W of a total of 245 W for operating speeds of 12,000 rpm.

A larger review of bearing technologies is beyond the scope of this thesis, but the reader is referred to Shah [46] for a comprehensive review of bearing technologies for high speed flywheels.

2.4.5. Aerodynamic losses

Aerodynamic losses for low speed flywheels are almost negligible compared to the bearing losses, however for high-speed flywheel rotating at speeds in the order of magnitude of tens of thousands of rpms they quickly become quite significant. The windage torque of the flywheel is dependent on the square of its rotational speed and its power losses on the cube. It is therefore crucial to operate the flywheel in a reduced pressure environment to keep these losses at an acceptable level.

The windage drag torque is the sum of the drag on its side and rim surfaces and can be expressed as

$$M_W = \rho_g \omega^2 r^3 (C_s A_s + C_{rim} A_{rim}) \tag{2.10}$$

Where ρ_g is the density of the environment; r is the flywheel radius; A_s and A_r are the surface areas of the sides and of the rim of the flywheel respectively; and C_s and C_r are non-dimensional drag coefficients that depend (according to the environment in which the flywheel rotates) on other non-dimensional parameters: the Reynolds number, the Mach number and the Knudsen number.

Under a vacuum environment, energy losses (including aerodynamic and bearing losses) between 2-3% can be expected as reported by Flybrid [45].

2.4.6. Safety

Probably the most common concerns with the integration of high-speed flywheels in transport vehicles are those involving safety. In particular, questions are raised about the transmission of gyroscopic moments to the vehicle and about the containment of the kinetic energy of the flywheel in case of a catastrophic failure.

In general gyroscopic reactions will tend to be negligible for the likely sizes of vehicular flywheels and the magnitude of movements during normal operation of the vehicle, to be of real concern for the manoeuvrability and overall safety of the vehicle. They can however apply significant forces in the bearings, particularly if magnetic bearings are used. It is also important to understand under what conditions gyroscopic forces may become significant. This is explored in more detail in section 2.4.7.

There is little environmental concern from the disposal of flywheel as the materials used in its construction are generally inert. The rotor and containment usually consists of aluminium, steel or carbon fibre. Only the resins used in composites might require special handling but are non-toxic nonetheless when cured [16].

2.4.6.1. Containment

In any flywheel design the containment must be able to withstand a sudden failure of the flywheel. This can occur due to a loss of vacuum (whether sudden or leak), bearings failure, or material fatigue for instance. Systems with electric flywheels also run the risk of flywheel over speed, and start up without flywheel, such as the one used by the University of Texas at Austin group [67].

Containment tests have been successfully carried out and reported by the groups reviewed in 2.1.2. The General Motors group [33] designed a flywheel unit that consisted of a stack of thin discs, which is advantageous in the case of a failure as the individual discs are able to bend absorbing much of the energy of the flywheel. Tests were carried out at 32,000 rpm in which a single cymbal was purposely failed and little damage was found in the containment ring.

Burst tests were also carried out at 38,200 rpm by the University at Texas [67], and at 64,500 rpm by Flybrid [43]. In particular the Flybrid test was able to spin down the flywheel to rest at an impressive 5.9 seconds [68].

2.4.7. Gyroscopic Torques

McDonald [69] presents a methodology by which to calculate the reaction torques arising from gyroscopic effects in vehicles carrying high-speed flywheels, this includes an analysis of the possible movements of the vehicle that will give rise to gyrodynamic reactions. This work was later expanded by Murphy at al. [38], from the group at the University of Texas to analyse the effect of the forces acting on their large flywheel on their proposed magnetic bearings. This is a special case as the flywheel package is large and heavy, but the mathematical model they presented can be used to analyse flywheels rotating in gimbals and other damped support systems.

A rotating mass will exhibit gyroscopic forces when the orientation of its spin axis changes. This will inevitably be the case for a vehicular flywheel as the car manoeuvres around curves

or as the slope of the road changes. The magnitude of the forces experienced by the vehicle will depend on the orientation of the flywheel, its angular momentum and the rate of change of its spin axis. These forces can be easily estimated as shown next.

The angular momentum of a rotating mass is a measure of its resistance to changes in the orientation of its spin axis, and it is given by

$$\vec{H} = \vec{I}\omega \tag{2.11}$$

As the car changes direction (i.e. moving around a curve), it does so at a certain *precession* rate $\vec{\Omega}$. This precession rate changes the angular momentum of the flywheel at a right angle to both the original angular momentum and the application of the precession. This relationship is shown in Figure 2.8 and is given by

$$\frac{d\vec{H}}{dt} = \vec{H} \times \vec{\Omega} \tag{2.12}$$

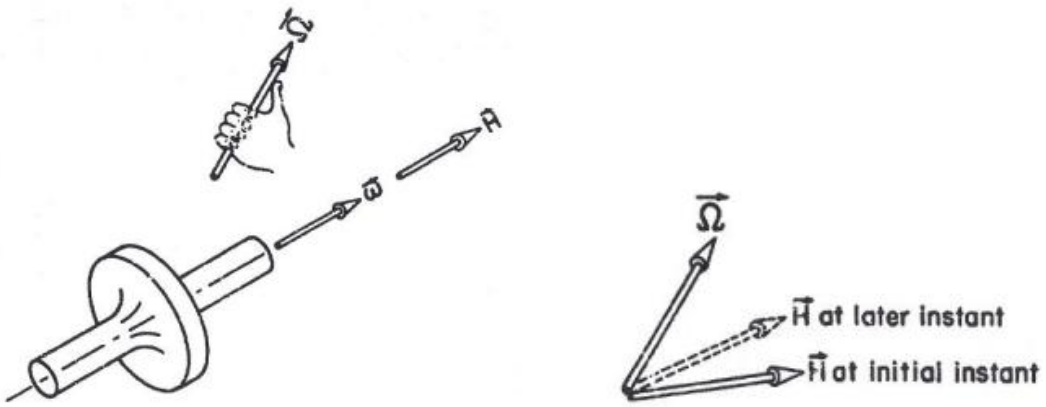

(a) (b)

Figure 2.8 (a) Schematic of angular momentum, angular velocity and precession rate, (b) Relationship of precession rate as the angular momentum changes [69].

Since angular momentum is conserved, a change in the direction of its spin axis results in an opposing torque being exerted on the flywheel package

$$\vec{\tau} = -\frac{d\vec{H}}{dt} \tag{2.13}$$

By combining equations (2.12) and (2.13), a relationship that relates the movements of the vehicle to the reaction torque exerted on the flywheel package is obtained

$$\vec{\tau} = \vec{H} \times \vec{\Omega} \tag{2.14}$$

This relationship can be used to determine the torques exerted on the flywheel package as the car manoeuvres. The effect that they will have on the vehicle will depend on their magnitude and direction. The magnitude of these reaction torques can be determined with the equation

$$\tau = H\Omega \, sin\theta_{H\Omega} \tag{2.15}$$

Where $\theta_{H\Omega}$ is the angle between the direction of the $\overrightarrow{H}$ and $\vec{\Omega}$ vectors.

It is only of interest to establish the maximum possible torques, which will occur when $\vec{\Omega}$ acts at a right angle to $\vec{H}$, and when the magnitude of $\vec{H}$ is the highest, which from equation (2.11) it can be seen to occur at the flywheel's maximum speed.

The manoeuvres of the vehicle can be described as yaw (going around a curve), pitch (going up or down a slope) or roll (an unlikely event of going down a ramp on the side of a highway), as shown in Figure 2.9.

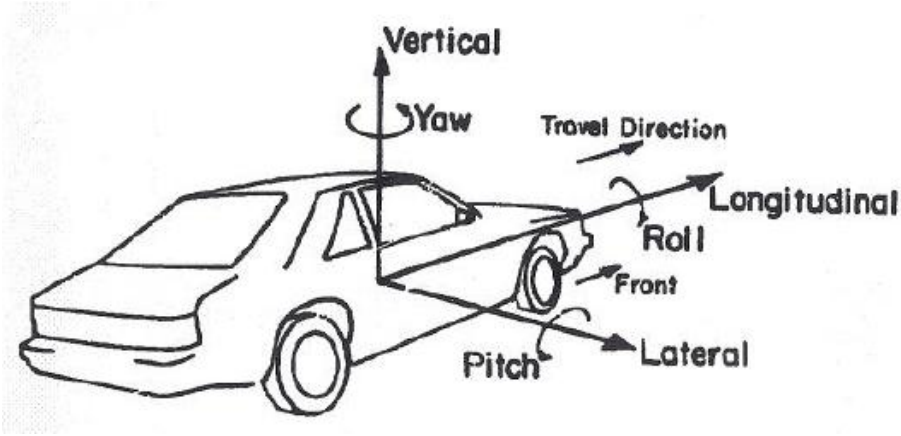

Figure 2.9 Vehicle axis system and vehicle manoeuvres used to describe gyroscopic motion [69].

T will be assumed that the flywheel will have one of three possible orientations: vertical, longitudinal or lateral. The direction of the torque reaction will depend on how the vehicle moves and it can be determined by using the right-hand rule, where the index fingers points in the direction of the angular momentum, the fingers warp around the precession direction, and the thumb gives the direction of the resultant torque. Table 2.2 shows the directions that the reaction torque will take for each possible case.

Table 2.2 Reaction torque sense depending on the orientation of the angular momentum (flywheel orientation)

Orientation of angular momentum	Direction of precession Ω		
	+ Yaw	+ Roll	+ Pitch
+ Vertical	None	- Pitch	+ Roll
+ Longitudinal	+ Pitch	None	- Yaw
+ Lateral	- Roll *	+ Yaw	None

The effect that varying the geometry of the flywheel will have in the magnitude of the induced gyroscopic torques can be examined with the use of an example.

From equation (2.14) it can be seen that the magnitude of the torque depends on the angular momentum and the precession rate. The precession rate is carried out by the vehicle and is thus independent of the geometry and size of the flywheel, but angular momentum is not (equation (2.11)). Its effect can be examined by a considering two flywheels, one with a cylinder-like geometry and radius r_1, and another one with a more disk-like geometry and radius $r_2 = x\, r_1$, both of which will carry the same amount of energy. Keeping the maximum tensile stress equal for both flywheels ($\sigma_{1\,max} = \sigma_{2\,max}$), and assuming that the maximum flywheel speed will be determined by stresses on its rotating material, it can shown by using equation (2.4) that

$$\omega_{2\,max} = \frac{\omega_{1max}}{x}$$

And since both flywheels have the same maximum energy ($E_{1max} = E_{2max}$), by using (2.2) and substituting the above equation, it can be shown that

$$I_2 = x^2 I_1$$

Finally, equation (2.11) can be used to compare the angular momentums for both flywheels and by substituting the expressions obtained above for $\omega_{2\,max}$ and I_2, and using equation (2.14) an expression relating the reaction torques is obtained

$$\tau_2 = x\, \tau_1$$

Although the actual stress concentration may vary for different flywheel designs (thus affecting the maximum rotating speed), the previous expressions show that induced gyroscopic torques will tend to increase with the flywheel's radius, favouring a long cylinder-like design. Significantly, it can also be shown that both flywheels will have the same mass.

This trend will be valid as long as the maximum tensile stress of the flywheel limits its allowable maximum angular speed, which tends to be the case for flywheels with large radius. As the radius decreases and the allowable maximum speed for the material increases, other limiting design parameters come into play, such as the bearing's maximum operating speed. In this case, to deliver the same amount of energy, equation (2.1) implies that without changing the maximum angular speed, the inertia must stay constant, and to keep the flywheel's inertia constant a reduction in radius must be accompanied by an increase in mass. This is illustrated in plot (b) of Figure 2.10 which shows how the angular momentum and mass of a flywheel change as the ratio R_{fw} = radius / length changes. For a flywheel with a given energy capacity, there is clearly a ratio R_{fw} that will provide the lightest flywheel with the lowest angular momentum and hence gyroscopic forces. The flywheels used in the simulations presented in Chapter 6 are dimensioned according to this principle.

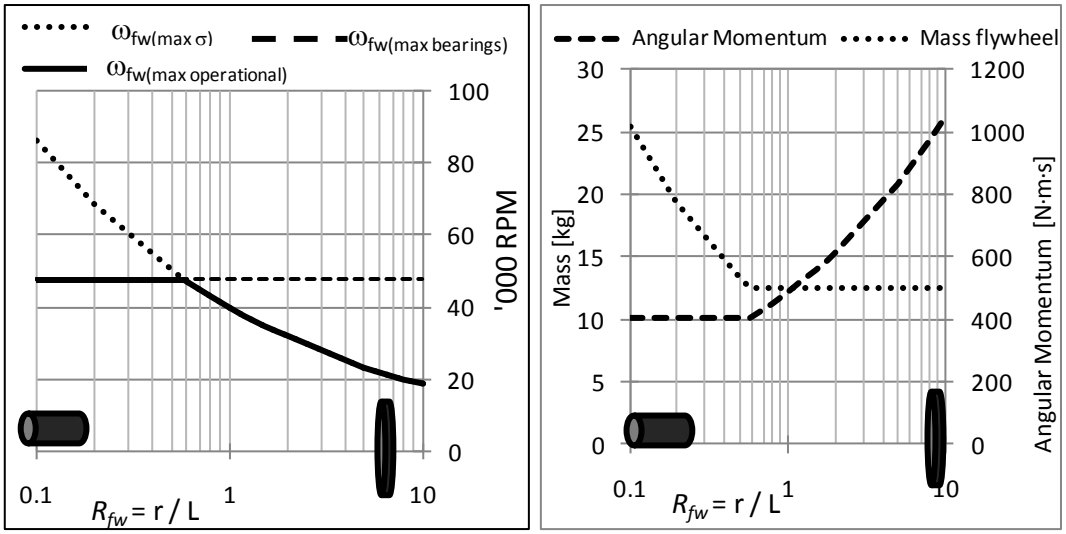

(a) (b)

Figure 2.10. Plot (a) on the left shows the dependency of ω_{max} changes from the ω_{max} allowed by the bearings to the ω_{max} allowed by the maximum tensile stress of the material as the ratio R increases. Plot (b) shows the effect that these dependencies have on the mass and angular momentum of the flywheel.

Appendix A shows an example on the calculation of the gyroscopic torques that a vehicle may encounter. It is shown there that these tend to be quite small to affect vehicle manoeuvring, especially if a careful orientation of the flywheel is chosen.

2.4.7.1. Designs with no net gyroscopic torques

The previous discussion assumed that the flywheel installation was stiff in the vehicle implying that a precession of the vehicle is also experienced by the flywheel. It is possible though, to mount the flywheel in a set of gimbals, so that its spin axis is maintained regardless of the vehicle's motion. This is rarely necessary unless a very large flywheel is used such as the one described in [38]. Mechanical power transfer with such mounting can be an important design challenge.

Another method for cancelling gyroscopic torques is to have two counter-rotating flywheels as the on e propose in [70]. This is shown in Figure 2.11. In this case the flywheels would experience opposed gyroscopic torques which would cancel the net torque that the flywheel package exerts on the vehicle.

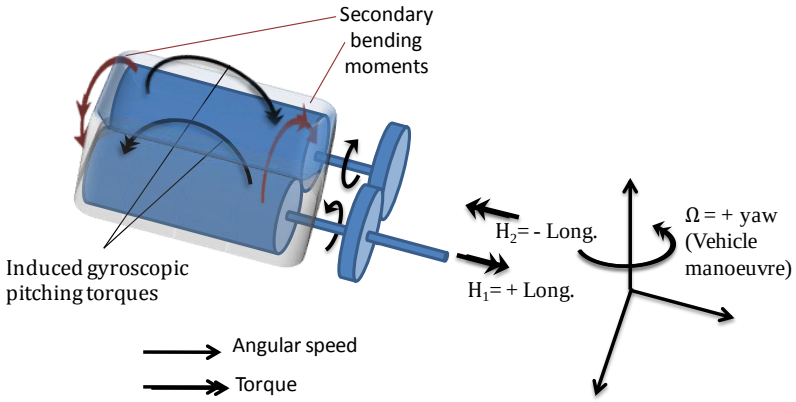

Figure 2.11 The figure shows the reaction torques for each flywheel, and the resulting bending moments on the flywheel package for a precession (Ω) yawing motion.

2.4.8. Maintenance and life service, expectancy

Maintenance costs are quite low depending on the system used, mechanical bearings could need replacing every 3 to 10 years and the vacuum pump every 5 years, while magnetic bearing are maintenance free [40,39]. It is important to note that in automotive applications, replacement of bearings might be needed sooner than as reported above, as these estimates are based on applications where the flywheel is stationary as is not subjected to dynamic road loads.

2.5. Continuously Variable Transmissions

One of the main challenges in the integration of high-speed flywheels in automobiles is the relatively complex challenge of controlling power flow in and out of the flywheel itself. During operation of the system, the flywheel and the vehicle's wheels will be rotating independently of each other, with the flywheel rotating in a wide range of angular speeds ranging from zero to perhaps tens of thousands of RPMs, while the vehicle's wheels will have a maximum angular speed that will probably top at around 150 RPMs. Virtually all speed ratios of flywheel to vehicle speed within their operating ranges may be possible, therefore the designed transmission must be able to accommodate a wide range of speed ratios in a continuous, non-discrete manner. This can be accomplished either with an electrical or a mechanical Continuously Variable Transmissions (CVT). The electrical transmission is briefly discussed in the next section.

It is worth noting that speed variator devices are increasingly known as CVTs. However in order to differentiate with other transmissions that may or not use speed variators to create a variable speed transmission, the term *variator* is used to refer to a component delivering variable speed ratio such as a toroidal or V-belt variator, while the term CVT is reserved for the whole section of the transmission that delivers variable speed. A CVT in this context may consist of a single or a set of variators, a planetary gear set, or a power split transmission combining these devices.

Mechanical CVTs are a main part of the study of this thesis and they are studied in more detail in Chapter 3. Those transmissions rely on the use of speed-variators and planetary gear sets which are introduced in sections 2.5.2 and 2.5.3 of the present chapter.

2.5.1. Electrical transmission

Transmitting power electrically to and from the flywheel as in [36] would render the flywheel an electrical machine, transmitting power as a motor/generator. The flywheel itself would be an energy storage device that would receive and deliver energy electrically and another set of motor/generator would be required to convert electrical energy to a useful mechanical energy to propel the vehicle.

During a regenerative braking a generator would convert the vehicle's kinetic energy to electrical energy and transmit this power to the flywheel, where an electrical machine acting as a motor would accelerate the flywheel inertial mass. Conversely during acceleration the flywheel's electrical machine acts as a generator decelerating the flywheel and transmitting power to the external motor where it can be used to propel the vehicle.

A major advantage of this system is that a flywheel package that holds vacuum is more easily designed with such a transmission system. Also the kinematic complexities of a mechanical connection are avoided.

However the flywheel must accommodate several design modifications. A cooling system must be designed into the flywheel package to dissipate the heat generated from electrical losses (eddy, resistive, etc). The choice of construction materials is severely constrained, and angular speeds will probably be constrained by the choice of rotor materials. Furthermore, the controller system would have to be able to control the flywheel and the propulsion motor/generator that will very likely be operating in very diverse and different conditions.

Furthermore, power flow from the vehicle to the flywheel and back to the vehicle entails four energy conversions, from mechanical to electrical to mechanical when braking regeneratively with the flywheel and back again when using this energy to drive the vehicle.

2.5.2. Planetary Gear Set

The use of a planetary gear set (PGS) is an attractive option in applications where a high ratio of reduction is required in a compact space [71]. It can also provide superior ratio coverage and higher efficiency than directly using a variator [20].

In many applications such as in automatic transmissions, it is common to fix one of the branches of the PGS. Such a configuration provides a fixed speed ratio between the rotating branches, and by changing the input and output branches and the branch that is fixed, many different speed ratios are available, including reverse. However, to provide a continuously variable ratio, it is necessary to use the PGS as a two degrees of freedom device with all the branches free to rotate.

Power flow through the PGS is better understood by examining its torque equilibrium and kinematic equations. These equations can be derived using the methods first developed by Robert Willis in his Principles of Mechanisms in 1841, and are presented and explained in great detail by White in [72].

The convention used is that positive power adds energy to the PGS while negative power draws energy from it. Thus, direction of power flow is determined by the direction of torque and rotational speed of the branches as shown in Figure 2.12. A torque applied in the direction of rotation adds power to the PGS while a torque in the opposite direction withdraws energy.

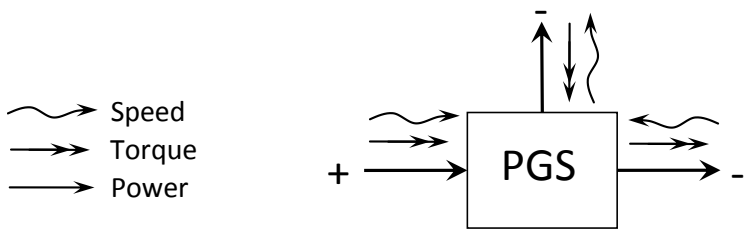

Figure 2.12. Sign convention used for the PGS. A torque applied in the direction of rotation produces positive power, which in the convention used means energy entering the system.

White suggests the definition of a PGS ratio R_P that can be used to simplify the description of the kinematic relationships of the branches of the PGS. This ratio is given by

$$R_p = \left(\frac{\omega_3}{\omega_1}\right)_{\omega_2=0} = \frac{\omega_3 - \omega_2}{\omega_1 - \omega_2} \tag{2.16}$$

Depending on how the branches of the PGS are assigned to ω_1, ω_2 and ω_3 in equation (2.16), R_p will be calculated differently and will have different lower and upper limits. Table 2.3 shows the six possible definitions of R_p according to these branch allocations. Notice that each definition can be found with respect to each other. This table will be useful later in the assessment of power-split transmissions in the next chapter.

Table 2.3 Planetary Gear Set ratio R_P depending on branch assignments.

Symbol	Definition	Basic ratio	Possible range
$\boldsymbol{R_1}$	$\frac{\omega_S - \omega_C}{\omega_R - \omega_C} = \frac{R_4}{(R_4 - 1)}$	$-\frac{D_R}{D_S}$	$-\infty < R_1 < -1$
$\boldsymbol{R_2}$	$\frac{\omega_R - \omega_C}{\omega_S - \omega_C} = \frac{(R_4 - 1)}{R_4}$	$-\frac{D_S}{D_R}$	$-1 < R_2 < 0$
$\boldsymbol{R_3}$	$\frac{\omega_C - \omega_R}{\omega_S - \omega_R} = 1 - R_4$	$\frac{D_S}{D_R + D_S}$	$0 < R_3 < 0.5$
$\boldsymbol{R_4}$	$\frac{\omega_C - \omega_S}{\omega_R - \omega_S}$	$\frac{D_R}{D_R + D_S}$	$0.5 < R_4 < 1$
$\boldsymbol{R_5}$	$\frac{\omega_S - \omega_R}{\omega_C - \omega_R} = \frac{1}{R_4}$	$\frac{D_R + D_S}{D_S}$	$1 < R_5 < 2$
$\boldsymbol{R_6}$	$\frac{\omega_R - \omega_S}{\omega_C - \omega_S} = \frac{1}{(1 - R_4)}$	$\frac{D_R + D_S}{D_R}$	$2 < R_6 < \infty$
$\boldsymbol{D_S}, \boldsymbol{D_R}$ = Pitch diameters of the sun and ring gears of the PGS respectively. The diameter of the planet gear is relative to both $\boldsymbol{D_S}$ and $\boldsymbol{D_R}$ and is not needed.			

There is no convention on how this assignment is done and routinely authors choose one of the six definitions described before and apply it consistently through the derivation of transmission equations. The problem with this approach is that depending on how the branches of the PGS are connected in a transmission, different equations (for example describing the transmission ratio) are required for each of the possible combinations of branch assignments, resulting in the derivation of different but equivalent equations (see for example [73,74,50]).

In this thesis the choosing of a particular definition for R_p is forfeited so that all the derived equations can be used for any PGS connections. This will become clearer and be particularly useful in the analysis of power-split continuously variable transmissions in section 3.4.

Equation (2.16) can be written as

$$\omega_3 = R_p\omega_1 + (1 - R_p)\omega_2 \tag{2.17}$$

The power and torque equilibrium equations for the PGS when ignoring losses are given respectively by:

$$\tau_1\omega_1 + \tau_2\omega_2 + \tau_3\omega_3 = 0 \tag{2.18}$$

$$\tau_1 + \tau_2 + \tau_3 = 0 \tag{2.19}$$

where τ_1, τ_2 τ_3 are the torques at the branches of the PGS. Using equations (2.17), (2.18) and (2.19) the following useful relationships are derived

$$-\tau_3 = \frac{\tau_1}{R_p} = \frac{\tau_2}{(1 - R_p)} \tag{2.20}$$

An interesting thing to note is that regardless of the planetary ratio definition chosen from Table 2.3, the sense of the torque at the carrier gear ($+\tau_C$) is always opposite to the senses of the torques at the sun ($-\tau_S$) and ring gears ($-\tau_R$).

Inspection of equation (2.20) also shows that given a known torque at one of the branches, the torque at the other branches is readily determined. However, as shown in equation (2.17), angular speeds (and therefore power flow) depends on known conditions at two of the branches.

This relationship is more easily visualised with the use of a nomogram (Figure 2.13) in which the linear relationship between the speed of the branches can be fully appreciated. In the figure, ω_2 is plotted on a vertical line crossing at $x = 0$, ω_1 is plotted on a line crossing at $x = R_p - 1$ and ω_3 on a line crossing at $x = R_p$. By plotting the known angular speeds of two of the branches, say ω_2 and ω_1 and drawing a straight line crossing through both values, the speed of the third branch ω_3 can be found by finding the intersection of the line with the vertical line crossing $x = R_p$.

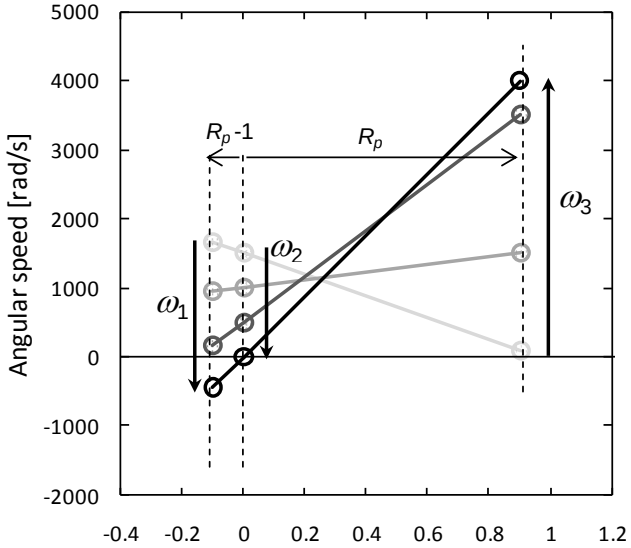

Figure 2.13 Nomogram for the kinematic equilibrium of a PGS with an R_4=0.9. The figure illustrates the equilibrium speeds during a regenerative braking event. It can be seen that as the ring and carrier (vehicle) decelerate, the sun (flywheel) accelerates, maintaining the linear kinematic relationship as defined in equation (2.17).

Figure 2.13 is actually representing a regenerative braking event in which the planetary ratio is defined as $R_p = R_4$, and where the flywheel is connected to the sun gear, the vehicle's driveshaft connects through the carrier branch, and the ring gear is used as a control gear which speed can be independently modulated (with a motor for example). Time progresses from the brightest to the darkest line. With the flywheel (ω_3) initially discharged, a torque is applied at the ring gear (ω_1), which causes the vehicle to decelerate (ω_2) and its kinetic energy to transfer to the flywheel accelerating it. The kinematic relationship of the PGS is such that the ring gear will reach zero speed before the vehicle stops completely. This means that in order for full regenerative braking to take place the ring gear must then be accelerated to a negative speed (relative to the sun and ring gears).

2.5.3. Speed Variators

Speed variators are increasingly being used in small, mid-sized and hybrid vehicles. These devices are unique in that they do not use fixed gears to provide the necessary speed ratios but instead rely in variable mechanisms capable of providing an infinite choice of speed ratios within a boundary ratio range. Variators usually have considerable friction losses compared to traditional transmissions where components are gear meshed. However, their capability to infinitely adjust transmission speed ratio allows the ICE to be used at its most efficient condition for a given power requirement, with most gains encountered at low speed and during acceleration and deceleration where speed ratios change constantly. At constant

cruising speeds, the lower efficiency of the variator means that a fixed gear transmission is more efficient [75].

The ratio coverage of a variator can be expressed as a ratio of its maximum to minimum speed ratios

$$V_t = \frac{V_{max}}{V_{min}} \tag{2.21}$$

Variators are an obvious choice for flywheel applications. The variability of speed demand and energy stored at the flywheel requires a variable and continuous matching of vehicle and flywheel speeds. However they have ratio coverage typically hovering around 5 to 6.25 which may be insufficient for applications with flywheels, and thus they may need to be complemented with other transmission elements that increase this ratio spread.

The most common type of variators in automotive applications are the V-belt and toroidal variators, but there are also hydrostatic and other roller-based variators.

V-belt speed variator

The variator most commonly used in vehicle applications if the V-belt variator. It is based on the Van Doorne transmission which uses two variable pulleys connected at the crankshaft and driveshaft ends of the transmission and a steel belt that transmits power between pulleys. Variable speed ratio is achieved by varying the distance between each pulley's halves changing the ratio between each pulleys radius. The distance between each pulley halves is adjusted with hydraulic pressure which increases the clamping pressure for higher loads.

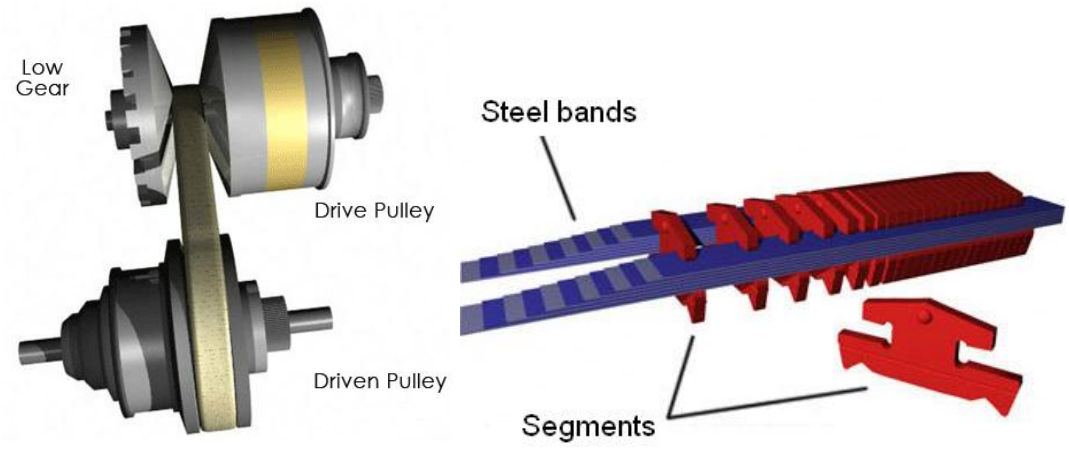

(a) (b)

Figure 2.14 (a) A V-belt variator in low gear, (b) elements of the transmission belt. Figures taken from [76].

The steel belt consists of a number of steel bands (typically 12) hold together by steel segments blocks. During operation the steel band work in tension while the interaction between the pulleys, segments and bands causes the segments to work in compression to transmit power [77]. These types of transmission tend to be favoured for low torque applications, however transmission torques of up to 450 Nm are claimed [78].

Sources of losses include friction between the variator elements, pulley deflect and belt slip [77,79,80]. Efficiency of the variator depends on the torque and speed being transmitted and on the regime operation (high or low gear) of the variator, with experimental measurements [77] suggesting poor efficiency at low torque operation and efficiencies hovering between 80-95% at high output torques.

Roller-based variators

The most common type of roller-base variator is the toroidal variator (Figure 2.14(a)). It consists of two toroidal shaped disks connected at opposite ends of the transmission and a pair of steerable rollers that transmit power between both disks by rolling at varying angles. A step-less ratio change is achieved by smoothly varying the relative angle at which the rollers revolve. The rotation of the rollers is set by a balance of forces between the contact forces at the rolling surfaces (set by a pressure chamber at the ends of the toroidal unit clamping the toroidal disks together) and a force being applied to the rollers. The speed ratio of this variator is thus said to be *torque actuated* [81]. This type of variator is used in the Flybrid-Torotrak transmission described in section 2.1.2.6.

Other roller based variators include the Milner variator [82] which uses a set of roller balls to change the effective radius of two transmissions disks. Experimental measurements reported in [82] give a maximum transmission efficiency of 90% occurring in high ratio and decreasing to a minimum of 75% as the ratio is decreased to low ratio regime.

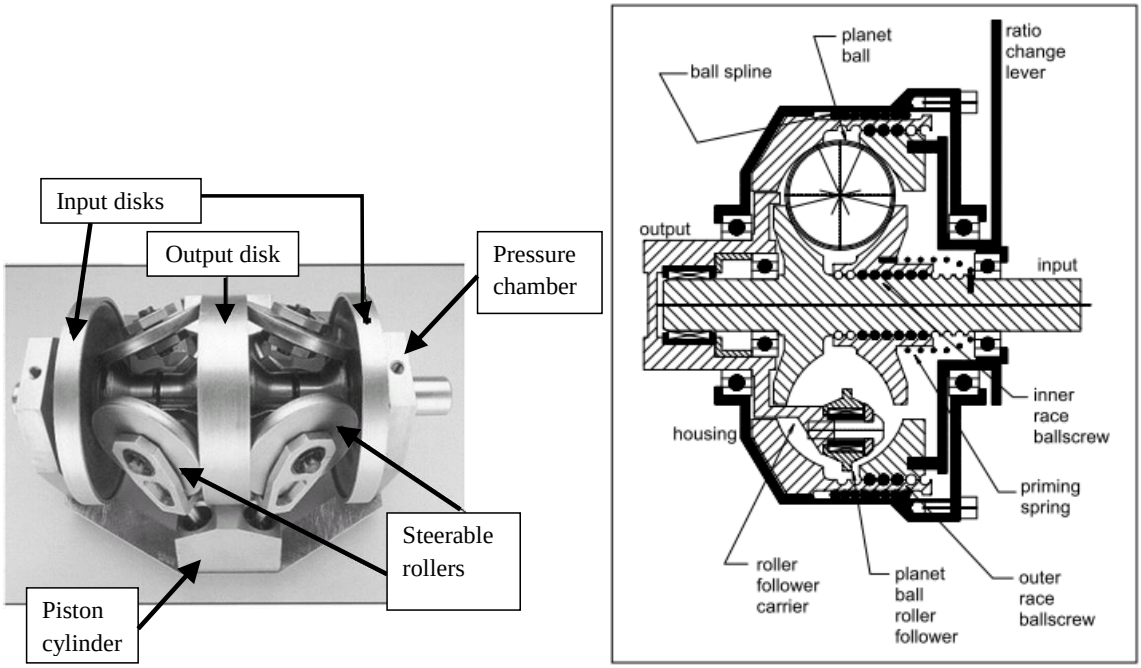

(a) (b)

Figure 2.15 (a) Parts of a Torotrak toroidal variator [83], (b) a Milner rolling variator [82].

2.6. Literature Survey and Technology Background Summary

In the first part of this chapter, the most relevant studies of vehicles incorporating flywheels have been reviewed. The survey has revealed a wide range of flywheel inertias used and types of transmissions proposed.

Thereafter, an introduction on energy storage technologies was presented; with an extensive section covering some fundamental characteristics of flywheels. The challenge of mechanically linking the flywheel with a conventional powertrain was recognised, and the use of a continuously variable transmission was identified as essential for this purpose.

In the latter part of the chapter, the fundamentals characteristics of the variators and planetary gear sets, which can be used to construct these transmissions have been presented. The kinematic behaviour, and the identification of performance limits of transmissions employing these components is the subject of study of the next chapter.

3. MECHANICAL CONTINUOUSLY VARIABLE TRANSMISSIONS

Using a mechanical transmission for the flywheel has several advantages compared to an electrical option. It does not have an energy conversion penalty and the cost is potentially less, as the expense of two electrical machines (one contained within the flywheel and another one in the driveshaft) and of the power electronics is avoided.

A major downside however is that it requires a transmission capable of providing a speed ratio for the disparate speeds of the vehicle and flywheel and to do this at a reasonable efficiency. The design and operation of the transmission is complex which may limit the use of the system, and packing of the system may be an issue. Any detail design must also provide a low loss vacuum seal allowing the flywheel to spin in a vacuum environment but permitting power to be transmitted in and out of the flywheel mechanically.

A mechanical transmission has two important design challenges: the kinematics of the transmission and the torque capacity of the components. Different designs have to find a compromise that will maximise the operability of the system which can be said to be constrained by the kinematics of the components, and its size and cost which are heavily dependent on the torque rating of the components.

There are a few ways of accomplishing a continuously variable transmission. One option is to use a speed variator, such as a V-belt or toroidal type. As discussed in section 2.5.3, these variators typically have a ratio spread between 5 and 6.25, and their direct use with a flywheel system requires the addition of a fixed set of discrete gears to provide wider speed ratio coverage. These transmissions are discussed in section 3.3.

Another approach is to use both a variator and a planetary gear set (PGS) to create a transmission in which power is split trough two transmission branches. Depending on the design used, these transmissions can offer when compared to a direct variator transmission, either higher efficiency but lower speed ratio spread, or higher ratio spread at lower efficiencies. These transmissions are studied in detail in section 3.4.

Finally, a PGS can also be used to provide continuously variable speeds if it is operated as a two degree of freedom device. The use of such a transmission is discussed in section 3.5.

These transmissions have different efficiencies and ratio spreads, and understanding their advantages and limitations is paramount for the design of an appropriate transmission for vehicles incorporating flywheels.

Simulations on the performance of these transmissions on a hybrid vehicle incorporating a flywheel are presented in Chapter 6.

3.1. Design Objectives

It is worth defining what is desired from a transmission system for the specific case of a vehicle with a flywheel.

Three main targets can be identified:

1. Wide range of operation allowing the system to capture braking energy and to reuse it at levels yielding significant energy savings.

2. The designed system should have reasonable efficiency.

3. Cost of the system should be minimised. The commercial success of a mechanical transmission depends highly on having a price to consumer well below of those of an electrical system.

There is a trade-off between all these objectives. As will be shown throughout this chapter, the operating range of the system can be greatly increased with the addition of various components at the expense of increase complexity and cost. An increased range of operation can also be accomplished at a low cost with the addition of brakes and slipping clutches, but at the expense of efficiency having the effect of diminishing energy savings and reduced life of components.

3.2. Modes of operation

To aid in the discussion of this chapter, three modes of operation are identified. These are: regenerative braking mode (RB) when energy is transfer from the vehicle's driveshaft to the flywheel; flywheel-acceleration mode (FA) when the flywheel provides the energy that propels the vehicle; and neutral (N) when no energy is transferred between the flywheel and vehicle.

The speed ratio of the transmission, which will be used extensively throughout this section is defined as

$$r = \frac{\omega_o}{\omega_i} \tag{3.1}$$

where ω_o is the rotational speed at the driveshaft side of the transmission, and ω_i is the rotational speed at the flywheel side.

3.3. Variator transmission

A transmission incorporating a high-speed flywheel requires ratio spreads that are beyond those offered by current variator technologies. However, this can be overcome with the addition of a gearbox in series providing different regime operations. A two-regime system for example can square the ratio spread of a variator. Such a concept was identified by the University of Wisconsin Group (section 2.1.2.2) and briefly discussed in [31].

The transmission analysed by General Motors and discussed in section 2.1.2.3 relies in the use of a V-belt push variator with a 5.6:1 ratio and with no gearbox. However a flywheel with a relatively low maximum speed (12,000 rpm) and with a step down gear of 6:1 was used.

As discussed in section 2.5.3, variators have lower transmission efficiencies than gearboxes with meshed elements, and it is therefore not surprising that both of the studies mentioned above identified losses at the variator unit as one of the key elements impeding the realisation of potential fuel savings. It is important to say however, that these are dated studies (early 80's) and that a better understanding of the origin of variator losses and lubricants have led to units with efficiencies rivalling those of meshed gears.

As the transmission ratio between a flywheel and a vehicle changes more rapidly than that of a conventional vehicle, care must be taken to design a system that minimises regime changes to accomplish these ratios. These might be accomplished at the expense of a flywheel with higher inertia requiring less ratio spread for the transmission.

The performance of this type of transmission under a standard drive cycle will be simulated along with other proposed transmissions in Chapter 6.

3.4. Power-split Continuously Variable Transmissions (PS-CVT)

One way of increasing the ratio coverage of a variator based transmission is to use a Power-Split Continuously Variable Transmission (PS-CVT). These transmissions have attracted some attention in the automotive industry as they offer several advantages over standard transmissions. Aside from the potential fuel economy improvement of operating the engine through an optimum low specific fuel consumption line, some power-split configurations allow for reverse and geared neutral gears without the need for a clutch or torque converter.

Such a transmission can be achieved by providing two branches as possible power paths: a variable speed ratio branch with a variator and a fixed-ratio mechanical branch. At an end of the transmission a PGS is then used to "sum" the power from each branch again.

Characterising the kinematics and power flow of these transmissions is a complex effort. It depends not only on the speed ratios of the fixed gears, the variator and the PGS, but also on how the branches of the PGS are connected in the system. Several authors have analysed many of these configurations [72-74,50,84], sometimes with slightly different powertrain architecture arrangements and ways of defining the PGS ratio. All this leads to equivalent but different equations for the description of the transmission and so it is important to be aware of how the derivations are reached.

In [72] White provides the most general case of the literature surveyed and the easiest to adapt for the particular requirements of the PS-CVT studied. In this section derivations for the specific system studied, the layout of the system is analysed and a methodology is proposed for system specification.

Vehicles with flywheels utilising power-split transmissions include the prototype vehicle developed by The University of Wisconsin Group (see section 2.1.2.2) that makes use of a hydrostatic variator, the one proposed by the Swiss Federal Institute of Technology (see section 2.1.2.4) which uses a V-belt variator, and the one proposed by Torotrak for road vehicles which is reported in [44] and uses a toroidal variator.

3.4.1. Configurations of PS-CVT

There are two basic configurations for a PS-CVT transmission depending on whether the variator branch is connected to the input or output branches of the PGS. These are shown in Figure 3.1 along with the possible operating modes depending on how power flows through the system. For transmission with a flywheel, the input side corresponds to the flywheel side and the output to the vehicle's driveshaft, therefore the figure below shows a system operating in flywheel assisted mode with power flowing from the flywheel to the wheels.

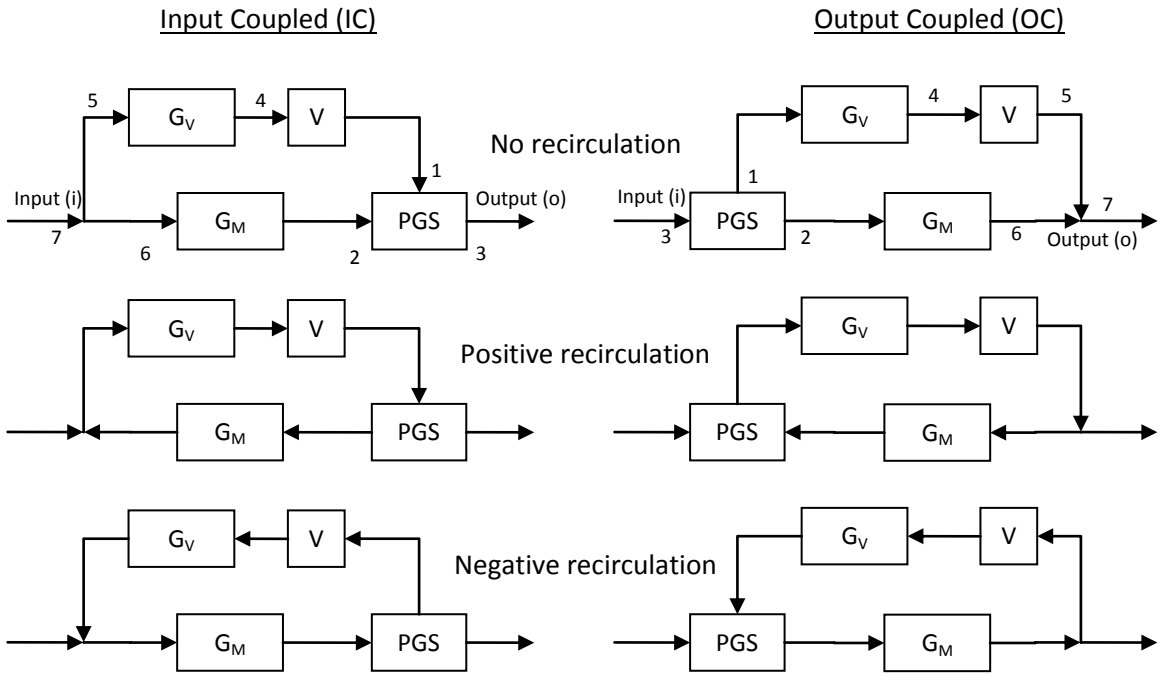

Figure 3.1 Operating modes for the Input Coupled and Output Coupled transmissions during FA mode. G_V and G_M are fixed gears of the variator and fixed ratio branches respectively. V is the variator unit and PGS is the planetary gear set.

In the input coupled (IC) transmission, power is *integrated* via the PGS at the end of the PS-CVT transmission. A zero speed output, or even a reverse speed is possible with some designs by adjusting the variator ratio. In such conditions a clutchless launch of the vehicle is possible by adjusting the variator ratio.

In an output coupled transmission (OC) power is *differentiated* at the PGS before going through the variator and fixed-ratio branches. A zero speed output is not possible unless the variator has capability for a zero speed ratio which may be possible with a hydrostatic variator as proposed in [73], this is similar to having a clutch in the variator branch and allowing it to slip.

The branches of the PGS can be connected differently within a PS-CVT. To name them, a convention found commonly in literature (see [73,74] for example) will be used. It consists of a prefix specifying whether it is input coupled (IC) or output coupled (OC), and a three letter code in which the first letter corresponds to the branch of the PGS connected to a variable speed branch (variator branch for PS-CVT), the second letter to the branch connected to the fixed-ratio branch and the third letter corresponding to either the output branch (for IC) or input branch (for OC). Thus an IC-RSC configuration corresponds to an input coupled transmission with the ring gear connected to the variator branch, the sun gear connected to the fixed-ratio branch and the carrier gear acting as the output branch. It follows that each IC and OC configurations have six possible combinations.

For a transmission with a flywheel, power flow will reverse during regenerative braking, and an input coupled transmission will behave as an output coupled one. In this section, derivations will be performed assuming an IC transmission and the nomenclature shown in Figure 3.1 is kept fixed for FA and RB modes except that the input and output labels are reversed.

3.4.2. Ratio coverage of PS-CVT

A disadvantage of PS-CVT transmissions is that in order to increase the ratio coverage of the transmission there must be power recirculation [72]. The problem is that the variator branch may be carrying more power than the output branch, and since the variator is likely to be the component with the lowest efficiency of the transmission, the overall efficiency of the transmission will suffer. This also means that in order to increase the efficiency of a variator based transmission with a power split arrangement a system with no power recirculation is required, which would come at the expense of decreased speed ratio coverage.

To understand this it is useful to first derive an equation for the transmission ratio of the PS-CVT. Similar derivations can be found in [72-74,85] with different gear arrangements or with defined PGS branch assignments. However, it is convenient not to assign a PGS configuration yet and to study this in a general PS-CVT system as the one shown in Figure 3.1.

Thus with ω_1, ω_2 and ω_3 as in Figure 3.1 for the IC configuration, the transmission ratio as defined by equation (3.1) can readily be written as

$$r = \frac{\omega_3}{\omega_7} \tag{3.2}$$

and the gear ratios as

$$G_V \cdot V = \frac{\omega_1}{\omega_7} \quad \text{and} \quad G_M = \frac{\omega_2}{\omega_7}$$

Where G_V and G_M are the gear ratios of the variator and fixed-speed branches of the PS-CVT and V is the speed ratio of the variator. It is also noted that the speed of branches 5, 6 and 7 is the same, thus $\omega_5 = \omega_6 = \omega_7$.

Using the above expressions in equation (2.16) the transmission ratio for an input coupled configuration can be written as

$$r = G_M(1 - R_p) + VG_V R_p \tag{3.3}$$

The form of equation (3.3) corresponds to the branch assignments of Figure 3.1. This means that depending on the value of R_p used an implicit arrangement of the PGS branches must be assumed in the system. So for a given PGS there is a unique value of R_p for each of the six power-split configurations that arise from different ways of connecting the PGS. These configurations are shown in Table 3.1, along with the equivalent planetary ratios for an example PGS.

Table 3.1 Power-split configuration corresponding to a value of R_p.

PGS Ratio	Power-split configuration	Possible range	Example planetary ratios for a PGS with $D_R = 3D_S$
$\boldsymbol{R_1}$	RCS	$-\infty < R_p < -1$	-3
$\boldsymbol{R_2}$	SCR	$-1 < R_p < 0$	-1/3
$\boldsymbol{R_3}$	SRC	$0 < R_p < 0.5$	1/4
$\boldsymbol{R_4}$	RSC	$0.5 < R_p < 1$	3/4
$\boldsymbol{R_5}$	CRS	$1 < R_p < 2$	4/3
$\boldsymbol{R_6}$	CSR	$2 < R_p < \infty$	4

Equation (3.3) can be used to find the maximum and minimum ratios attainable which occur at the speed-ratio limits of the variator V_{max} and V_{min}. The ratio coverage of a transmission is usually measured with the parameter

$$r_t = \frac{r_{(V\max)}}{r_{(V\min)}} \tag{3.4}$$

However this is an unsatisfactory parameter for transmissions capable of achieving zero-speed or reverse, and it is convenient instead to use a normalised ratio coverage C_r as proposed by Beachly et al. [30], which is defined as

$$C_r = \frac{r_{(V\max)} - r_{(V\min)}}{r_{(V\max)}} \tag{3.5}$$

An equation for the ratio of input power that goes through the variator branch can also be written. Neglecting losses at the variator and fixed-ratio branches, this can be written for either FA or RB mode as

$$\frac{P_V}{P_i} = \frac{\tau_5\omega_5}{\tau_i\omega_i} = \frac{\tau_5\omega_5}{\tau_5\omega_5 + \tau_6\omega_6} = \frac{\tau_1 V G_V}{\tau_1 V G_V + \tau_2 G_M}$$

This is further simplified by using equations (3.3) and (2.20) and substituting them in the expression above to get

$$\frac{P_V}{P_i} = \frac{V G_V R_p}{G_M(1 - R_p) + V G_V R_p} = \frac{V G_V R_p}{r} \tag{3.6}$$

To keep losses at a minimum and given that the variator losses are likely to be the highest of any of the components of the PS-CVT, the most desirable area of operation is the region with no power recirculation: $0 < P_V/P_i < 1$.

An example will now be used to understand the different kinematic behaviours possible with a PS-CVT. A variator with transmission ratio $0.4 \leq V \leq 2.5$ will be used with gear ratios G_V and G_M equal to unity, and the planetary ratios of Table 3.1 representing six different PGS branch connections for the same PGS. For each one of these configurations two theoretical operations are possible as the output speed of the variator can be reversed or not relative to its input depending on the variator used (a toroidal variator reverses the input speed while a V-belt will not). Figure 3.2 shows two plots of the expressions in (3.3) and in (3.6) with the values used in the example. The former plot shows how the transmission ratio changes as the variator ratio changes (with the axis interchanged), and the latter plot shows the fraction of input power that goes through the variator at different transmission ratios. The figures only show the curves that are possible within the ratio coverage of the variator. The labels for each curve correspond to the PS-CVT configurations as described in Table 3.1. A negative value on the label does not signify a negative PGS ratio but rather than the variator speed output is reversed relative to its input (i.e. a toroidal variator is used).

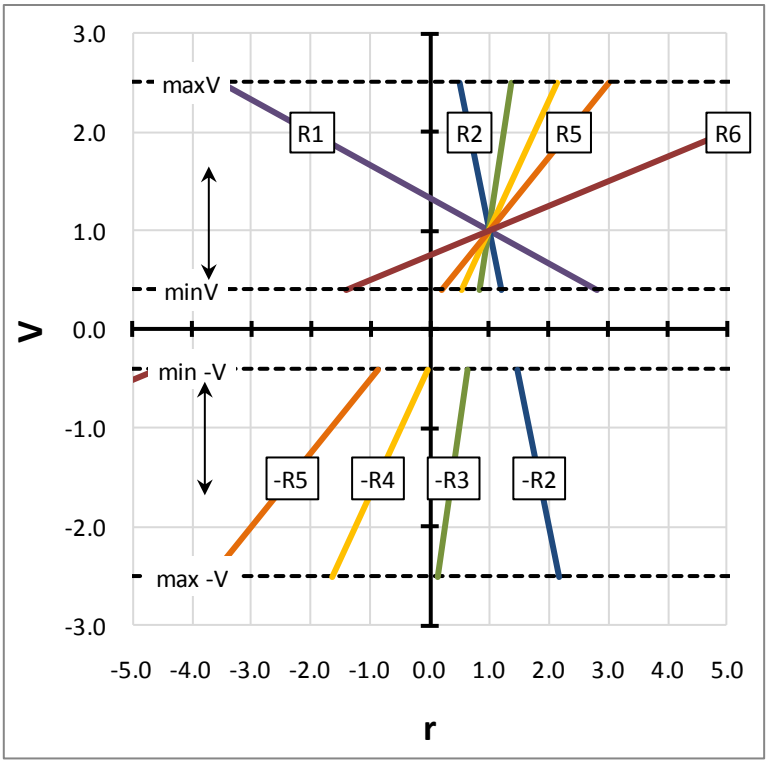

(a)

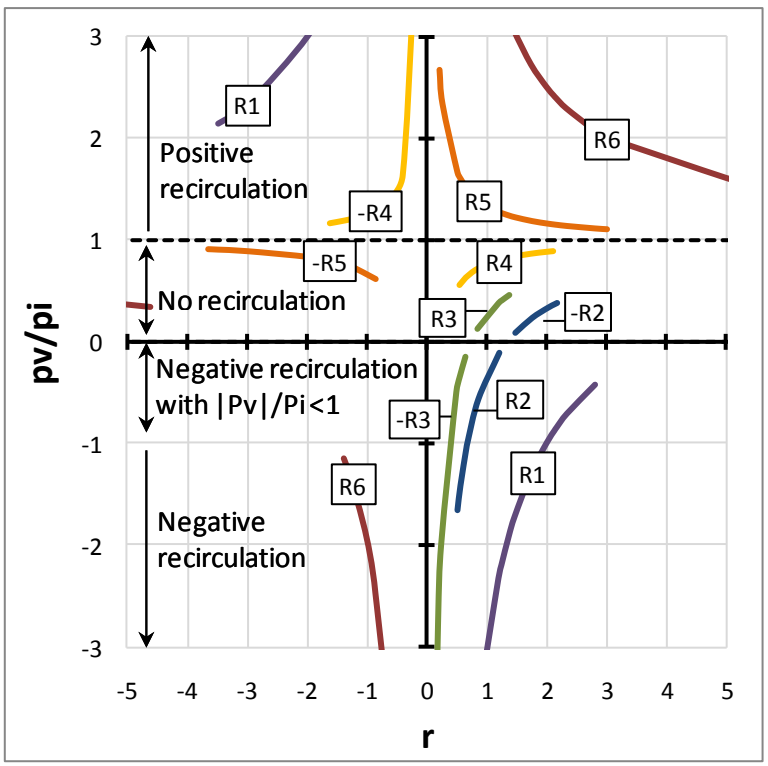

(b)

Figure 3.2 (a) Variator ratio as transmission ratio changes and (b) fraction of input power through the variator for six different PGS configurations with equal gear ratios G_V, G_M and PGS size. Only the possible operation areas attainable through the variator range are shown.

It can be appreciated from the second plot that the configurations with no power recirculation also have more limited ratio coverage. The opposite is clearly seen in case R_1 that has a large C_r value but has to operate at high power recirculation to accomplish it. Table 3.2 presents a summary of some of the cases showing their normalised ratio coverage along with their possible operating modes and C_r values.

Table 3.2 Summary of transmission characteristics for the configurations shown in Figure 3.2

PGS Ratio	Power-split configuration	C_r	Possible vehicle operating modes	Recirculation type	$\frac{P_V}{P_i}$
$\boldsymbol{R_1}$	RCS	1.8	Reverse, neutral and forward	(-) and (+)	very high >>1
$\boldsymbol{R_3}$	SRC	0.38	Only forward	None	low < 0.5
$\boldsymbol{R_4}$	SRC	0.74	Only forward	None	0.5< moderate < 1
$-\boldsymbol{R_5}$	CRS	0.76	Only reverse	None	0.5< moderate < 1
$\boldsymbol{R_5}$	CRS	0.93	Only forward	(-)	high >1

3.4.3. Gear sizing

It is now important to understand the role that the gearing of the variator and fixed-speed branches can play in the configuration of the system. Fussner et al. [74] propose a methodology where equation (3.3) is used to build two expressions that can be solved to dimension the components of the PS-CVT transmission to satisfy target transmission ratios limits of $r_{(V_{\max})}$ and $r_{(V_{\min})}$.

$$\begin{bmatrix} r_{(V_{\max})} \\ r_{(V_{\min})} \end{bmatrix} = \begin{bmatrix} (1-R_p) & V_{max}\cdot R_p \\ (1-R_p) & V_{min}\cdot R_p \end{bmatrix} \begin{bmatrix} G_M \\ G_V \end{bmatrix} \tag{3.7}$$

With these expressions, assuming that variator spread is defined (V_{max} and V_{min}) and fixing the value of either the planetary ratio (R_p) or of any of the fixed gears of the branches of the transmission (G_V or G_M) the rest of the components can be dimensioned

It is interesting to note that a solution can be found for any planetary ratio. This means that a transmission can be dimensioned regardless of how the branches of the PGS are allocated, although the gearing required for some configurations might be impractical.

This is better illustrated by again using an example. Continuing with the PGS used before ($D_R = 3D_S$) with planetary ratios as shown in Table 3.1, a transmission will be designed for each of the configurations resulting in the same transmission ratio coverage and power split. In this case a $C_r = 0.8$ was chosen giving a power split ratio $0.55 \leq P_V/P_i \leq 0.88$. This corresponds to the operation of curve R_4 in Figure 3.2. Recognising that for each configuration this can be accomplished with a variator with either a positive or negative ratio (same or reverse input and output speed senses). The resulting variator and power split curves as transmission ratio changes are shown in Figure 3.3. And the gearings required for each configuration is shown in Table 3.3.

Table 3.3 Gear ratios G_V, G_M for all possible configurations for a transmission with $C_r = 0.8$ and $0.55 \leq P_V/P_i \leq 0.88$, corresponding to the operation shown in Figure 3.3.

PGS Ratio	Power-split configuration	G_V,	G_M
$\boldsymbol{R_1}$	RCS	1 : -4	1 : 16
$\boldsymbol{-R_1}$	RCS	1 : 4	1 : 16
$\boldsymbol{R_2}$	SCR	-2.25 : 1	1 : 5.33
$\boldsymbol{-R_2}$	SCR	2.25 : 1	1 : 5.33
$\boldsymbol{R_3}$	SRC	3 : 1	1 : 3
$\boldsymbol{-R_3}$	SRC	-3 : 1	1 : 3
$\boldsymbol{R_4}$	RSC	1 : 1	1 : 1
$\boldsymbol{-R_4}$	RSC	-1 : 1	1 : 1
$\boldsymbol{R_5}$	CRS	1 : 1.78	1 : -1.33
$\boldsymbol{-R_5}$	CRS	1 : -1.78	1 : -1.33
$\boldsymbol{R_6}$	CSR	1 : 5.33	1 : -12
$\boldsymbol{-R_6}$	CSR	1 : -5.33	1 : -12

It is evident from the table above that for the parameters chosen in this example some configurations (RCS and CSR for instance) require gearing that could be impractical, but for the most part the required gearing is reasonable. All these configurations have the same torque and speed conditions at the output branch and the same power split ratios through its branches, but the specific torque and speed combinations through the branches will be different, which will have a direct impact on the losses though the variator as well as its size and the specification of bearings. This is studied in more detail in subsection 3.4.5 of the present section.

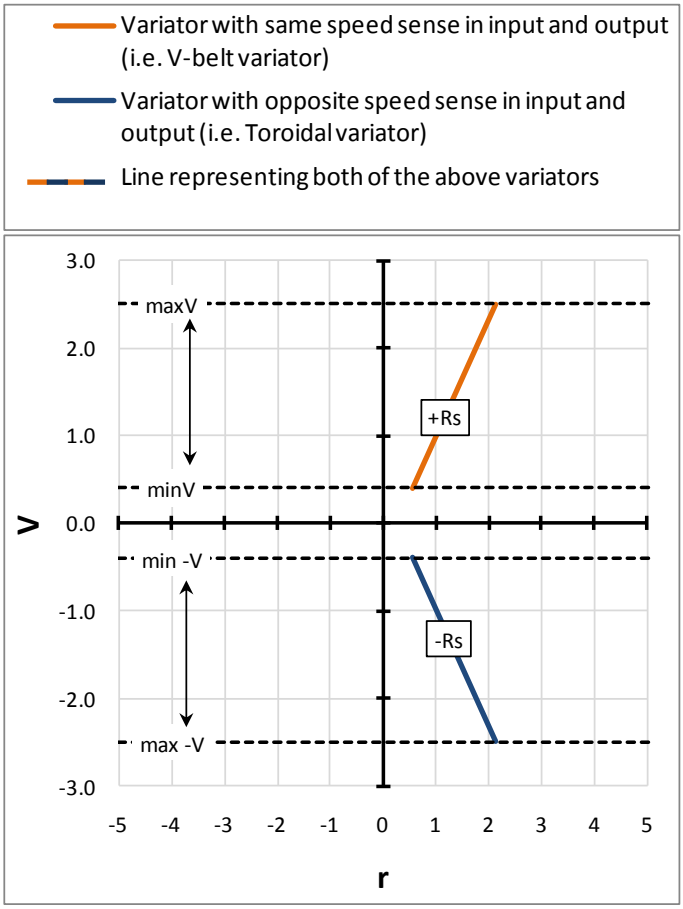

(a)

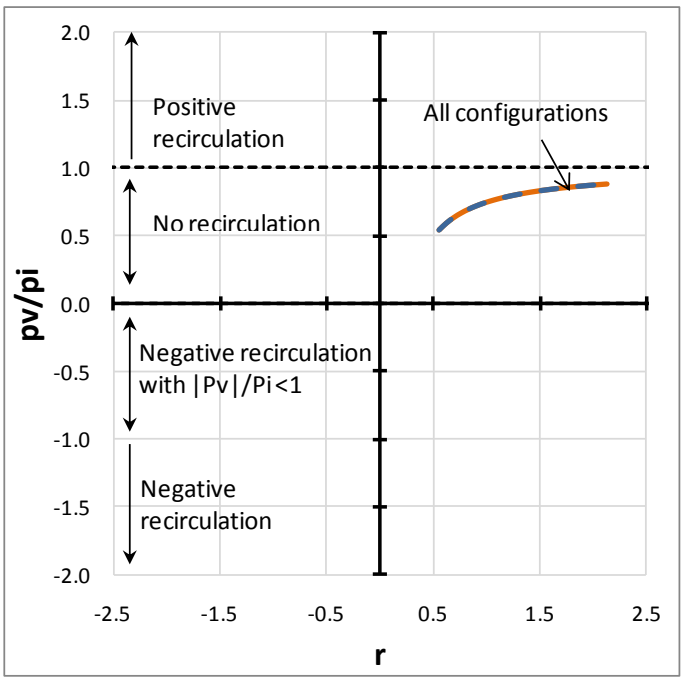

(b)

Figure 3.3 (a) Variator ratio as transmission ratio changes and (b) fraction of input power through the variator for six different configurations with different gear ratios G_V, G_M and PGS size, providing the same power split and transmission ratios. The (+R) and (-R) labelled curves corresponds to a variator where the input and output angular speeds have the same sense and an opposite sense respectively.

3.4.4. Dimensioning for specific modes of operation

Plot (b) in Figure 3.2 shows the power ratios P_V/P_i that give rise to the modes of operation of the PS-CVT shown in Figure 3.1. The limits of these power ratios will now be studied.

A useful expression for the value of G_V can be derived by using the expressions of equation (3.7), namely,

$$G_V = \frac{1}{R_p}\frac{r_{(V_{\max})} - r_{(V_{\min})}}{V_{max} - V_{min}} \tag{3.8}$$

It is now possible to rewrite equation (3.6) using equations (2.21), (3.5) and (3.8) as

$$\frac{P_V}{P_i} = \frac{V}{r}\frac{r_{(V_{\max})} - r_{(V_{\min})}}{V_{max} - V_{min}} = \frac{V}{r}\frac{r_{(V_{\max})}}{V_{max}}\frac{C_r}{C_{Var}} \tag{3.9}$$

where

$$C_{Var} = \frac{V_{max} - V_{min}}{V_{max}} \tag{3.10}$$

The power split at the variator ratio limits can thus be simply written as

$$\frac{P_V}{P_{i\,(V_{min})}} = \frac{r_t}{V_t}\frac{C_r}{C_{Var}} \tag{3.11}$$

$$\frac{P_V}{P_{i\,(V_{max})}} = \frac{C_r(1 - C_{Var})}{C_{Var}(1 - C_r)} \tag{3.12}$$

The normalised ratio coverage of the variator C_{Var} is always positive and less than one. The modes of operation can then be deducted from the equations above and are summarised in Table 3.4.

Table 3.4 Normalised ratio coverage and power split ratios for different operating modes

C_r	$r_{(V_{max})}$	$r_{(V_{min})}$	r_t	$\frac{P_V}{P_i}$	PS-CVT operating mode
$C_r < 0$	+	+	$r_t < V_t$	$\frac{P_V}{P_i} < 0$	Negative recirculation
$0 < C_r < C_{Var}$	+	+	$r_t < V_t$	$0 < \frac{P_V}{P_i} < 1$	No recirculation
$C_r = C_{Var}$	+	+	$r_t = V_t$	$\frac{P_V}{P_i} = 1$	Variator-only transmission
$C_{Var} < C_r < 1$	+	+	$r_t > V_t$	$1 < \frac{P_V}{P_i} < \infty$	Positive recirculation
$1 < C_r$	-	+	NA	$-\infty < \frac{P_V}{P_i} < 0, 1 < \frac{P_V}{P_i} < \infty$	Negative and positive recirculation

Bearing in mind the design targets identified in section 3.1, the following conclusions can be made about the operating modes:

Working in negative power recirculation mode only would yield no benefits compared to a variator-only transmission as the ratio coverage of the PS-CVT is less than of its variator and the power through the variator branch will sometimes be more than the input power, so a less efficient energy transfer can be expected.

Operating with no power recirculation offers reduced power through the variator decreasing the required size of the variator and increasing the overall transmission efficiency. However this comes at the expense of reduced ratio coverage.

Positive recirculation offers an interesting trade off. The system can be designed to expand the ratio coverage of the PS-CVT at the expense of higher power going through the variator and less transmission efficiency. This can be a controlled increase though, for example a twofold increase in ratio coverage can be accomplished with power split ratios remaining between unity and just above double the power input (similar to curve R5 in plot (b) in

Figure 3.2). An example of such a unit is the one proposed by Torotrak in [44], which uses a variator with ratio spread of 6 in a PS-CVT to produce a transmission with ratios spread of 9.

Operating in a mode allowing for both positive and negative recirculation does allow for a reverse and a clutchless start, however this is a very inefficient mode of operation as the power through the variator branch is much higher than the input power. This operating mode only becomes acceptable if it used as a regime for low power operation (low vehicle speeds for example) and a higher efficiency regime (i.e. with lower power recirculation or no recirculation) is employed at higher power demands.

It is known from the PGS torque equilibrium equations (equation (2.20)) that the torque τ_1 at the variator branch is fixed by the planetary ratio to the output torque. This means that an increase in power through the variator branch (i.e. power recirculation) has to come from an increase in speed at ω_1. Whether this translates into increased speeds at the variator depends on the arrangement of gear G_V within the variator branch. This will be explored next.

3.4.5. Torque and speed through the variator

The determination of the torque through the variator is of special interest as it is one of the most important factors in sizing the device, ultimately affecting its efficiency and cost. Two different configurations for the variator branch will be examined in this section, where the position of the variator and the fixed gear G_V are interchanged as in Figure 3.4 (b).

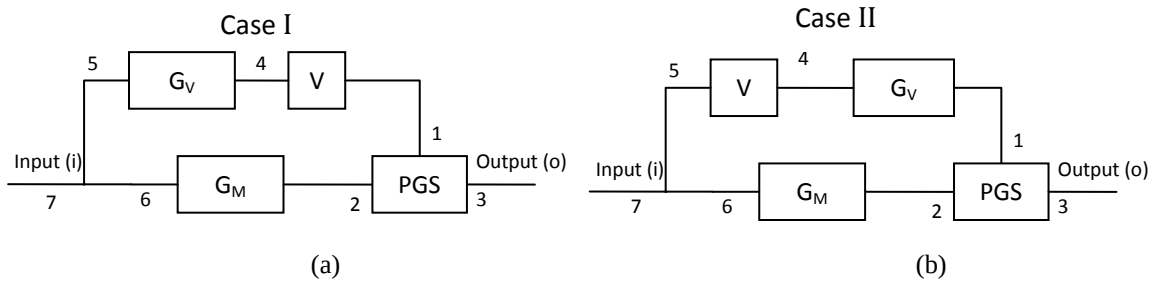

(a) (b)

Figure 3.4 IC transmissions with (a) G_V at the input side of the variator, and (b) G_V at the output side of the variator.

For Case I as in Figure 3.4 (a), given known τ_3 and ω_3 at the output the transmission, allows for the torque at the output of the variator (τ_1) to be determined by using equation (2.20). Ignoring losses, the torque at the input of the variator (τ_4) is given by $\tau_4 = -\tau_1 V = \tau_o R_p V$. It is clear from this expression that the torques through the variator are dependent on R_p, and that the highest variator torque will occur at $\tau_4(V_{max})$. Thus, expressions for the highest and lowest ratios of variator torque to output torque can be written as $\left|\frac{\tau_4}{\tau_o}\right|_{max,min} = |R_p|V_{max,min}$. This is a convenient ratio to use as ideally the maximum torque should be encountered at the output of the transmission. Similarly, the maximum rotational velocity of the variator can be calculated by noting that $\omega_1 = V\omega_4 = VG_V\omega_i$. Using equation (3.8) and defining $k = \frac{r_{(V_{\max})} - r_{(V_{\min})}}{V_{max} - V_{min}}$, expressions relating the highest and lowest rotational speed of the variator to input speed can be written as $\left|\frac{\omega_1}{\omega_i}\right|_{max,min} = \frac{kV_{max,min}}{|R_p|}$. Again this is a convenient ratio as the highest rotational speed is likely to be found at the flywheel side ω_i.

For Case II, a torque at the input of the variator (τ_5) is given by $\tau_5 = \tau_4 V = \tau_1 G_V V = -\tau_3 R_p G_V V = -\tau_3 kV$. The highest and lowest variator torque to output torque ratios are thus given by $\left(\frac{\tau_5}{\tau_o}\right)_{max,min} = kV_{max,min}$. From Figure 3.4 (b) the variator rotational speed is given by $V = \frac{\omega_4}{\omega_5} = \frac{\omega_4}{\omega_7}$, it follows that the highest and lowest variator to input rotational speed ratio

is given simply by $\left(\frac{\omega_4}{\omega_i}\right)_{max,min} = V_{max,min}$. These ratios are summarised in Table 3.5 along with the values for a variator-only transmission (i.e. no power split).

Table 3.5 Maximum ratios of variator to output torques, and variator to input rotational speeds.

	Case I	**Case II**	**Variator-only**
Max. variator torque	$\left\|\frac{\tau_4}{\tau_o}\right\|_{max} = \|R_p\|V_{max}$	$\left(\frac{\tau_5}{\tau_o}\right)_{max} = kV_{max}$	$\frac{\tau_i}{\tau_o} = V_{max}$
Max. variator rotational speed	$\left\|\frac{\omega_1}{\omega_i}\right\|_{max} = \frac{kV_{max}}{\|R_p\|}$	$\left(\frac{\omega_4}{\omega_i}\right)_{max} = V_{max}$	$\frac{\omega_o}{\omega_i} = V_{max}$

As previously mentioned only the Case I configuration is sensitive to the choice of planetary ratio and PGS arrangement. But it is also worth noting how both arrangements are affected by factor k. This factor is dependent on the relationship between the ratio spread of the transmission and that of the variator, and it is higher for a transmission with positive power recirculation than for one with no power recirculation.

To further understand these relationships and contrast the above transmissions an example contrasting three transmission objectives will be used. Two of the transmission will be operating with power splits, with one operating with no power recirculation and the other one with positive recirculation. Each power split transmissions can be configured either as Case I or Case II. The third transmission consists of only a variator and does not include a power split. The parameters for each transmission are presented in Table 3.6.

Table 3.6 Parameters for the three transmissions studied.

	No power recirculation	Positive power recirculation	Variator-only
$r_{(V_{min})}$	0.5	0.2	0.4
$r_{(V_{max})}$	2	5.45	2.5
r_t	4	27.25	6.25
r_t/V_t	0.64	4.36	1
C_r	0.75	0.963	0.84
k	0.71	2.5	1
Range of P_V/P_i	$0.57 < P_V/P_i < 0.89$	$1.15 < P_V/P_i < 5$	1

Plotting of the ratios shown in Table 3.5 will be helpful to understand how they are affected by different planetary ratios, choice of power split configuration (SCR, RCS, etc) and operating mode choice. They are presented in Figure 3.5. Plot (a) shows the maximum torque and rotational speed ratios of both transmissions for a Case I configuration, and plot (b) shows the same transmissions but with a Case II configuration.

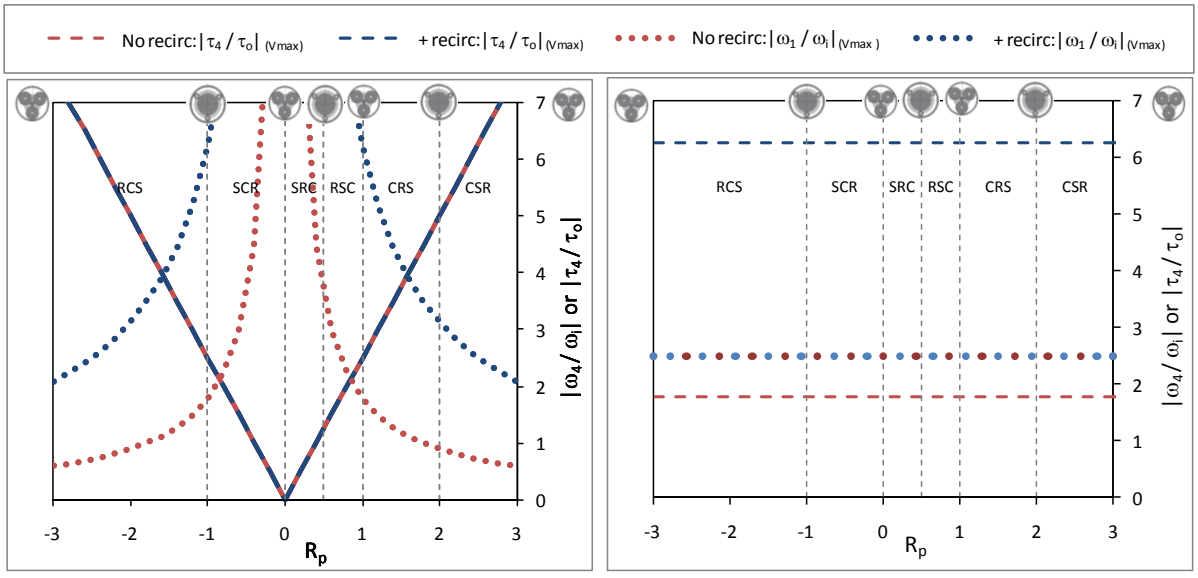

Figure 3.5 Maximum and minimum ratios of torque through the variator to output torque as R_p and PS-CVT configurations change for Case I (a) and Case II (b). The figures also show the ratio of variator speed to output speed for those conditions. The relative size of the sun to ring gears is also shown at the transition lines between the PS-CVT configurations for reference.

It can be seen that most Case I configurations have high torques through the variator except for a few planetary ratios of the SRC and SCR configurations. These lower torques come at the expense of higher variator rotational speeds though. It can also be appreciated that for this case the maximum torque trough the variator stays the same regardless of the operating mode with the increase in power accomplished by an increase in rotational speed.

For Case II configurations, the highest torque and speeds are independent of planetary ratios and therefore of PS-CVT configurations. Variator speeds remain constant for increasing levels of positive recirculation (increasing k), and the increase in power is thus accomplished by higher levels of torque.

Any given transmission objective (defined $r_{(V_{\max})}$and $r_{(V_{\min})}$ can in theory be accomplished using any planetary ratio, and the torques and speeds of the variator can be adjusted to acceptable limits by gearing the input or output of the PS-CVT. But it can also be inferred from Figure 3.5 that the gearing required to accomplish some transmissions will be impractical for some arrangements and planetary ratios.

3.4.6. Efficiency considerations

For a power split with no recirculation the power balance and torque equilibrium equations for FA mode at the PGS (equations (2.18) and (2.19) respectively) can be rewritten as

$$\eta_{PGS}(\tau_1\omega_1 + \tau_2\omega_2) + \tau_3\omega_3 = 0 \tag{3.13}$$

$$\eta_{PGS}(\tau_1 + \tau_2) + \tau_3 = 0 \tag{3.14}$$

Multiplying (3.14) by ω_2 and subtracting it from (3.13) yields

$$-\tau_3(\omega_3 - \omega_2) = \eta_{PGS}\tau_1(\omega_1 - \omega_2)$$

Using the definition for the planetary ratio (equation (2.16)) and then the torque equilibrium equation (3.14) yields the following expressions

$$-\tau_3 = \eta_{PGS}\frac{\tau_1}{R_p} = \eta_{PGS}\frac{\tau_2}{(1 - R_p)} \tag{3.15}$$

It is important to note that the above expressions hold for both FA and RB mode. However in RB mode power is transferred from branch 3 to branches 1 and 3, and so the efficiency of the PGS η_{PGS} in the equations above becomes $1/\eta_{PGS}$.

Attention is now shifted towards determining how power is split when considering efficiencies. Useful expressions for power split are different for FA and RB modes as the power split of interest is that of the power through the variator to that of the input power to the PS-CVT which is different for both modes.

Following the same procedure in deriving the lossless power ratio equation (3.6) and using equation (3.15), the power ratio equation considering the efficiencies of the PGS and variator can now be written. For FA mode this becomes:

$$\frac{P_V}{P_i} = \frac{\tau_5 \omega_5}{\tau_7 \omega_7} = \frac{V G_V R_p}{V G_V R_p + \eta_{Var} G_M (1 - R_p)} \tag{3.16}$$

And for RB mode:

$$\frac{P_V}{P_i} = \frac{\tau_1 \omega_1}{\tau_3 \omega_3} = \frac{\eta_{PGS} V G_V R_p}{V G_V R_p + G_M (1 - R_p)} = \eta_{PGS} \frac{V G_V R_p}{r} \tag{3.17}$$

The transmission will thus have a different power split though its variator branch for FA and RB modes.

3.5. Planetary Gear Set Transmission

The complex kinematics of planetary gear sets were previously discussed in section 2.5.2. It will now be explored how these devices can be used as the sole components in a flywheel-powered transmission.

3.5.1. Configuration of the PGS transmission

Using the same notation as in the previous section, a PGS transmission using a brake as a control device can be defined as in Figure 3.6.

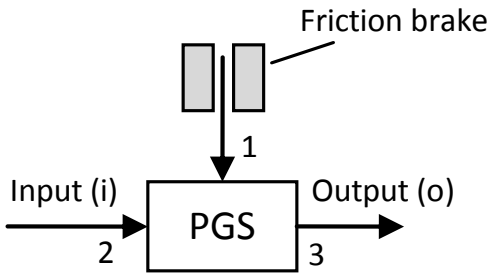

Figure 3.6 Transmission with a planetary gear set and a friction brake as control device in FA mode. During RB mode the input becomes branch 3 and the output branch 2.

Such a system was proposed by Diego-Ayala et al. [50] in which a friction brake is used as the sole control device. Diego-Ayala and the author of this thesis validated the operation and computational model of this system experimentally and it is presented in [50]. The Gyreacta concept discussed in 2.1.2.1 also uses PGSs to create a variable speed transmission.

In the system proposed by Diego-Ayala, the brake is used to apply a torque at one of the branches of the PGS to establish a power transfer between the other two branches of the PGS (corresponding to the vehicle and flywheel). This system can operate in RB, FA or N mode. The transmission is clutchless as the neutral operating mode is achieved by allowing the ring to rotate freely, in this manner a kinematic equilibrium is achieved regardless of the operating speed of the vehicle and flywheel.

3.5.2. Operating range of the PGS transmission

Keeping in mind the convention for power used (positive power adds energy to the PGS), three conditions must be met for power transfer to occur between the input and output branches:

1. Power at the brake (P_1) must to be negative.

2. The brake cannot extract more energy than is available.

   Thus, for RB the condition $-1 < \frac{P_1}{P_3} < 0$ is needed (that is opposite signs for P_1 and P_3), and for FA $-1 < \frac{P_1}{P_2} < 0$ is needed. But for FA it is desirable for most of the energy extracted from the flywheel to be transferred to the vehicle (P_3), thus complying with the condition $0 < \frac{P_1}{P_3} < 1$ is desirable.

3. P_2 and P_3 should have opposite signs for any transfer of energy between the vehicle and the flywheel.

To find an expression for P_1, the torque balance equation (2.19) is first multiplied by ω_1 and then the relationship $\tau_2 = -\tau_3(1 - R_p)$ from equation (2.20) along with the speed balance equation (2.17) are used to get

$$P_1 = -\tau_3 R_p \omega_1 = -\tau_3 R_p \left[\left(1 - R_p\right)\omega_2 - \omega_3\right]$$

By using the transmission ratio from (3.1) this simplifies to

$$P_1 = P_3 \left[\frac{1 - R_p}{r} - 1\right] \tag{3.18}$$

A similar process yields

$$P_1 = P_2 \left[\frac{r}{1 - R_p} - 1\right] \tag{3.19}$$

For the first and second conditions to be met it can be shown that:

During RB when $P_3 > 0$ and using equation (3.18) the following must condition must be met

$$-1 < \frac{1 - R_p}{r} - 1 < 0 \tag{3.20}$$

During FA when $P_3 < 0$ and using equation (3.19) the following must condition must be met

$$-1 < \frac{r}{1 - R_p} - 1 < 0 \tag{3.21}$$

It is also noted that reversing the sense of the output (or input) speed with a gear, the kinematics of the PGS are affected, reversing the sign of the transmission ratio $r = \frac{\omega_3}{\omega_2}$.

For condition 3 to be met, the condition $\pm(\tau_2\omega_2) = \mp(\tau_3\omega_3)x$ is needed, where x is a positive number. By using equation (2.20) it can be shown that condition 3 is met when

$$1 - R_p > 0 \text{ for } r > 0 \tag{3.22}$$

and

$$1 - R_p < 0 \text{ for } r < 0 \tag{3.23}$$

It can readily be seen that these conditions are independent of power demand. Noting as well, that since the transmission ratio approaches zero for low vehicle speeds, these ratios will only encounter negative power at brake branch P_1 for planetary ratios R_p approaching unity. These narrows down the possible arrangements of the branches of the PGS to two options: an RSC arrangement (brake at the ring, flywheel at the sun and vehicle at the carrier) as the one used in [50]; and a CRS arrangement with a geared output, which is kinematically equivalent to the RSC and SRC arrangements. These planetary ratios can be accomplished with two-stage planetary gear sets as described in Appendix B.

Requiring a negative power at the brake has a different effect on the RB and FA modes with important implications in the operation of the system. This can be seen by exploring plots (a) and (b) in Figure 3.7 which show the ratio of power at the brake branch to the PGS input power for different planetary ratios and transmission ratios for RB and FA modes respectively.

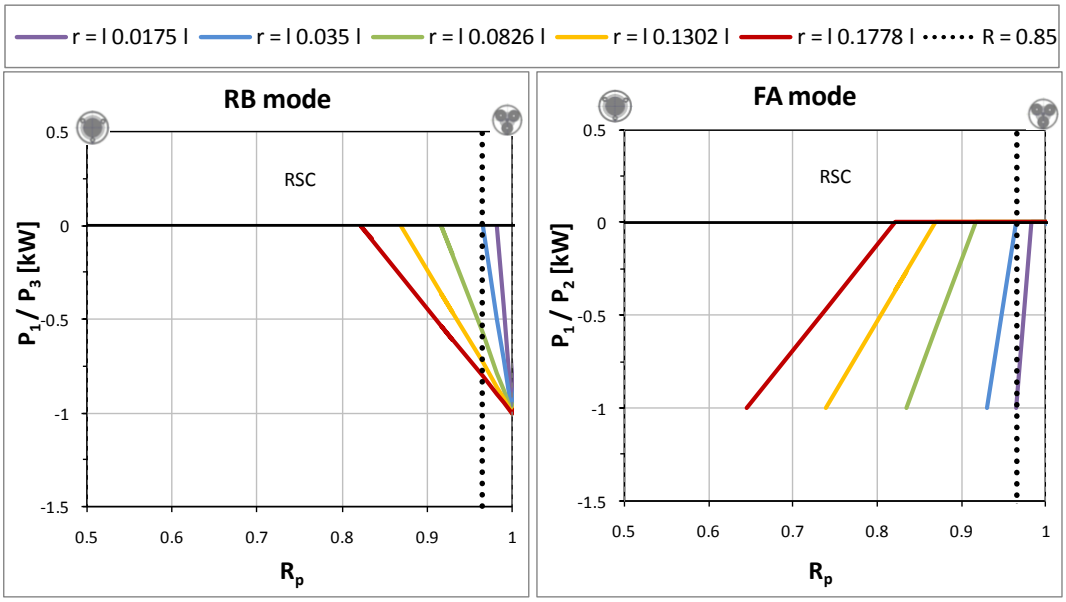

(a) (b)

Figure 3.7 Ratio of power at the brake to PGS input power against planetary ratio R_p for different transmission ratios r at (a) RB mode (P_1/P_3), and (b) FA mode (P_1/P_2).
The dotted line corresponds to a PGS with $R_p = 0.965$ as the one used in [50].

In Figure 3.7 a planetary ratio of $R_p = 0.965$ as the one used in [50] is used to illustrate the different transmission ratios at which the system can operate for RB and FA modes. It can be seen that for a given R_p the system can operate at many transmission ratios for the RB mode, but the same ratios are not attainable during FA mode. This is a main disadvantage of using this system on its own. The transmission is able to recuperate a substantial amount of the energy available during braking but it can hardly deliver any.

Increasing the gear ratio of the final drive or stepping down flywheel speed can bring more ratios within the operation of the system, but there will always be a disparity between the ratios attainable in RB and FA modes. Alternatives to overcome this problem could include a gearbox in series with the PGS or a series of PGS in parallel; however this would require fast gear shifting and possibly unacceptable exercising of the transmission.

3.5.3. Experimental work

The results reported in [50] were based on experimental work carried between Diego-Ayala and the author of this thesis. These experiments consisted on the use of a PGS transmission with a brake at the ring branch to control the power flow between two inertias representing the vehicle and the flywheel. The experimental rig and setup are discussed in detail in [47,50]. These experimental results can be used to confirm the boundary conditions suggested in the previous section.

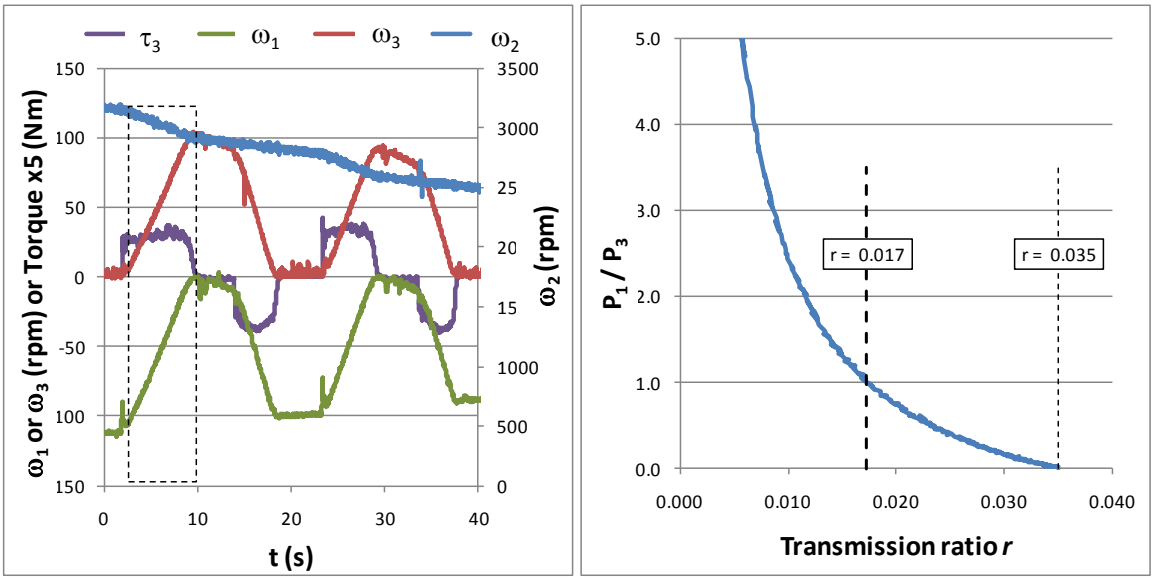

(a) (b)

Figure 3.8 (a) An experimental run for FA mode and (b) the transmission ratio versus ratio of power at the brake to power at the output (P_1/P_3) for the boxed area in plot (a).

From plot (b) of Figure 3.7 it can be seen that power at the brake branch will be negative for transmission ratios lower than 0.035 and that the ratio P_1/P_3 is less than one only for ratios higher than 0.0175. These boundary conditions are confirmed in the experimental data shown in plot (b). In the experiments FA was also applied for lower transmission ratios but at the expense of very high P_1/P_3, dramatically lowering the effectiveness at which energy was transferred from the flywheel to the vehicle.

In [50] it was reported that the simulations for this powertrain predicted improvements in fuel economy between 4 and 11% depending on the drive cycle. However, almost of the savings could be attributed to turning off the engine during idling and braking periods (compare to a stop-start system with typical savings of 7.5%) with very little improvement attributable to reutilisation of braking energy. However, this system is capable of providing inertial mass to assist in the restart of the ICE when as it is turned on and off. The experimental work carried

out for this research helped to validate the PGS model and to identify areas of improvement. The brake system though is better suited as a complement for a transmission capable of delivering the stored energy, such as in a PS-CVT transmission.

3.6. Other CVT transmissions

An alternative to increase the speed ratio coverage of the transmission while improving efficiency requires a reconfiguration of the system such as the proposed by Mantriota [84] or the Perbury transmission which is proposed by Torotrak for conventional vehicles [86]. Both of these systems have two regimes of operation to increase the speed ratio coverage of the transmission. The regimes are chosen by coupling and decoupling clutches depending on the speed ratio of operation, however as the clutches are only actuated when its plates are rotating synchronously there is no wear and the transition between regimes is smooth.

Another alternative is to use a power split transmission together with a brake on one of the branches of the PGS. Such a system was proposed by Diego-Ayala [47] and numerical simulation on their performance carried out with the author of this thesis can also be found in [50]. This type of PS-CVT arrangement delivers higher ratio coverage although at the expense of higher losses. This would be prohibitive in a conventional vehicle transmission, but for a hybrid with a flywheel the increase in ratio coverage may compensates in fuel savings the decrease in transmission efficiency.

3.7. Mechanical Continuously Variable Transmissions Summary

This section has presented extensive analyses on continuously variable transmissions. The tradeoffs between efficiency and ratio coverage have been examined and discussed. Particular attention has been devoted to tackling the complex kinematics of PS-CVT and PGS-only transmissions.

In section 3.4, as synthesis of work published by White [72] and by authors from the Southwest Research Institute [73,74], led to the development of simple expressions that can be used in the analysis of PS-CVTs with different PGS branch assignments, greatly reducing the complexity of the analyses of these powertrains. Defined operating ranges for PS-CVTs were identified using this approach and are shown in table 3.4.

A methodology for the design of PS-CVT transmission to provide specific ratio coverage and mode of operation was presented and is used to design the PS-CVT transmissions incorporating flywheels analysed in Chapter 6.

The section covering the use of the brake at the PGS, analyses the system proposed by Diego-Ayala and which the author of this thesis assisted Diego-Ayala in conducting experiments and simulations on. Extended analyses on the system (section 3.5) showed that the ratio coverage for this transmission is quite limited, which rules out the use of this system for many PGS branch assignments. It also showed that the system is able to regenerate more braking energy than it can deliver and that most of the predictions in fuel economy arose from turning off the engine and not from its reuse of energy from regenerative braking.

4. POWERTRAIN MODELLING TOOL (CAPTAIN)

In order to study the energy requirements of hybrid vehicles and to assess the performance of different powertrains a computer model was built. The program is called Car Advanced PowerTrain Analysis, which is shortened to CAPTAIN to aid in the discussion. The purpose of the program is to simulate the energy requirements of the vehicle, determine power flows throughout the powertrain and produce a forecast of the energy consumption of the vehicle. Its intended use is an evaluation tool for vehicle performance rather than a design tool.

This chapter will explain the general structure of CAPTAIN as well as the different vehicle and powertrain models used and developed. This simulation tool is used in the studies on the fuel economy potential of hybrid vehicles presented in Chapter 5, and on the analyses of different flywheel-hybrid powertrains presented in Chapter 6.

A general schematic of the vehicle and powertrain models and how they fit in the program is shown in Figure 4.1. The schematic also presents the sections in which the specific parameters for the powertrains are presented in this chapter.

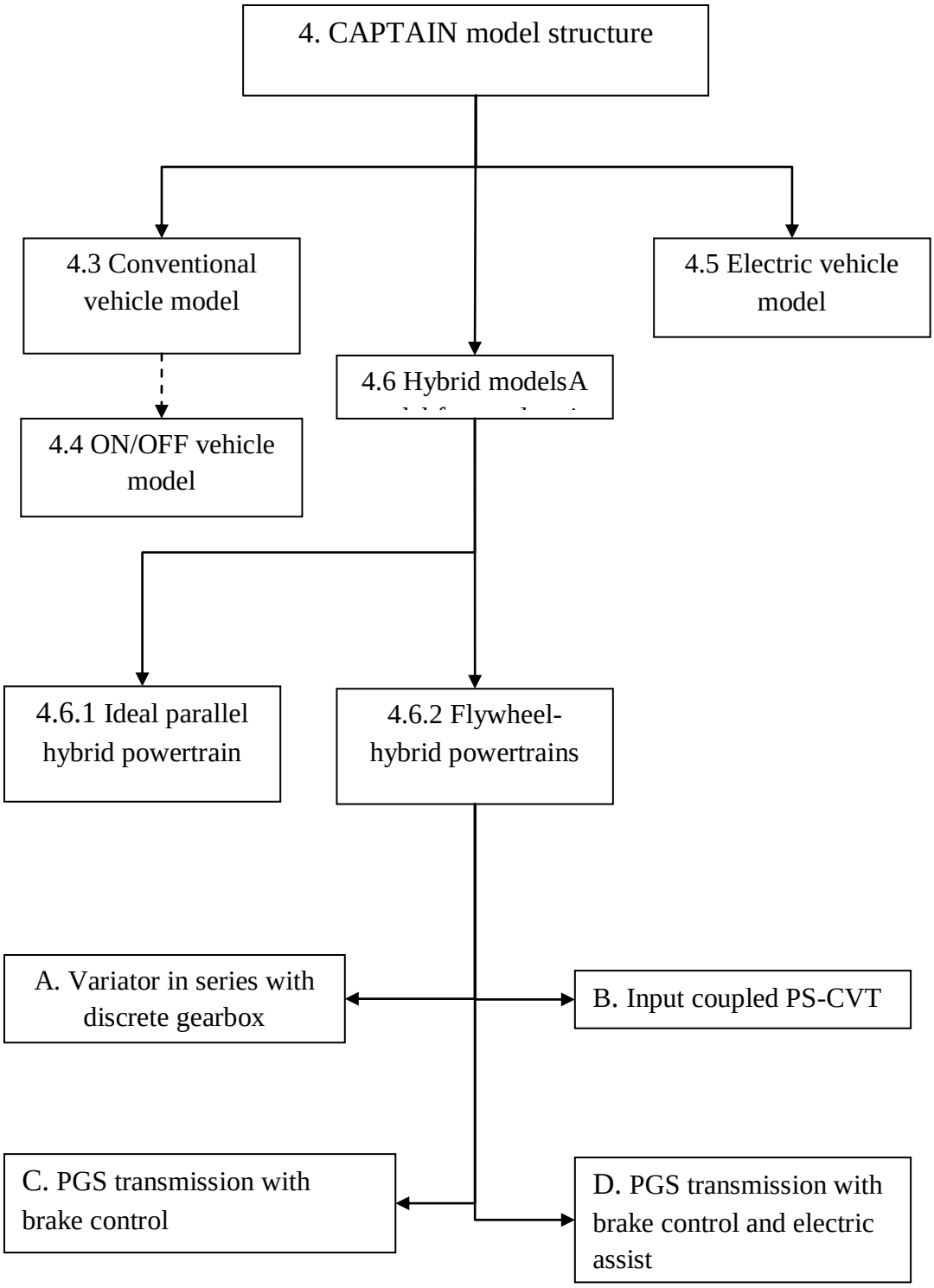

Figure 4.1 General structure of CAPTAIN and location of models within the chapter.

4.1. CAPTAIN validation

CAPTAIN was modelled similarly to the well known program ADvanced VehIcle SimulatOR (ADVISOR) that was developed by the US National Renewable Energy Laboratories (NREL).

ADVISOR has an extensive library of maps for fuel consumption and efficiency of components including the ICE and gearboxes. Many of these maps as well as some component models were taken from ADVISOR and adapted for CAPTAIN. Data and models coming from ADVISOR are specified in this chapter. ADVISOR was distributed free of charge until 2002 and all the data used in CAPTAIN was marked as unprotected and free to distribute.

The models and forecasts in ADVISOR have been validated against real data by NREL and industry partners as stated in [87] and [88]. Simulations on a vehicle were undertaken using CAPTAIN and ADVISOR (with the vehicle shown in Table 4.2) and the results proved to be in good agreement for both programs. Table 4.1 shows the predicted fuel consumption and percent difference between the predictions of both programs for various drive cycles.

Table 4.1 Fuel economy predictions for CAPTAIN and ADVISOR for various drive cycles using the vehicle parameters shown in Table 4.2.

Drive Cycle	CAPTAIN Fuel economy prediction [km/l]	ADVISOR Fuel economy prediction [km/l]	Difference
ECE -15	12.5	12.05	3.75%
UDC	13.1	12.35	6.11%
EUDC	17.4	16.67	4.40%
NEDC	16.6	14.71	12.88%
UDDS	16.1	14.71	9.48%
FTP-75	16.5	14.93	10.55%

4.2. General structure

For each time step, CAPTAIN determines the forces that the vehicle will experience in order to reach a target instantaneous vehicle speed. It then works backwards through the powertrain (this is usually termed backward-facing) from the wheels to the engine to determine the necessary torque and speeds of the powertrain's components, calculating and applying the appropriate efficiencies at operating conditions and ultimately determining the fuel consumption of the ICE for associated the time step. The values calculated over the time steps are integrated over the duration of the drive cycle to determine average requirements and expenditures of the vehicle.

For each component of the powertrain, once the torque and speed requirements are known, it can be determined based on its operational limits whether the demanded operating condition is possible. However, due its backward-facing structure, CAPTAIN cannot be used to determine a vehicle response based on a defined operating condition for a component. So for example, if the power demanded of the ICE is greater than what it can deliver, then the program will assume that the driving trace was met and thus it will not change for the next time step. CAPTAIN will however flag that the demanded operation was outside the power limits of the ICE. In all the simulations shown in this thesis (unless specifically noted) the operation of the components fell within their operating ranges. This approach has its limitations and to design specific powertrain components, a response based software is more appropriate.

Therefore the strength of CAPTAIN lies in the ability to compare the performance of different powertrains over the same conditions. This is considered an appropriate tool for the objectives of this thesis and the studies presented in chapters 5 and 6.

Some of the general features of the program common to the different vehicle models are detailed next.

4.2.1. Drive cycles

The raw velocity data used by this program is based on the recorded velocities (in case of experimental driving cycles) or on target instantaneous velocities for a particular time (for the standard driving cycles). In any case, the time steps employed for calculations by the program can vary in magnitude and are adjusted for each time step.

Different drive cycles are available in CAPTAIN. The drive cycles used most frequently in the analyses presented in this thesis are based on the European drive cycles, the US Urban Dynamometer Driving Schedule (UDDS) and the ARTEMIS (Assessment and Reliability of Transport Emission Models and Inventory Systems) drive cycles. These cycles have been designed to provide a standard cycle easily repeatable by different users to assess diverse driving conditions and are intended to represent typical driving conditions. This is certainly the case of the Urban (UDC) and Extra Urban (EUDC) Drive Cycles, which are part of the New European Drive Cycles (NEDC) (shown in Figure 4.2). These cycles are used by automotive manufacturers as standard drive cycles for determining and reporting the fuel economy of their vehicles.

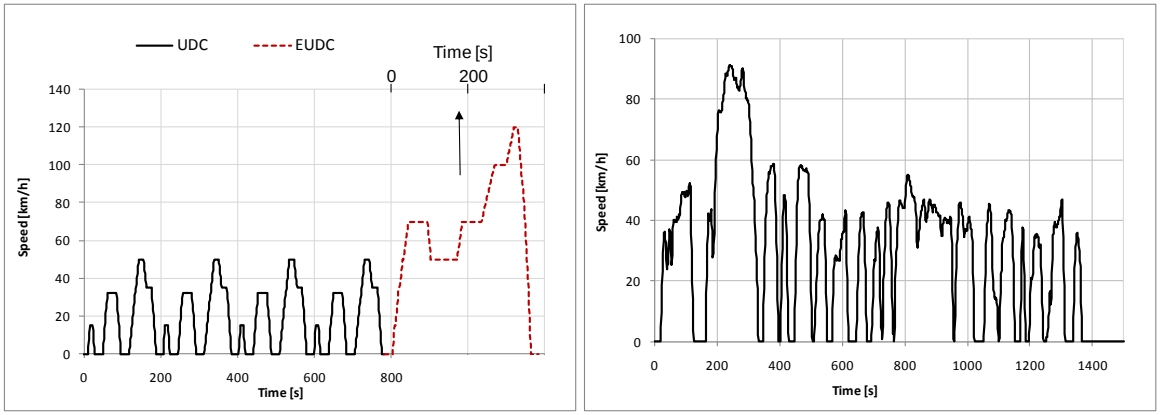

(a) (b)

Figure 4.2. (a) the Urban (UDC) and Extra Urban (EUDC) Drive Cycles, and (b) the US Urban Dynamometer Driving Schedule (UDDS).

The NEDC cycles have long been criticised for not displaying the aggressive driving behaviour that is typically encountered in real driving conditions. Other drive cycles exhibiting more frequent and harder braking and accelerating events are available in CAPTAIN, including the ARTEMIS drive cycles and real drive cycles that are used later in the thesis and discussed in section 5.2.

4.2.2. Road topology

The program can simulate a driving cycle over different road topologies. This allows the study of the effect that road gradients have on the performance of the vehicle. These topologies can be real tracks corresponding to recorded drive cycles or computer generated tracks with varying road gradients.

In particular, two algorithms were developed to generate different tracks. One is a sinusoidal track that in which the user can adjust the amplitude and periodicity of the wave to simulate a road track. The other one creates a random road based on a maximum road gradient constraint and on a desired road roughness. These road tracks are used extensively in Chapter 5 where they are explained in more detail.

4.2.3. Vehicles

Several vehicles are available for the simulation. Vehicle data includes weight, aerodynamic drag and wheel rolling coefficients, vehicle frontal area, transmission and engine fuel maps. It is also possible to combine different components to form a specific powertrain arrangement.

Throughout the simulations presented in this thesis, the same vehicle was used in order to provide a proper basis for comparing different powertrains. The vehicle chosen was a Ford Focus Estate with a 1.8 L diesel engine with direct injection, turbocharged, intercooled, and with exhaust gas recirculation. Fuel and emission maps for this vehicle were developed by North based on dynamometer testing of the vehicle and reported in [89].

The vehicle weight was adjusted depending on the powertrain used (e.g. conventional, ideal parallel hybrid, flywheel-based hybrid, etc) according to the weight of the components of the powertrain. The specifications shown in Table 4.2 correspond to the vehicle with the conventional powertrain.

Table 4.2. Specification for the 1.8 L diesel Ford Focus Estate used in the simulations.

Parameter	Value	Unit
Gross Vehicle Weight	1439	kg
Load weight	70	kg
Frontal area	2.06	m^2
Radius of wheels	0.282	M
Friction coefficient	0.009	--
Drag coefficient	0.312	--
Transmission ratio (manual)	3.50 / 1.97 / 1.30 / 0.98 / 0.74	--
Final drive ratio	3.84	--
Maximum engine speed	4400	rpm
Maximum engine power	65 @ 4400 rpm	kW
Maximum engine torque	184 @ 2000 rpm	Nm

4.3. Conventional vehicle model

4.3.1. Tractive force

For each time step, the tractive force is calculated by first determining the forces resisting the vehicle's movement

$$F_{resist(n)} = F_{aero(n)} + F_{roll(n)} + F_{g(n)} \tag{4.1}$$

and noting then that the tractive force must overcome the resistance forces and provide the target acceleration. Thus it can be written that:

$$F_{tract(n)} = F_{resist(n)} + F_{acc(n)} \tag{4.2}$$

The resultant force F_{Tract} needed at the vehicle's wheels is thus:

$$F_{tract(n)} = \frac{1}{2} C_d A_f \rho \left(\bar{V}_{veh(n)} - V_{air}\right)^2 + C_{rr} m_{veh} g \cos\theta_{(n)} + m_{veh} g \sin\theta_{(n)} + m_{veh} \bar{a}_{veh(n)} \tag{4.3}$$

The required torque and angular speed of the drive axle are calculated as

$$\tau_{tract(n)} = F_{tract(n)} r_{wheel} \tag{4.4}$$

$$\omega_{axle(n)} = \frac{\bar{V}_{avg(n)}}{r_{wheel}} \tag{4.5}$$

4.3.2. Transmission

The model applies the same shifting strategy as used in ADVISOR, which aims to keep engine speed and torques within a defined operating region of the engine. It does so by applying a gear ratio for required speed and torque values at the gearbox output. If the corresponding engine speed and torque lie outside the regions defined by the up-shift and down-shift torques (as shown in Figure 4.3) then it applies a gear shift to bring the torque-speed operating point within the defined range.

The model calculates the friction losses associated with gearing of the transmission, including the efficiency of the final drive gearing and the gearbox. The efficiency of the gearbox transmission is determined with the use of efficiency maps for each of the gears which were

obtained from maps available in ADVISOR. Thus the torques at the engine side of the gearbox are calculated with,

$$\tau_{eng,prev(n)} = \frac{\tau_{axle(n)}}{FD_{ratio} \cdot \eta_{FD} \cdot GR_{(n)} \cdot \eta_{GR(n)}} \tag{4.6}$$

and the angular speed with

$$\omega_{eng(n)} = FD_{ratio} \cdot GR_{(n)} \tag{4.7}$$

4.3.3. Engine

Once the required input power of the gearbox is determined, the torque and speed required from the engine can be calculated. The power required by ancillary systems (e.g. air conditioner, alternator, etc) can also be included as part of the power requirements of the engine. This power (P_{anc}) can be simulated either as a constant mechanical power demand on the engine (for a conventional vehicle) or a constant electrical power demand on a bank of batteries (for a hybrid vehicle to ensure power availability during the intermittent use of the ICE). The simulations presented later in Chapters 5 and 6 assume no ancillary power demand.

Engine power is thus calculated as:

$$P_{eng(n)} = \tau_{eng,prev(n)} \omega_{eng} + P_{anc} \tag{4.8}$$

The final torque demanded from the engine is simply calculated as:

$$\tau_{eng(n)} = \frac{P_{eng(n)}}{\omega_{eng(n)}} \tag{4.9}$$

With the speed and torque requirements of the engine determined for a particular time step, the fuel consumption for the time step is estimated using a specific fuel consumption map of the engine. A heat transfer model of the ICE estimates the temperature of the engine and adjusts the fuel consumption estimate based on the current operating temperature of the engine.

Figure 4.3 presents an example on the operation of the ICE of the Ford Focus vehicle of Table 4.2 as it follows the UDC drive cycle. The map in the background shows the thermal efficiency of the ICE (at 95°C) and an up-shift and down-shift lines within which the operation of the ICE is aimed to be kept in. The red triangles in the figure represent the operating points for the vehicle with the conventional powertrain, and the yellow circles are the operating points for the vehicle with the ideal parallel hybrid powertrain.

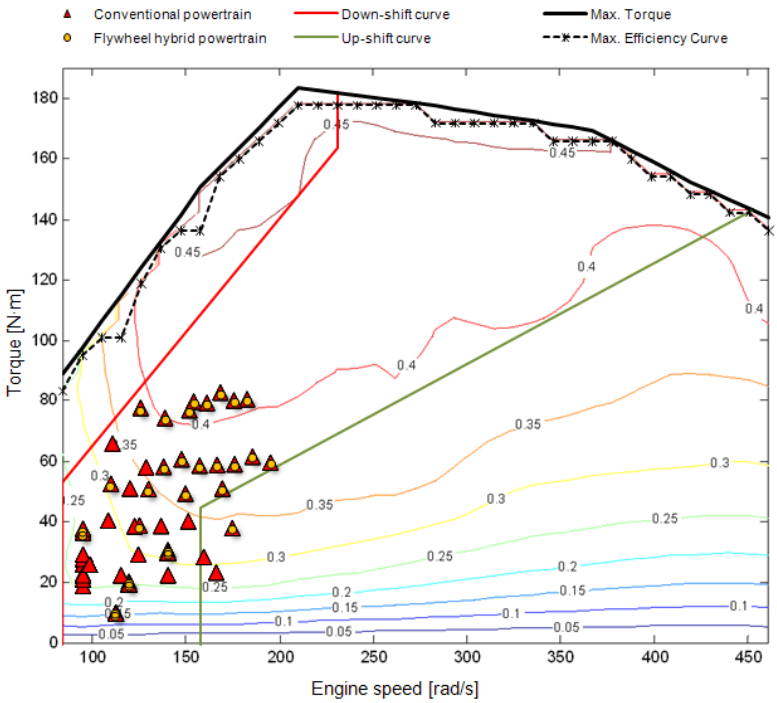

Figure 4.3 The figure shows in the background, the contours of the thermal efficiency map for the Ford Focus (developed at at 95°C ±5°C) . The solid black line at the top is the maximum torque curve and the dotted line just underneath is the line of best specific fuel consumption for the engine, which shows the operation of the ICE that would result in the lowest fuel usage. The up-shift and down-shift lines used in determining the gear ratio at the gearbox are shown in green and red respectively.
The foreground shows an example on the operation of the Ford Focus vehicle following the UDC cycle, with the red traingles representing the operating points of the vehicle with a conventional powertrain and the yellow circles the operation of the vehicle with an ideal parallel hybrid powertrain.

Finally the estimated fuel economy of the vehicle is calculated by

$$Fuel\ economy = \frac{\rho_{diesel} \cdot Total\ Distance}{\sum_{o}^{N} Fuel\ consumption\ (n)} \tag{4.10}$$

In the conventional powertrain, all the braking required from the vehicle is done by conventional brake and thus engine braking is not modelled.

4.4. ON/OFF vehicle model

Within the conventional model, a simple model of a vehicle that turns off the engine when it is not needed was also modelled. The purpose of this model is to assess the potential fuel savings from simply turning off the engine during braking and engine idling periods.

Corrections are applied on specific fuel consumption estimates due to the lower operating temperatures of the ICE. However transient effects from the intermittent use of the engine are not taken into account.

The model of the *ON/OFF vehicle* is not an assessment tool for vehicles with start-stop technology, but rather a point of comparison for the fuel savings of different hybrid powertrains. With much of the fuel savings from hybrid vehicles coming from turning off the engine, it is necessary to use this point of comparison when estimating fuel savings from other strategies, such as reusing regenerative braking energy and the selective use of stored energy.

4.5. Electric vehicle model

A model for an electric vehicle was also included in CAPTAIN. This model was not used in the simulations presented in this thesis and will not be further discussed. However an explanation of the model is included in Appendix C.

4.6. Hybrid models

Three hybrid systems with different energy storages were modelled in CAPTAIN. These include an *Ideal-parallel-hybrid powertrain*, a *Hybrid-electric powertrain* and a *Flywheel-hybrid powertrain*. All of these hybrid powertrains were modelled as parallel systems…

4.6.1. Ideal parallel hybrid powertrain

The *Ideal-parallel-hybrid powertrain* was modelled in order to understand the potential limits for the performance of parallel hybrid vehicles. This powertrain has in principle, no energy storage or power transfer limitations. Therefore it is capable of storing all the energy available during braking and to deliver any amount of power as required by the vehicle provided enough energy is available in its energy reservoir. However, upper and lower limits for these values can be defined if desired. It is also weightless and imposes no weight penalty on the vehicle.

The proposed parallel installation of the hybrid powertrain is shown in Figure 4.4. It functions as a full-hybrid, in which both the engine and the energy reservoir are capable of independently propelling the vehicle.

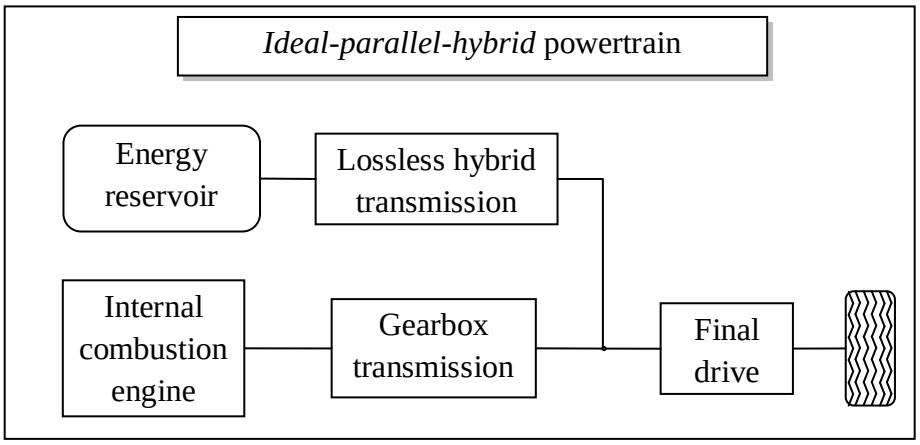

Figure 4.4. Schematic representation of the *Ideal-parallel-hybrid* powertrain

Although an actual hybrid powertrain will be quite restrained by some or all of these characteristics, defining such an ideal powertrain is nevertheless useful for identifying some of the characteristics desired of hybrid powertrains. This includes power and energy rating of the energy storage unit (i.e. batteries, ultra-capacitors, flywheels) and control strategies according to the performance objectives of the powertrain. Some of these characteristics and control strategies are discussed in more detail in section 5.3.

4.6.2. Flywheel-hybrid powertrains

The *Flywheel-hybrid powertrain*, was modelled considering the use of different powertrain alternatives and control methods. These are:

A. Variator in series with discrete gearbox

B. Input coupled PS-CVT

C. PGS transmission with brake control

D. PGS transmission with brake control and electric assist

A schematic representation of these powertrains is shown in Figure 4.5.

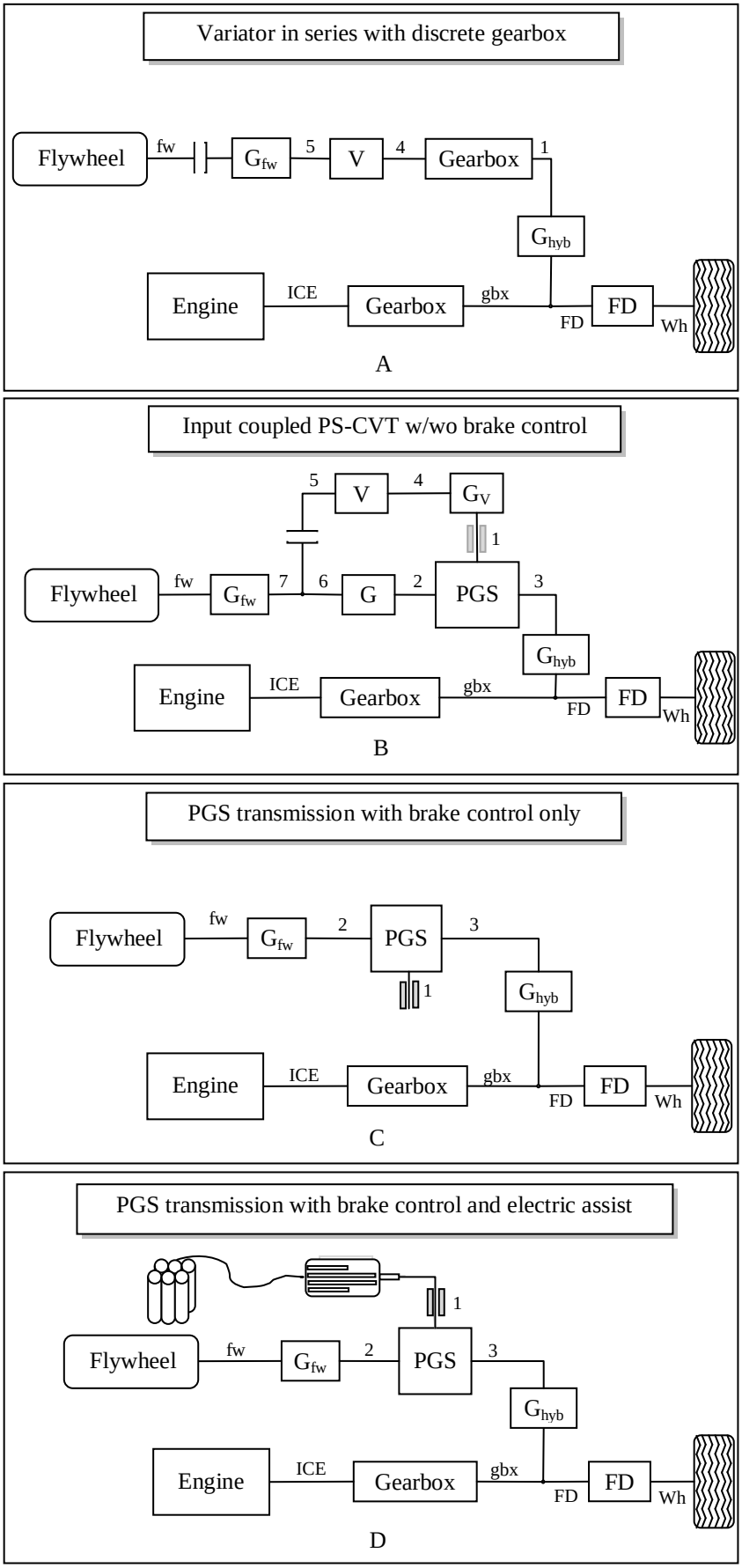

Figure 4.5 Schematic representation of the flywheel-hybrid powertrains simulated in CAPTAIN.

4.6.2.1. Clutch

An important consideration on the powertrains presented in Figure 4.5 is that they should be able to decouple the flywheel from the vehicle's wheels. Powertrains C and D accomplish this by allowing branch 1 of the planetary gear set to rotate freely (i.e. when neither the friction brake nor the motor/generator are used), permitting the other two branches to rotate at independent speeds.

In powertrains A and B either a hydrostatic variator (which allows zero-speed and slips until fully engaged) or a clutch can be used to decouple the flywheel from vehicle's wheels.

In the model developed in CAIMAN and in the subsequent analyses, the use of a dog clutch with a synchromesh engagement and with no-slipping is assumed. This type of clutch and engagement was chosen in order to isolate the ratio spread of the CVT as the variable of study.

However, it is important to note that the use of a slipping clutch increases the ratio spread of the hybrid transmission, albeit with some friction losses. Thus, although it is not modelled and simulated in the analyses presented in this thesis, such a system is recognised as an alternative worth studying.

4.6.2.2. Components losses

Flywheel losses:

Losses at the flywheel (bearing, aerodynamic and sealing losses) were approximated with an exponential decay function where the energy at time (t) is

$$E(t) = E_o e^{-\lambda t} \tag{4.11}$$

and where λ is calculated as

$$\lambda = -\frac{\ln\left(100 - fw_{rate\_loss}\right)}{60}$$

and fw_{rate_loss} is the rate of energy losses per minute in percent. A value of 3% energy losses per minute was chosen for the analyses presented in this thesis, which is similar to values reported in the literature [45]. Figure 4.6 shows the energy content of a flywheel with energy losses of 3% pre minute. The energy content of the flywheel is expressed as a state of charge (SOC) (similar to the one used for batteries; i.e. 100%=full, 0%=empty).

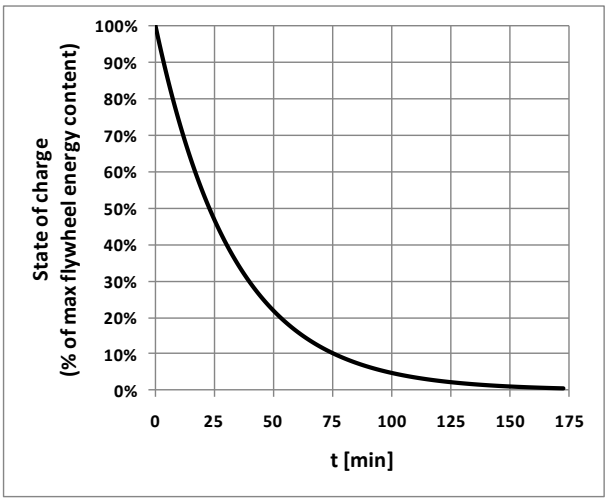

Figure 4.6 Flywheel state of charge with energy losses of 3% per minute.

PGS losses:

The PGS model uses the equations presented in section 2.5.2 covering the kinematics of planetary gear sets, and the equations presented in section 3.4.6 that cover efficiency. Transmission efficiency between branches of the PGS was approximated with the use of an efficiency map for gear meshed transmission. This is considered to be a valid approximation of the losses of a PGS, as power transmission through a manual gearbox is accomplished via a layshaft where two gear meshes are needed for power transfer between the input and output shafts. This is similar to what happens in a PGS where gear meshes occur between the carrier planets and the sun and ring gears.

The map (taken from ADVISOR and corresponding to the first-gear efficiency of a Volkswagen gearbox), was normalised to nominal torque and speeds to accommodate different speed and torque ratings of the PGS. The map is shown in Figure 4.7.

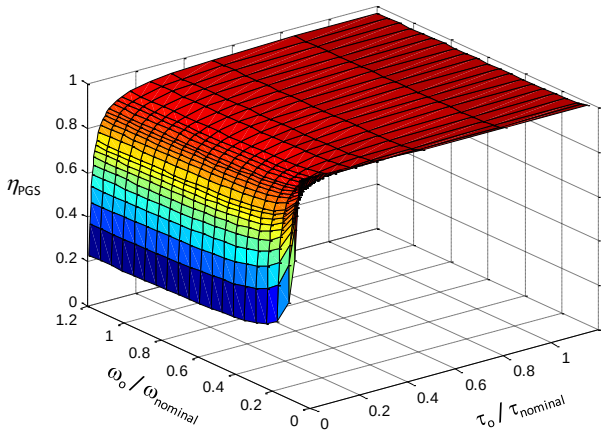

Figure 4.7 Efficiency map used to estimate the efficiency of the PGS. The map was normalised from an existing map in ADVISOR for the first gear of a Volkswagen 5-gear transmission.

Variator losses:

Similarly to the PGS, to estimate the variator losses a normalised map is used. The map was digitised form a map developed by Soltic with data from a dry belt variator and presented in [90]. The map used in the model is presented in Figure 4.8.

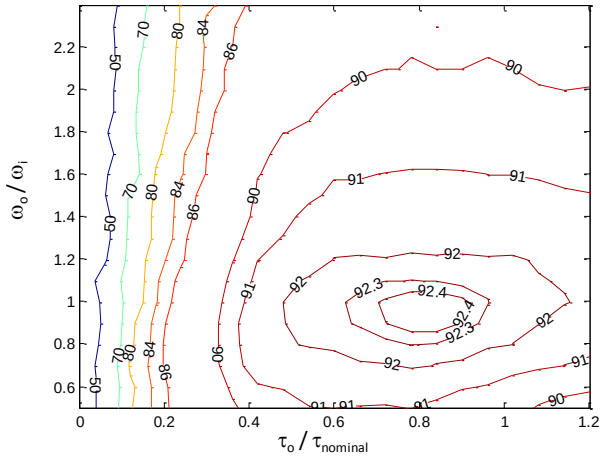

Figure 4.8 Efficiency map for the variator, adapted from Soltic [90].

4.6.2.3. Transmission logic

For each *Flywheel-hybrid powertrain* slightly different procedures were employed, however the overlying principle is the same for all:

1. The power requirements to comply with the drive schedule for a particular time step are determined.

2. The power is then geared backwards through the transmission and efficiencies are applied as appropriate until a power demand reaches a part of the transmission requiring an iterative calculation. Up until this point all the calculations are done on a standard Excel spreadsheet.

3. Iterative calculations are performed with code in Visual Basic (integrated with Excel) where a solution is found and the operation of the hybrid-powertrain is determined (i.e. variator engaged, brake at the PGS engaged, neutral). The efficiencies of components are taken into account as well.

4. Based on the operation of the hybrid-powertrain the power demanded (or delivered) to the flywheel is determined and a new SOC is found.

5. Finally, based on whether the hybrid-powertrain is capable of powering the vehicle the operation of the conventional part of the powertrain is defined. If the ICE must be

used then the corresponding transmission losses and specific fuel consumption calculations are determined just as in the case for the conventional vehicle.

The specific operations involved for each powertrain are too numerous to be shown in detail for each powertrain. Instead flowcharts showing the calculation process for the *Flywheel-hybrid powertrain* B are presented in pages 119, 120 and 121. The operation for other powertrains is similar though. For instance the PGS transmission with brake control uses the flow chart in page 119 and 121, but not the one in 120.

The nomenclature used to explain the flow diagrams is shown in Figure 4.9.

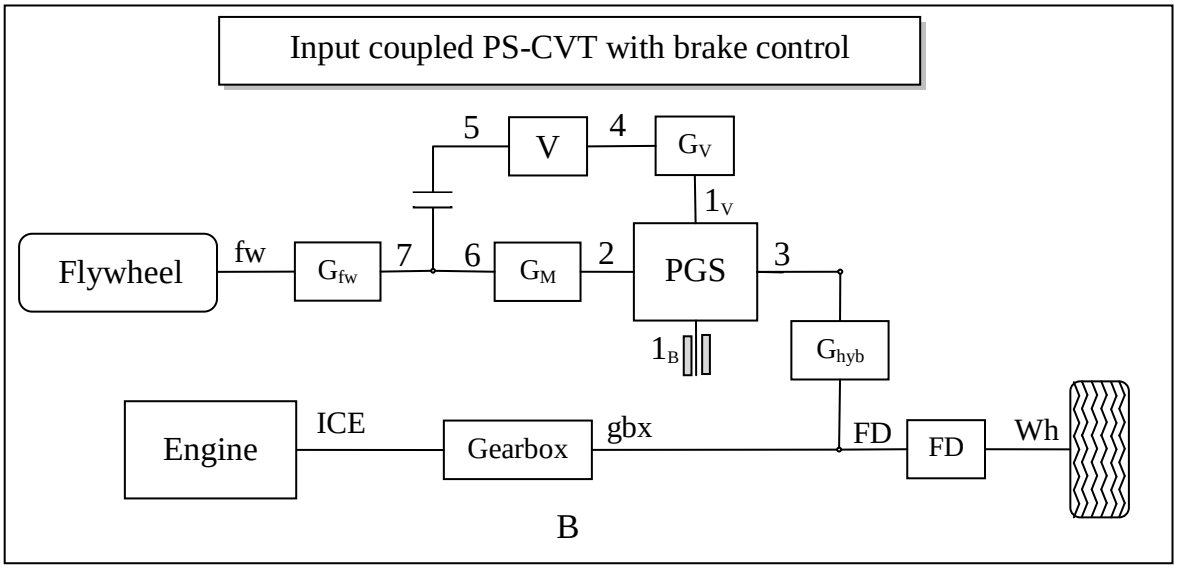

Figure 4.9 Nomenclature used for the flow diagrams presented in pages 119, 120 and 121.

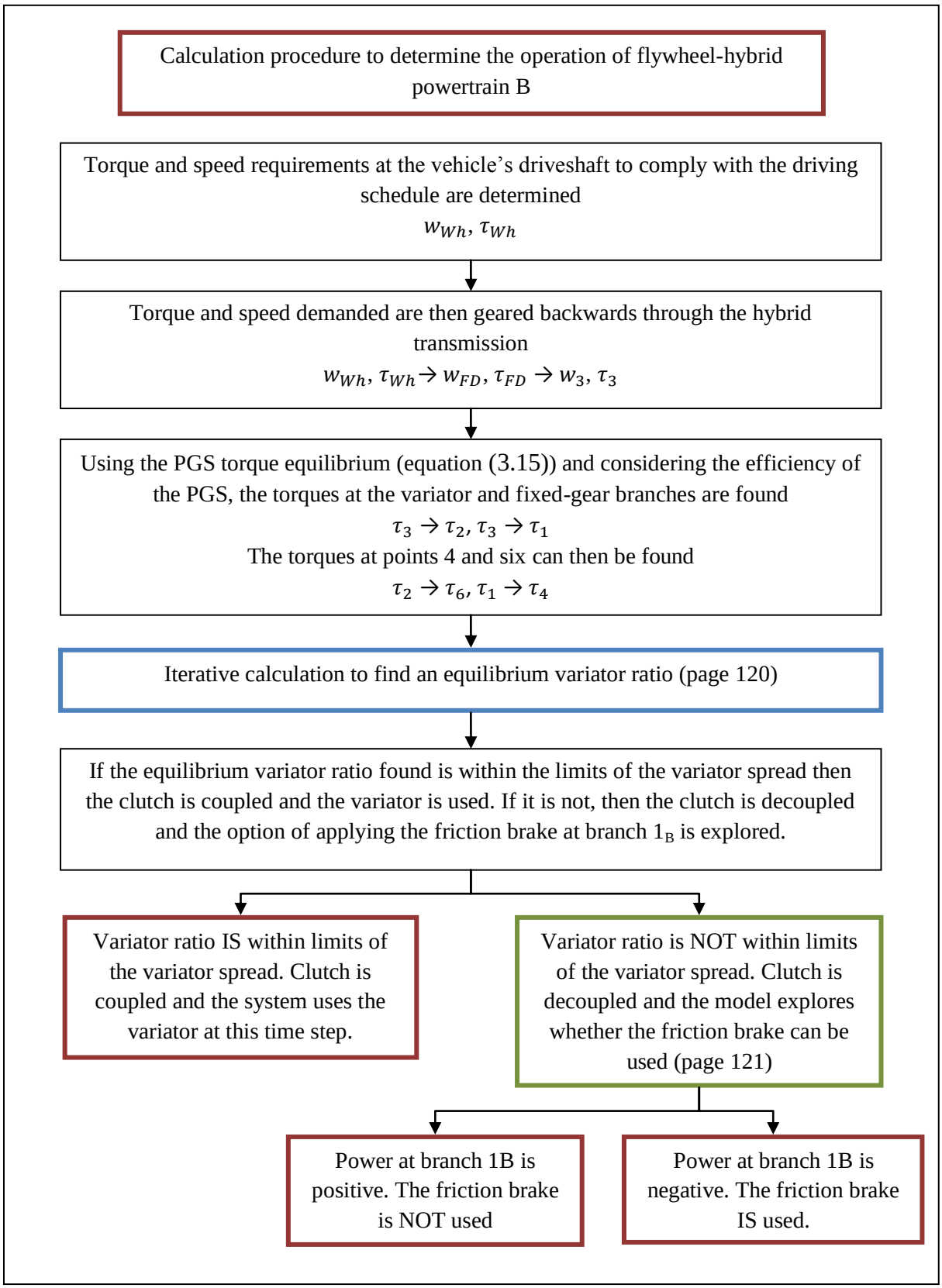

Figure 4.10 Flow diagram of the calculation procedure for the operation of *flywheel-hybrid powertrain* B. The procedure for other powertrains is similar.

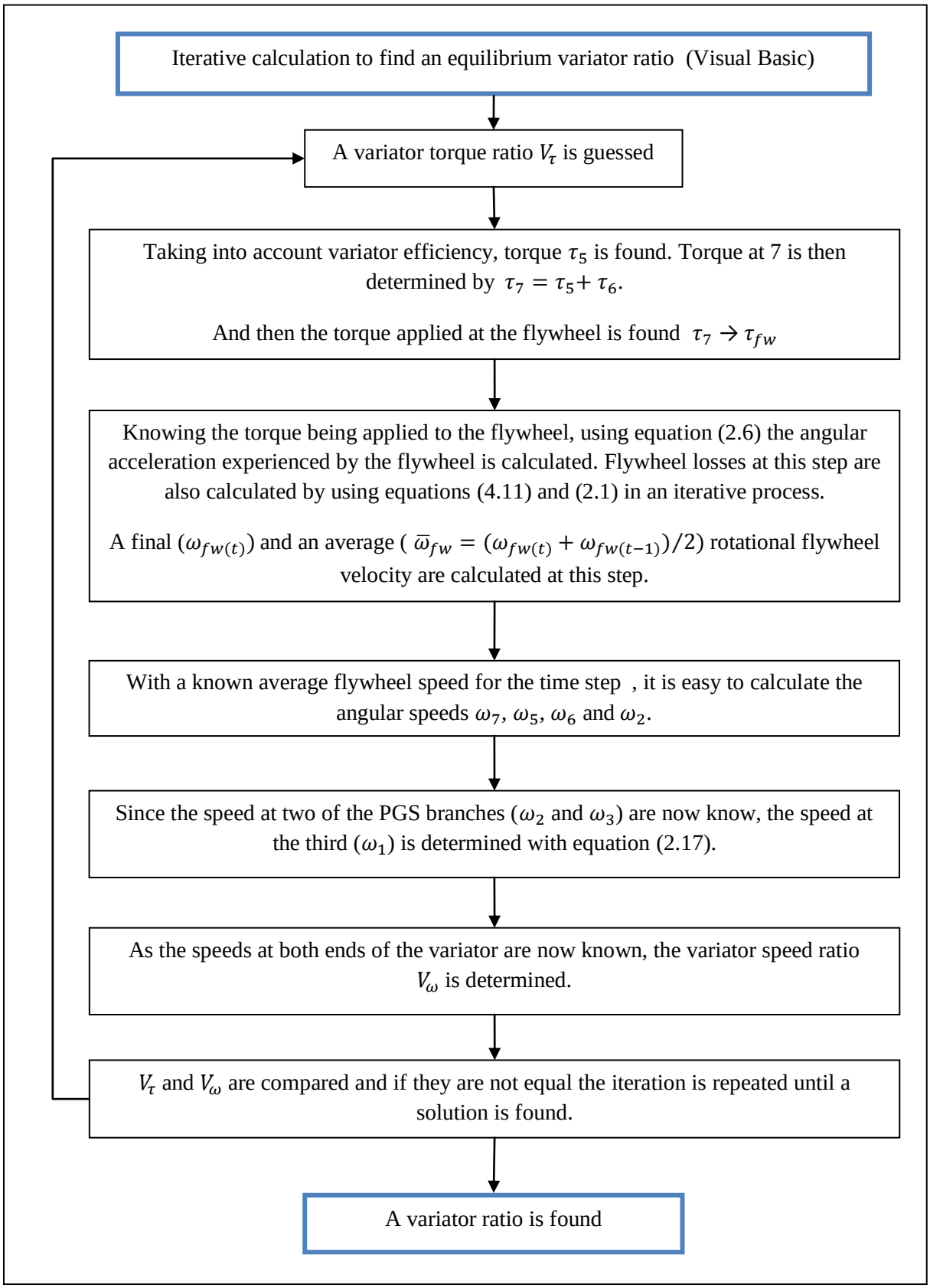

Figure 4.11 Flow diagram for the iterative calculation to determine an equilibrium variator ratio. This calculation s performed in Visual Basic.

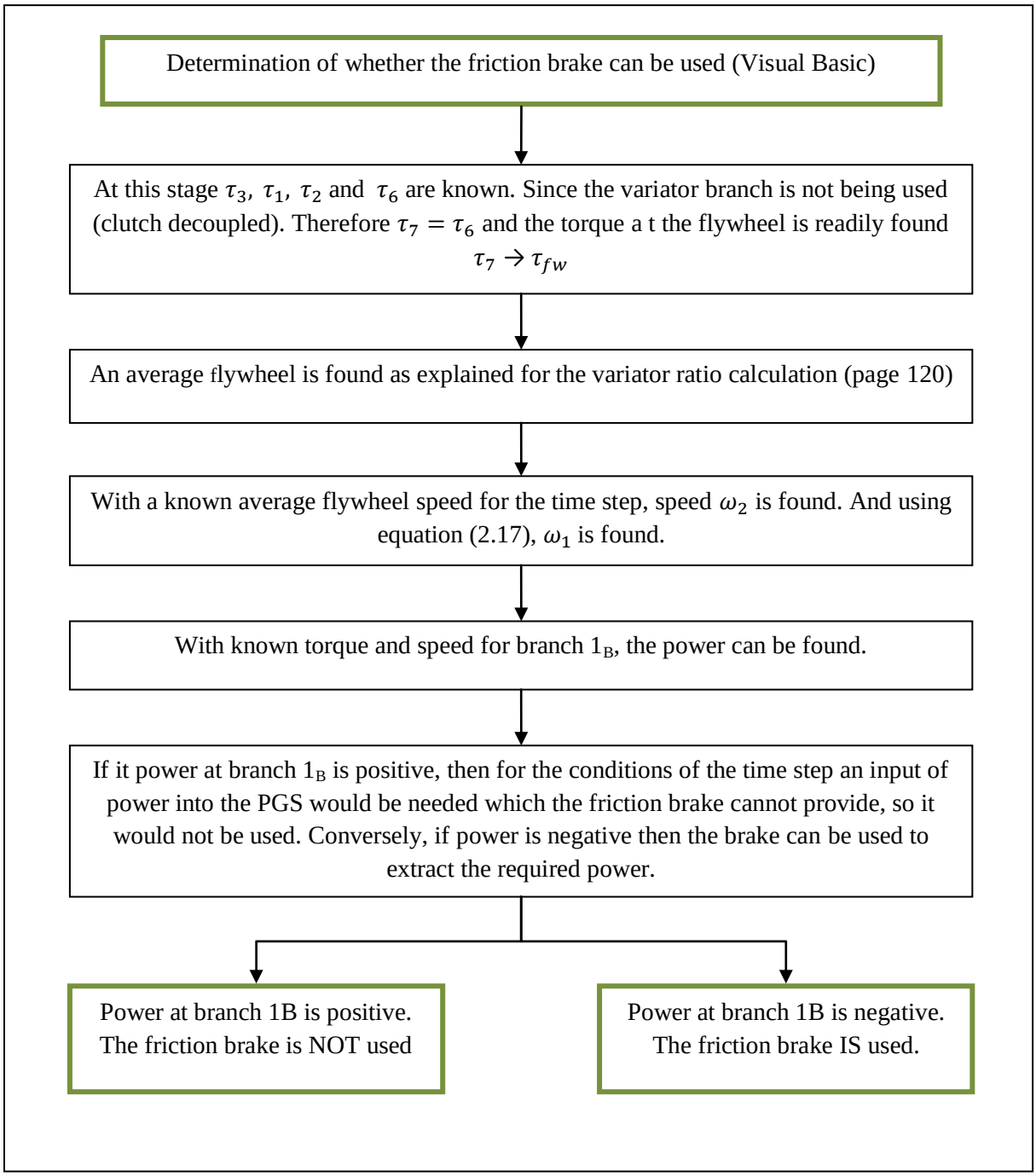

Figure 4.12 Flow diagram for the calculation that determines whether the friction brake can be used. This calculation s performed in Visual Basic.

4.6.3. Control strategy

In general, the control strategies used for all the hybrid powertrains work on the following three principles:

- Provided the hybrid powertrain is able to operate then all the braking is provided by the regenerative system which stores available power in an energy reservoir (which which can be a flywheel, a bank of batteries or a reservoir with infinite capacity for the *Ideal-parallel-hybrid powertrain*).
- When the vehicle requires power, it is first provided by the reservoir and the engine only provides power if the energy reservoir is empty or the hybrid powertrain cannot operate under current conditions.
- The engine is turned off during the periods when it is not needed. These include periods when the vehicle is not moving, when it is braking and when it is being propelled solely by the hybrid powertrain.

As can be seen, the control strategy employed is simple and blind to future road conditions, and as such it is unbiased to varying road conditions, it is thus termed *blind control strategy*. There is great potential for a control strategy that accurately anticipates the requirements that the vehicle will encounter and adjusts its control strategy. This could lead to real-time optimisation of a control strategy that could deliver higher fuel economy savings or greater power at the wheels. This is explored in more detail in section 5.4.

4.6.4. Engine management

An important aspect in the logic of the hybrid vehicle is engine management. As has been previously stated and as will be shown in the next chapter, the ability to turn off the ICE is an important strategy to substantially reduce fuel consumption.

The process by which the operation of the hybrid system is determined has been shown in the previous section. That allowed to determine whether the vehicle can be powered by the energy storage reservoir of the hybrid powertrain (whether it is a flywheel or bank of batteries) or whether the vehicle is decelerating or at rest and the use of the ICE is not required. The engine strategy employed is aimed at minimising fuel consumption and thus if the ICE is not required it is turned off.

This modelling strategy might be useful in estimating the savings available from the intermittent use of the ICE, but it is a poor estimate of engine behaviour and of emissions

other than CO_2 (which is closely linked to the amount of fuel consumption). Transient effects on the ICE are ignored and the effect that this may have on emissions. Some provisions are taken to better predict fuel consumption by applying temperature correction for decreased ICE usage and by not allowing the ICE to stay on for less than a certain period of time.

Therefore fuel economy predictions for hybrid powertrains are better indicators for their energy saving potential when compared in relation to one another, rather than as definite saving predictions over the consumption of a conventional vehicle.

4.7. Powertrain Modelling Tool (CAPTAIN) Summary

In this chapter, the simulation tool (CAPTAIN), which was developed to assess the performance of various hybrid powertrains has been presented. The general vehicle and model parameters and with their assumptions have been discussed.

Several vehicle models were introduced, including the conventional, the ON/OFF, and the Ideal-parallel-hybrid vehicle models, which are useful in assessing the performance of the *Flywheel-hybrid powertrains* which were also introduced in this chapter as well.

The information presented in this chapter details the common methodology used in the analyses presented in Chapters 5 and 6, which use the powertrains presented in this chapter. The specific methods and assumptions particular to each of the analyses presented in the next chapters are described in their own sections.

The hybrid powertrain control strategy and the engine management strategy employed by CAPTAIN were also discussed. These strategies have an important effect in the fuel economy performance of the hybrid vehicle and will be explored in more detail throughout the next chapter.

5. FUEL ECONOMY POTENTIAL FOR HYBRID VEHICLES

This chapter presents a set of computational studies performed on different hybrid powertrains with the aim of understanding some of the parameters that determine the effectiveness of hybrid vehicles in reducing fuel consumption.

It is generally accepted that hybrid vehicles have the most comparative advantage over conventional vehicles under low speed driving conditions with intermittent stops such as those encountered in urban areas. There are two main reasons for this. First, frequent stops give ample opportunities for a storage system to recuperate kinetic energy during braking and to reuse it during acceleration, thus avoiding fuel usage of the ICE. Second, the ICE used by conventional vehicles typically shows lower efficiencies at low speeds and remains idling during periods in which is not needed such as braking and at rest; hybrid vehicles may use their secondary power unit under these conditions and turn off the ICE when not in use to avoid using fuel unnecessarily.

Furthermore, hybrid vehicles may also exhibit additional advantages when they encounter road gradients. If the hybrid vehicle incorporates regenerative braking capabilities, then speed modulation may be carried out by an energy storage unit instead of the conventional brakes leading to increased opportunities to store energy. Section 5.2 of this chapter presents a study on the effect that road gradients may have on hybrid vehicles.

Section 5.3 will then use the same set of results to further investigate and present the factors that affect fuel economy the most. These factors will shed a light into the principles that control strategies could use to maximise fuel economy. This is briefly discussed in section 5.2.

5.1. Energy flow in a vehicle

Before assessing the potential fuel economy of hybrid vehicles, it is important to first review how energy is spent in a *conventional vehicle*. In this manner the areas of opportunity that will have the biggest impact in reducing fuel consumption can be established.

Figure 5.1 shows how the mechanical energy developed by the ICE for the whole cycle is typically spent by the powertrain for a vehicle following an urban drive cycle. The particular case shown corresponds to the Ford Focus (presented in section 4.2.3) following the UDC drive cycle (shown in Figure 4.2 (a)) and simulated with CAPTAIN

In the figure, the energy lost in aerodynamic and rolling losses (plus the energy spent in powering the vehicle's ancillaries when simulated, which are not in this case) is the minimum amount of energy required to drive the vehicle for this particular drive cycle. Other losses, such as transmission losses and ICE friction losses are powertrain dependant, thus a hybrid powertrain will not encounter those losses, although it will incur in losses associated with its own powertrain.

The energy dissipated in the brakes is the energy required to accelerate the apparent inertia of the vehicle (considering only the mass of the vehicle and not any friction losses from the vehicle or losses from the powertrain) and is the target of the regenerative braking strategy.

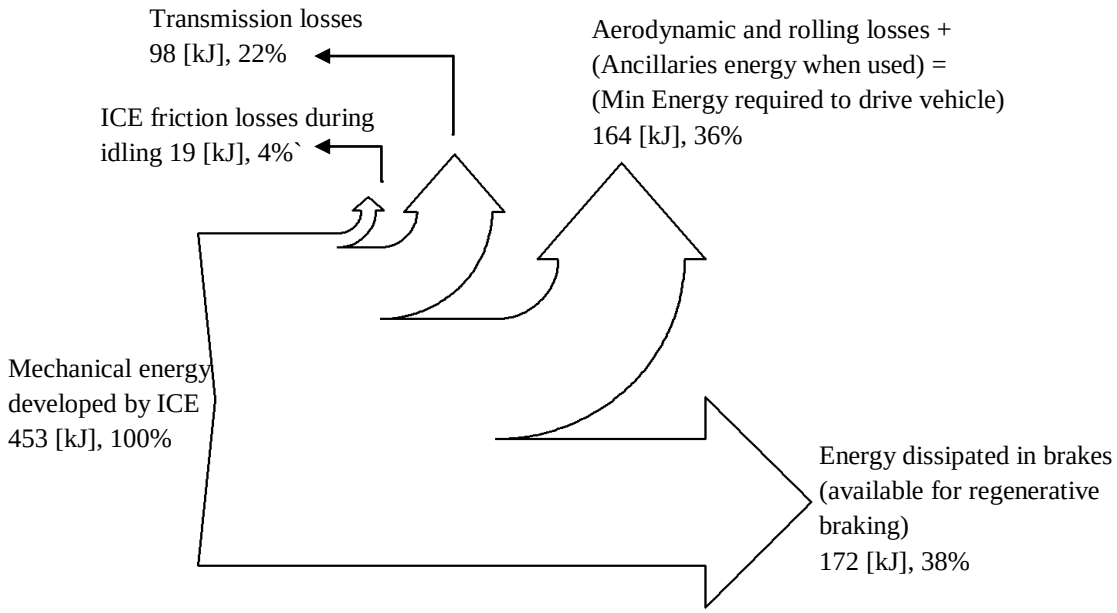

Figure 5.1 Final destination of the mechanical energy developed by the internal combustion engine for a vehicle following an urban drive cycle (Ford Focus Estate following the UDC cycle).

However the biggest gain in vehicle effectiveness does not come from the reutilisation of this inertial energy, (although it is significant), but rather from the energy that its use displaces. In the case of a *conventional vehicle* with a hybrid powertrain, the recuperation and reuse of the inertial energy of the vehicle displaces mechanical energy that is produced inefficiently by the ICE. This is especially the case for the driving conditions of this example (low average velocity and prolonged idling periods) over which the ICE operates with an average efficiency of 16% for the drive cycle as shown in Figure 5.2.

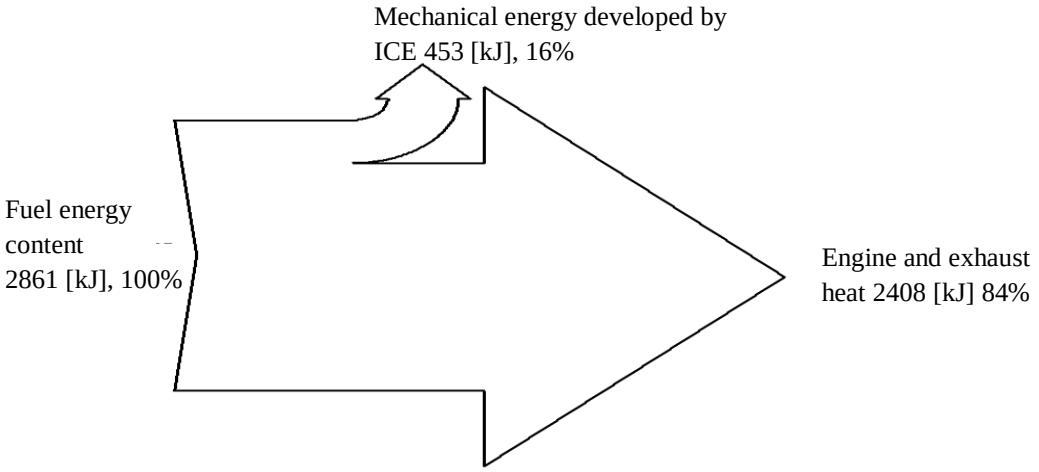

Figure 5.2 Thermal efficiency of the ICE following the UDC cycle.

It is now useful to define a vehicle effectiveness which can be used to compare the ability of different powertrains in maximising fuel economy. This effectiveness is defined as

$$\eta_{Veh} = \frac{Minimum\ Energy\ required\ to\ drive\ vehicle}{Energy\ content\ of\ used\ fuel} \tag{5.1}$$

In the example above the *conventional vehicle* has a very low effectiveness of only 5.7%

The strategies and conditions that allow this effectiveness to increase is the purpose of this chapter and will be examined throughout the next sections.

5.2. Road gradients study

In recent years, considerable effort has been devoted in developing fuel economy tests that more accurately reflect the fuel economy achieved by drivers. In the US, the Environmental Protection Agency (EPA), which is the body in charge of developing and administering these tests, recently published new procedures for these tests [91]. These procedures claim to better reflect real conditions more accurately and have a much better prediction of fuel usage. Under the new tests fuel economy predictions for conventional and hybrid vehicles decreased on average 13% and 22% for city driving conditions respectively compared to the previous tests. This has been attributed primarily to a higher impact of temperature on fuel used in hybrids and to the inclusion of a new driving cycle in the procedures.

Road topology is an important factor affecting the performance of vehicles, and under certain conditions it may dramatically reduce the fuel economy and increase the emissions of vehicles. Although this is widely recognised, the difficulty of simulating road gradients on a dynamometer and the wide variability of road topology that may be encountered by drivers in different locations, have led to either their disregard or the introduction of approximations to account for them during standardised fuel assessments.

The new EPA tests apply correction factors for certain phenomena which are not easily replicated under dynamometer tests and that are not currently part of the tests procedures. The EPA devoted particular effort in revising previous correction factors, and as a result the factors for wind, road surface and tire pressure effects, were updated. However, the effect of road gradients was considered to be small in magnitude and as a result, the correction factor was not updated and was left at its previous value of -1.9%.

This might be justifiable for comparing vehicles of similar size and with conventional powertrains, as their performance can be assumed to be affected relatively equal for varying road gradients. However, this might not be the case for hybrid powertrains, especially for hybrid powertrains with high regenerative capabilities, as they are (at least to a certain extent) able to tap into potential energy gains by controlling vehicle speed when going downhill by using the regeneration system, rather than conventional brakes or by ‘engine braking’. Therefore the comparative fuel economy advantage of hybrid over conventional vehicles under these conditions can be expected to increase. The aim of the study presented in this section is to analyse and quantify what this comparative advantage might be when road gradient are considered. For this aim, three study-sets were designed and simulated using CAPTAIN. Their definition is presented next.

5.2.1. Definition of case studies

The three study-sets are:

A. Sinusoidal gradients

B. Random gradients

C. Real gradients

All the study-sets use the same vehicles, powertrains and control strategies. They differ in the drive cycles used and in the manner in which road topology was simulated.

The vehicle used is a Ford Focus Estate with specification shown in Table 4.2. Two vehicles with different powertrains are used. These are a *conventional vehicle* (described in section 4.3), and an *ideal-parallel-hybrid vehicle* (described in section 4.6.1) but with varying limits on the capacity of its energy reservoir. In one instance the *ideal-parallel-hybrid vehicle* energy reservoir is limited to a zero-capacity, which is equivalent to the *ON/OFF vehicle* described in section 4.4. This particular case is referred to as the *ON/OFF vehicle* in the results to stress the point on the limits of the capabilities of this powertrain.

For each study-set, several single cases were simulated, with each case representing a unique set of conditions with a defined drive cycle, road topology and energy reservoir capacity. These conditions were artificially selected and cover a wide range of driving conditions, many of which may not represent typical driving behaviours, but are nevertheless useful in identifying the most important set of factors affecting fuel economy and in determining the potential benefits from adopting specific driving strategies.

The maximum road gradients recommended in road construction are typically in the range of about 9m/100m for highways and 13m/100m for urban roads [92]. The road topologies used for all the study sets were restricted to roads giving a maximum rise within the above mentioned limits.

For some simulated conditions, the torques required were too high for the ICE or powertrain components to handle, in which case the simulation was discarded and was not included in the results. Thus all the cases presented are plausible driving conditions.

Since the drive cycle usually ends up with a final regenerative braking event, the energy reservoir will end up charged. In order to get a real potential fuel economy for the hybrid vehicle, simulations were repeated with the energy reservoir initially charged, until there was no net difference between the initial and final energy contents of the energy reservoir.

The drive cycles and road topologies particular to each study-set are explained next.

A. Sinusoidal gradients

This set consists of the UDC drive cycle superimposed over varying road topologies, and considering 5 different energy reservoir capacity limits.

The varying slopes of the tracks used for this set were simulated using a sine function in which the amplitude and period were altered to generate a wide range of roads with varying gradients, as shown in Figure 5.3. The period was adjusted to ensure that the vehicle ended at the same height as it started to avoid any net change in potential energy. The notation used implies that for a positive amplitude the vehicle would commence the cycle with an upward slope and conversely a negative amplitude implies an initial downward slope. The tracks used in the simulation include a flat track and sinusoidal tracks ranging from 1 to 10 full-cycles with amplitudes ranging from -50 to 50 meters (at increments of 1 meter).

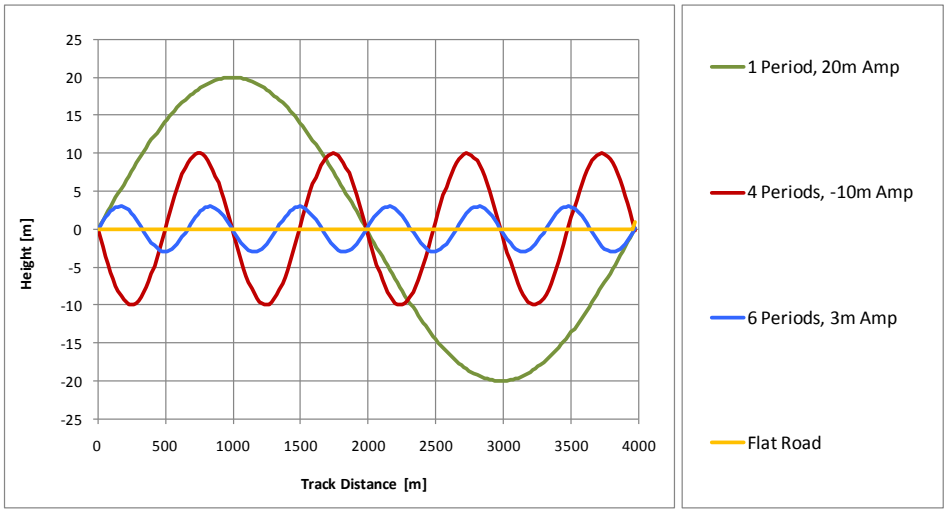

Figure 5.3 Examples of the road topology employed for the *Sinusoidal gradients* study-set.

For the *ideal-parallel-hybrid vehicle* a total of 5000 cases were simulated out of which 789 were considered successful (within the power range for the ICE and maximum road gradient limit for the road topology); and for the *conventional vehicle* 168 cases were simulated and considered successful.

B. Random gradients

This set consists of 8 drive cycles superimposed over 25 different road topologies and considering 6 different energy reservoir capacities. A total of 900 cases were simulated for the *ideal-parallel-hybrid vehicle* with 807 of them considered successful. For the *conventional vehicle* 150 cases were simulated with 120 of them successful.

This study-set uses a set of 6 drive cycles sectioned from existing drive cycles developed within the frame of the ARTEMIS European research project (the follow up project of the HYZEM project discussed in section 1.1.3), and that more closely reflect real-world driving conditions compared to the NEDC cycle. The ARTEMIS drive cycles represent urban, rural and highway driving conditions with varying degrees of traffic [93]. These driving cycles can be disaggregated allowing for the study of various driving conditions. The main ARTEMIS cycles are shown in Figure 5.4.

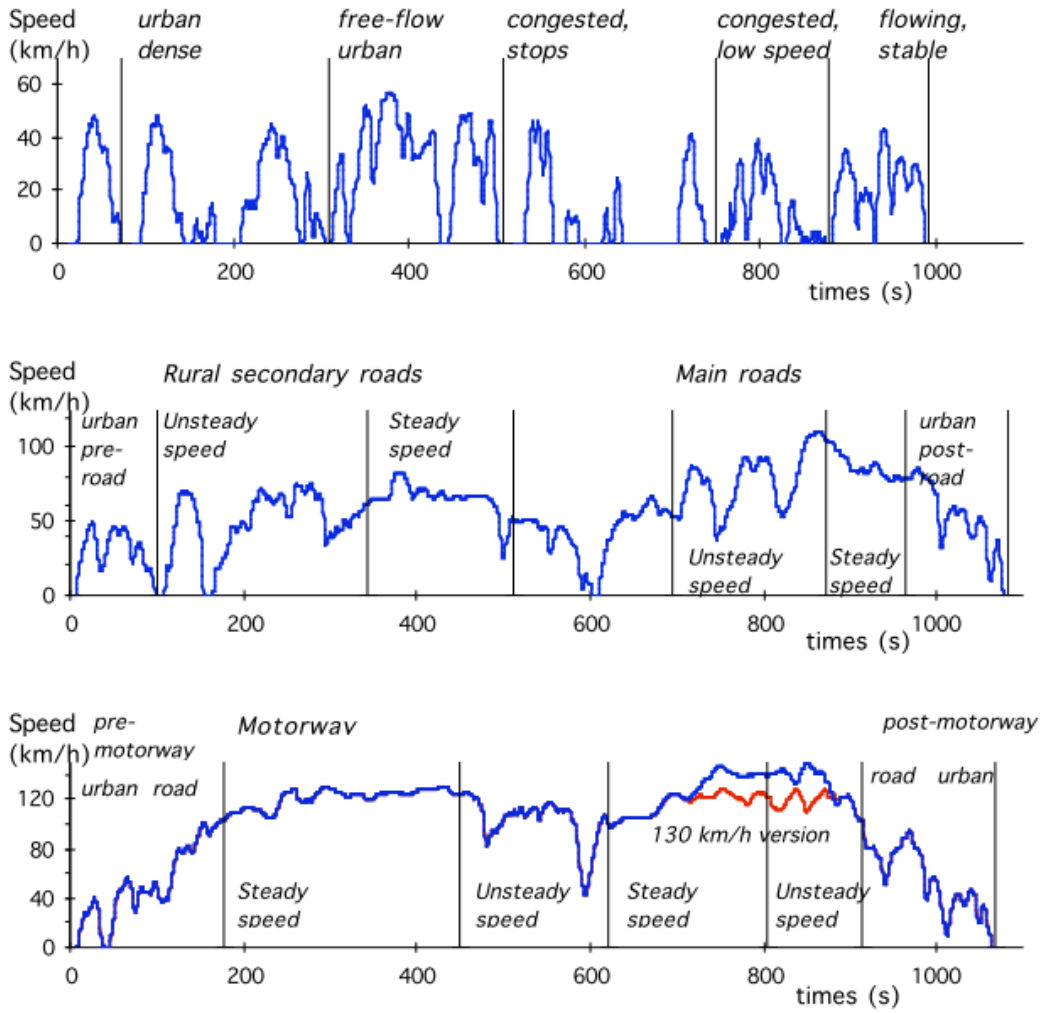

Figure 5.4. . From top to bottom, urban, rural and highway ARTEMIS driving cycles showing regions with varying traffic. Figure from [93].

The road topology for this study-set was randomly generated by an algorithm that kept road gradients and road roughness within defined limits. The purpose of this is set of data was to avoid any cyclic effects from the topology of sine waves and to test the effect on drive cycles of a topology more closely resembling real driving conditions.

For this purpose a program was built into CAPTAIN to generate the track within defined constraints. The limiting parameters for the cycle generation program are road roughness and maximum gradient. At regular intervals the program generates a random gradient which is limited by a defined maximum gradient. The length of the interval is defined by a roughness factor so that a low number generates a smooth curve with infrequent gradient changes, while a large number produces a topology with frequent and abrupt gradient changes. Figure 5.5 presents four examples of randomly generated topologies with varying maximum gradient and road roughness.

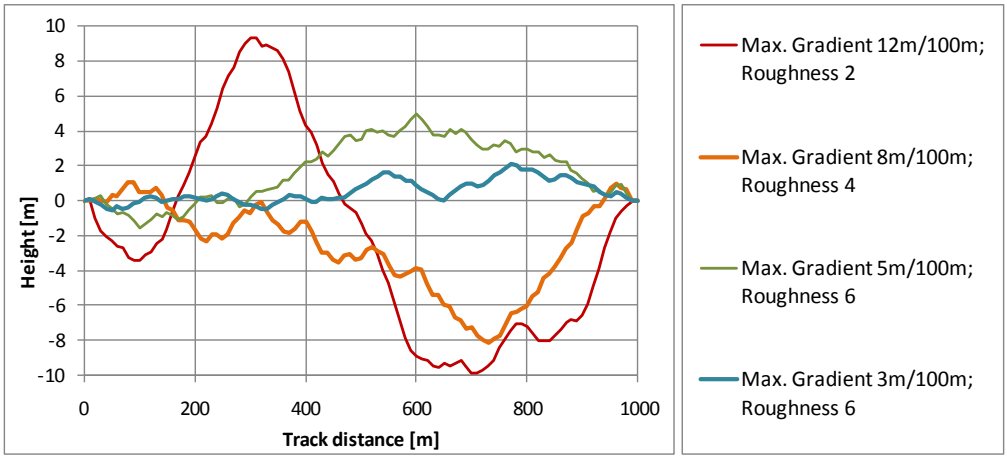

Figure 5.5 Two examples of randomly generated road topologies with varying maximum gradients and road roughness.

C. Real gradients

This final study-set is an effort to simulate real-driving conditions and road topologies as accurately as possible. Real-world velocity and road topology data recorded in GPS devices was used for this set. The drive cycles and road gradients were obtained from data posted by drivers on the internet [94] which was collected between March 2006 and August 2009, covering 13 cities from around the globe.

This set consists of 12 drive cycles, each with its unique road topology. Details on the original data is shown in Appendix D. This data had to be filtered first to get rid of inaccurate readings demanding unrealistic acceleration or road gradients. Net gains in potential energy were avoided by sectioning the drive cycle to the longest stretch possible starting and ending at the

same height. In order to study the effect of gradients of different magnitudes over the same driving cycle, seven different roads with the same contour but with varying gradient magnitudes were generated based on the original road topology for the drive cycle. The roads generated corresponded to magnitude fractions of 0, 0.25, 0.5, 0.75, 1, 1.25 and 1.5 of the original road.

Figure 5.6 shows an example of one of the sectioned drive cycles used (corresponding to a recorded trip in Vancouver) along with its original full drive cycle. Figure 5.7 shows the sectioned part of the road used with the original topology (green line) along with the various fractions of gradient magnitudes used in the simulations.

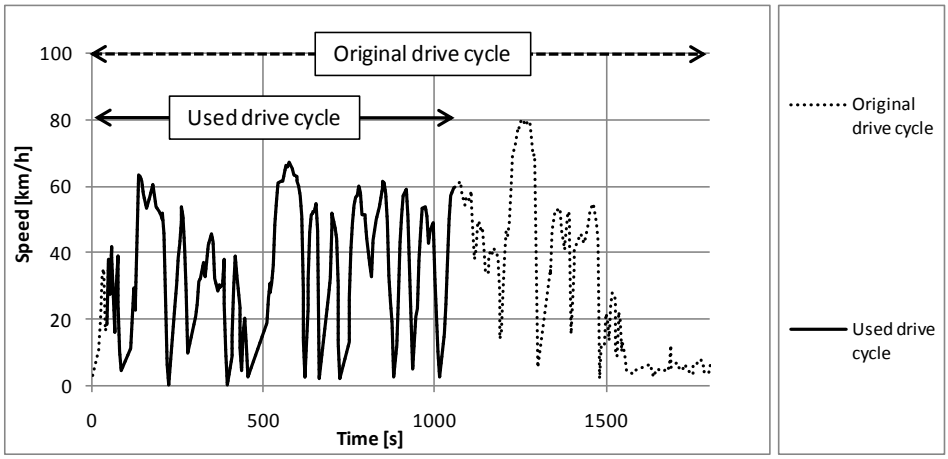

Figure 5.6 A Vancouver drive cycle with the original full drive cycle and the section used in the simulations.

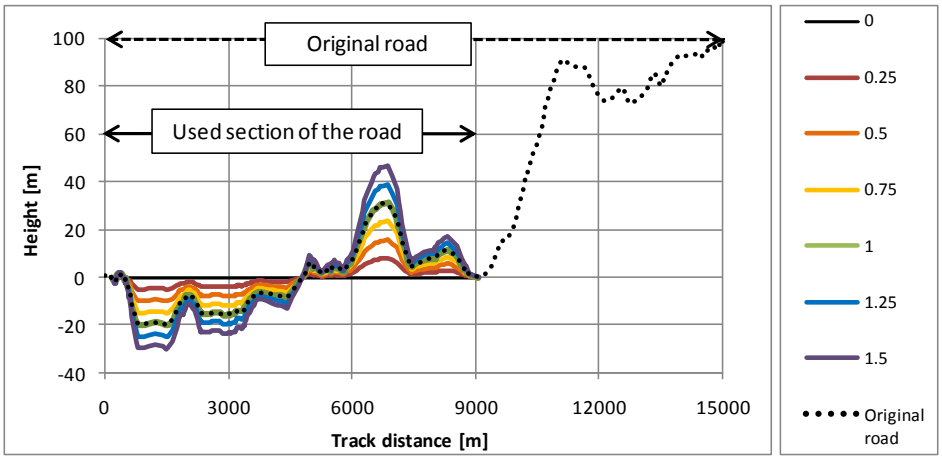

Figure 5.7 The corresponding topology for the drive cycle shown above, showing the section used of the road along with the different fractions of road gradients magnitudes used.

These drive cycles and road topologies were then simulated considering 6 different energy reservoir capacities for the *ideal-parallel-hybrid vehicle*. A total of 570 cases were simulated for the *ideal-parallel-hybrid vehicle* with 370 of those considered successful, and a total of 84 cases were simulated for the *conventional vehicle* with 55 of them successful.

5.2.2. Road gradients study results

As expected, the fuel economy of the *conventional vehicle* tends to decrease with increasing gradients, with the best fuel economy occurring at near zero road gradient conditions for all cases simulated. The conventional vehicle will only experience minor improvement in fuel economy under gentle gradients when the topology of the road is such that the most demanding acceleration periods of the driving schedule coincide with a negative slope that assists on the acceleration of the vehicle thus compensating for the extra energy required when going uphill. The benefit under these conditions is marginal though, and further increasing the magnitude of the gradients is not beneficial for the *conventional vehicle* as gains in potential energy can rarely be fully converted to useful kinetic energy at the vehicle. Energy management of the vehicle when going downhill is usually carried out by regular vehicle brakes or through engine braking and thus most of the potential energy gained is dissipated as heat.

The results for the *ideal-parallel-hybrid vehicle* are quite interesting. The fuel economy with this configuration rarely suffers as gradients are increased. This can be expected since the gains in potential energy that the vehicle makes when going uphill can be stored in its energy reservoir as the hybrid powertrain uses its regenerative braking capabilities to modulate speed when going downhill. Thus any extra power required to propel the vehicle as a result of increased gradients comes from energy stored in the energy reservoir. This is specially the case as the capacity of the energy reservoir is increased to accommodate this extra available energy. Moreover, at higher energy reservoir capacities, the fuel economy of the vehicle actually tends to increase as the magnitude of gradients increase.

The behaviour described above can be discerned from examining plots (a) through (d) in Figure 5.8, which show the predicted fuel economy of the *Sinusoidal gradients* study-set for the *conventional vehicle*, the *ON/OFF vehicle*, the *ideal-parallel-hybrid vehicle* with an energy reservoir capacity limited to 200 kJ and the *ideal-parallel-hybrid vehicle* with a limitless energy reservoir capacity respectively. The plots show how the predicted fuel economy of the powertrains changes against the amplitude of its road topology for various numbers of cycles.

For the *conventional vehicle*, the fuel economy decreases as the periodicity and amplitude increase (that is under increasing road gradients). For the *ON/OFF vehicle*, it can be seen that at low gradients (corresponding primarily to lower amplitudes) the fuel economy starts to

increase against the base case of zero gradients. As the energy capacity of the hybrid reservoir is increased, the vehicle is able to store more of the extra energy available at higher gradients. This extra energy serves not only to overcome the extra energy required when going uphill, but it also allows the engine to be turned off for longer periods. The performance of the *ideal-parallel-hybrid vehicle* thus tends to increase as the energy capacity of its reservoir is increased as shown in Figure 5.8 (c) and (d).

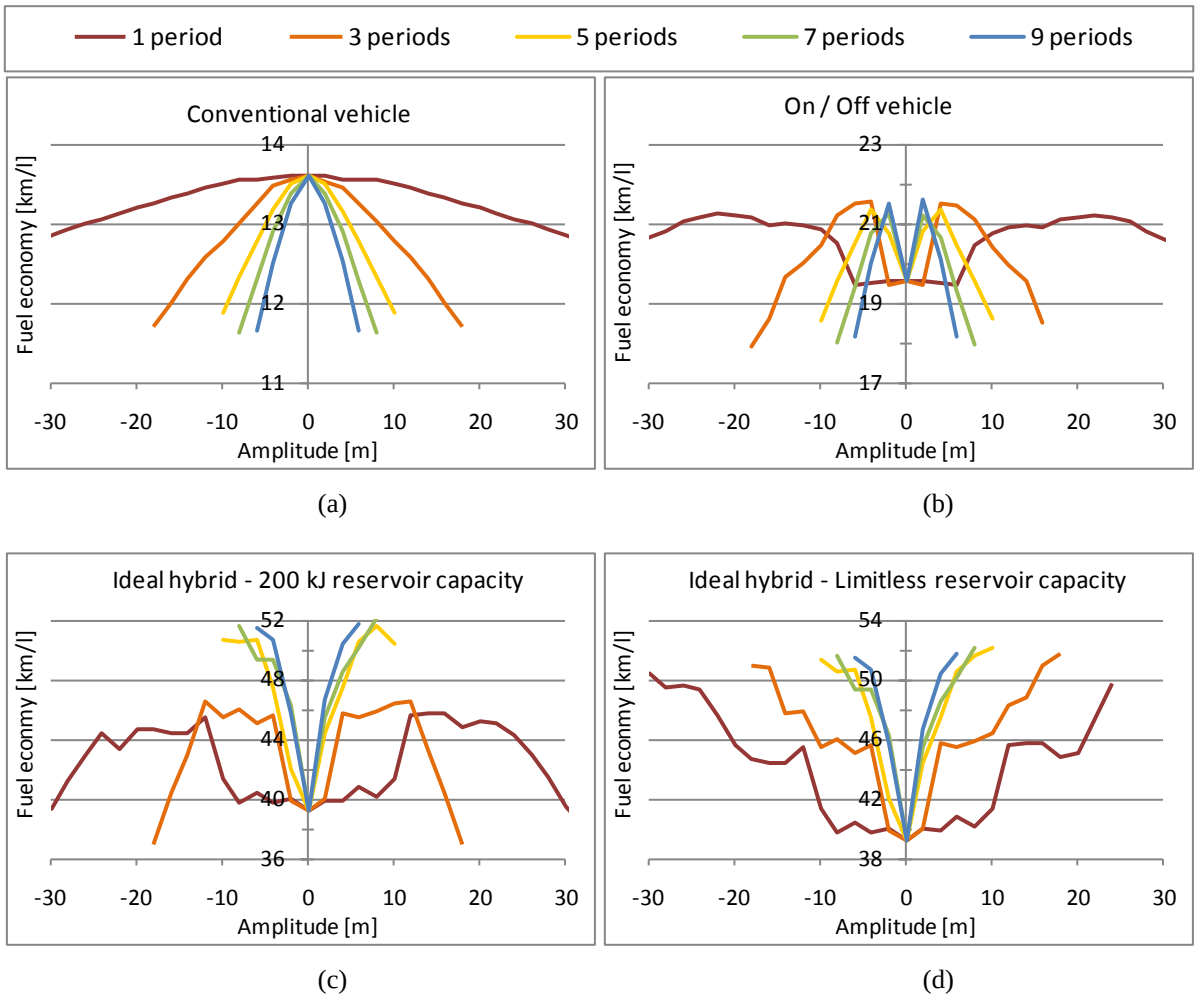

Figure 5.8 (a) The fuel economy of the *conventional vehicle* (b), the *ON/OFF vehicle* (b), the *ideal-parallel-hybrid vehicle* with a 200 kJ energy reservoir capacity (c), and the hybrid powertrain with a limitless energy reservoir capacity.

This trend is also evident in the *Real gradients* study-set. Figure 5.9 shows the fuel economy for a (a) Rome and a (b) Santiago drive cycles under increasing maximum road gradients. As expected the fuel economy of the *conventional vehicle* decreases with increasing road gradients. As in the previous study-set, the fuel economy achieved by the *ideal-parallel-hybrid vehicle* under higher road gradients is dependent on capacity of its energy reservoir,

with the highest fuel economy achieved under conditions of high road gradients and with hybrids with the largest energy reservoir capacities.

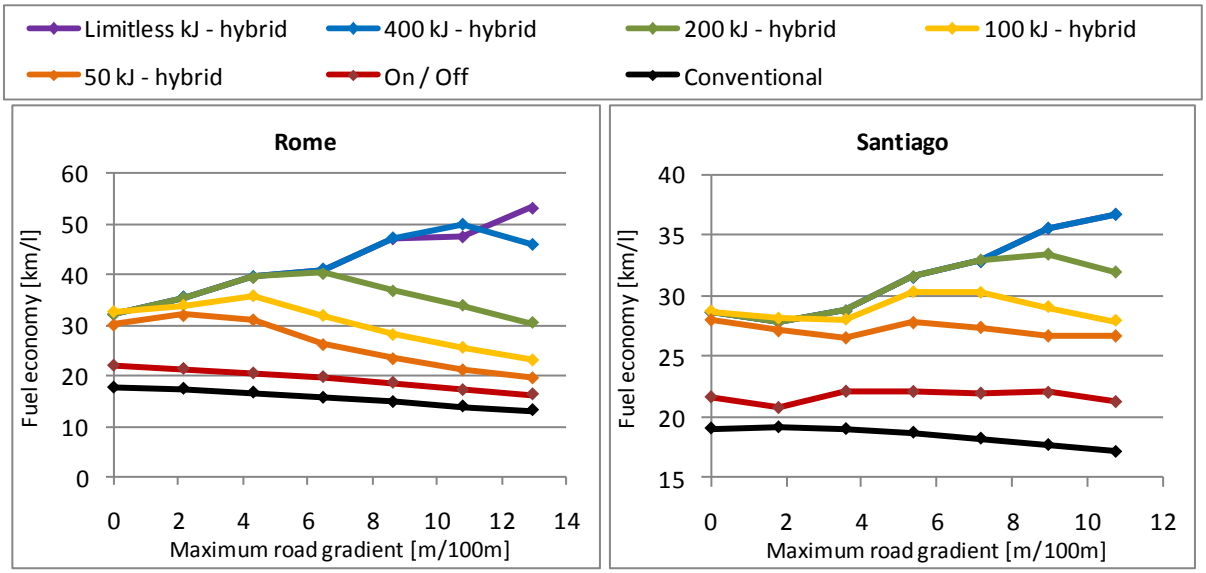

(a) (b)

Figure 5.9 Fuel economy versus maximum road gradient encountered for (a) a Copenhagen drive cycle and (b) a Singapore drive cycle. The different lines represent different vehicles and varying maximum capacity of the energy reservoir for the *ideal-parallel-hybrid vehicle*.

The same trend repeats itself for all drive cycles of the *Real Gradients* study-set as shown in Figure 5.10. This figure shows the average improvement in fuel economy for all the drive cycles over a base case with a flat road, as the fraction of road gradients magnitude increases (a fraction of zero represents a flat road while a fraction of one represents the original topology).

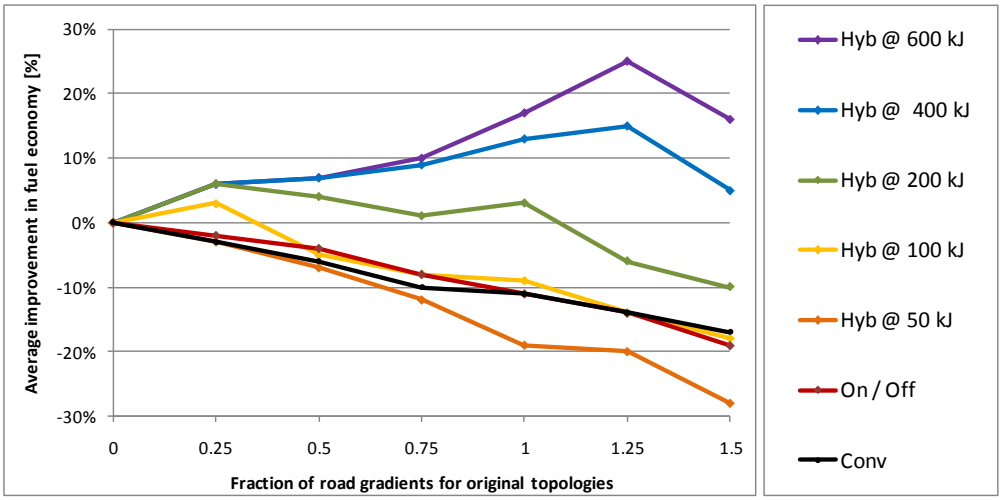

Figure 5.10 Average fuel economy improvement (compared to the base case of a road with zero-gradients) as the magnitude of road gradients in increased, for various vehicle and with different energy reservoir capacity limits. In the graph, a fraction of road gradients of zero corresponds to a flat road, and a magnitude of one corresponds to the original topology of the road.

Figure 5.11 can be used to try to determine the reason behind the fuel economy improvement for the *hybrid vehicle* when in the presence of larger gradients. It is important to note that in the presence of large road gradients, the amount of energy that needs to be spent to accelerate the vehicle is higher than for small gradients. Of course, this also means that there is more energy available for regeneration. The figure shows the operation of the *ideal-parallel-hybrid vehicle* with an infinite energy reservoir for a UDC cycle under two different topologies, one on a flat road and another one on a road with an average gradient of 2.27 m / 100 m (2 cycles and 10 meters amplitude). The top chart of the figure shows the amount of energy in the hybrid energy reservoir for both road scenarios, as well the gradient of the road and the driving schedule. The bottom chart shows the state of the engine, that is, ON or OFF. For both cases, the energy reservoir starts uncharged.

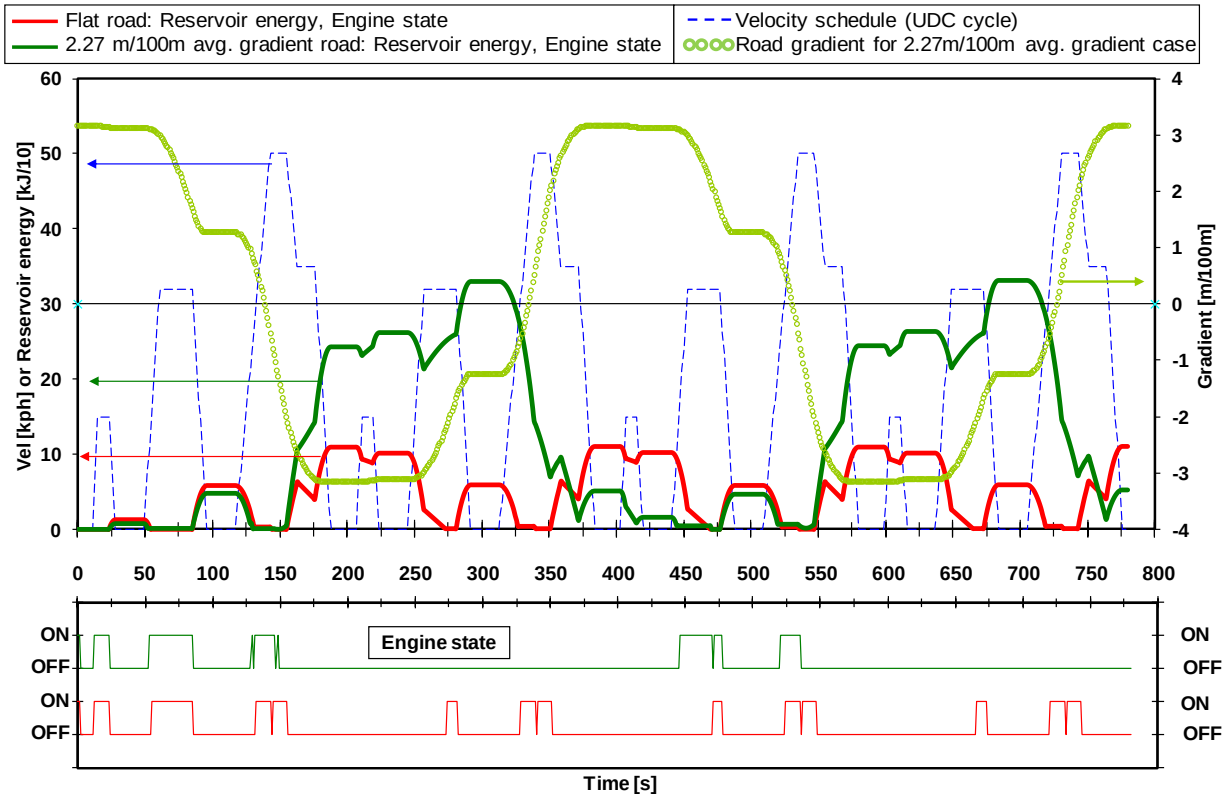

Figure 5.11 Operation of two simulations with different gradients: one on a flat road and one with 2.27 m / 100 m average gradient for the *ideal-parallel-hybrid vehicle* with a limitless energy reservoir capacity. The top chart shows the energy contained in the energy reservoir for each of the cases, as well as the gradient curve over time of the second case, and the driving cycle (UDC). The bottom chart shows the engine state (ON or OFF).

It can be seen in Figure 5.11, that for the flat road case the hybrid energy reservoir will periodically regenerate and store a considerable amount of energy (i.e. period from ~150 to ~250 sec), but that it will be spent quickly and deplete completely (i.e. period from ~250 to

~275 sec). This pattern is repeated consistently, albeit with varying intensity, throughout the driving schedule.

The case with road gradients follows a similar energy regeneration-delivery pattern, but with a crucial difference. The period running from ~150 to ~320 sec is characterised by the prevalence of negative road gradients which the energy reservoir uses in its favour by regenerating a larger amount of energy. When a considerable amount of energy is finally demanded by the engine, at around ~320 sec, it takes around 120 seconds for the reservoir to deplete completely, even under the presence of positive road gradients.

As the engine is turned off when power demand is met by the hybrid system, the end result is that for the flat road, the *ideal-parallel-hybrid vehicle* only requires the engine to be on for 20% of the time; and for the case with road gradients, the engine will be on for only 14% of the time, accounting in part for the impressive fuel economy improvement under the presence of gradients.Finally the overall fuel economy improvement for the *Random Gradients* study-set in shown in plots (a) through (d) in Figure 5.12. The plots show a frequency distribution function on the fuel economy improvement for the cases simulated over the base case of zero gradients for a specific powertrain. The red green and blue columns represent the frequency of cases exhibiting a worse, equal (or insignificant) or better fuel economy than the zero-gradients case respectively.

The significance of these charts is that they show unequivocally that the comparative advantage of the *ideal-parallel-hybrid vehicle* (on a fuel economy basis) increases in the presence of hills. An even starker difference is exhibited by the other two study cases which are presented in Appendix E.

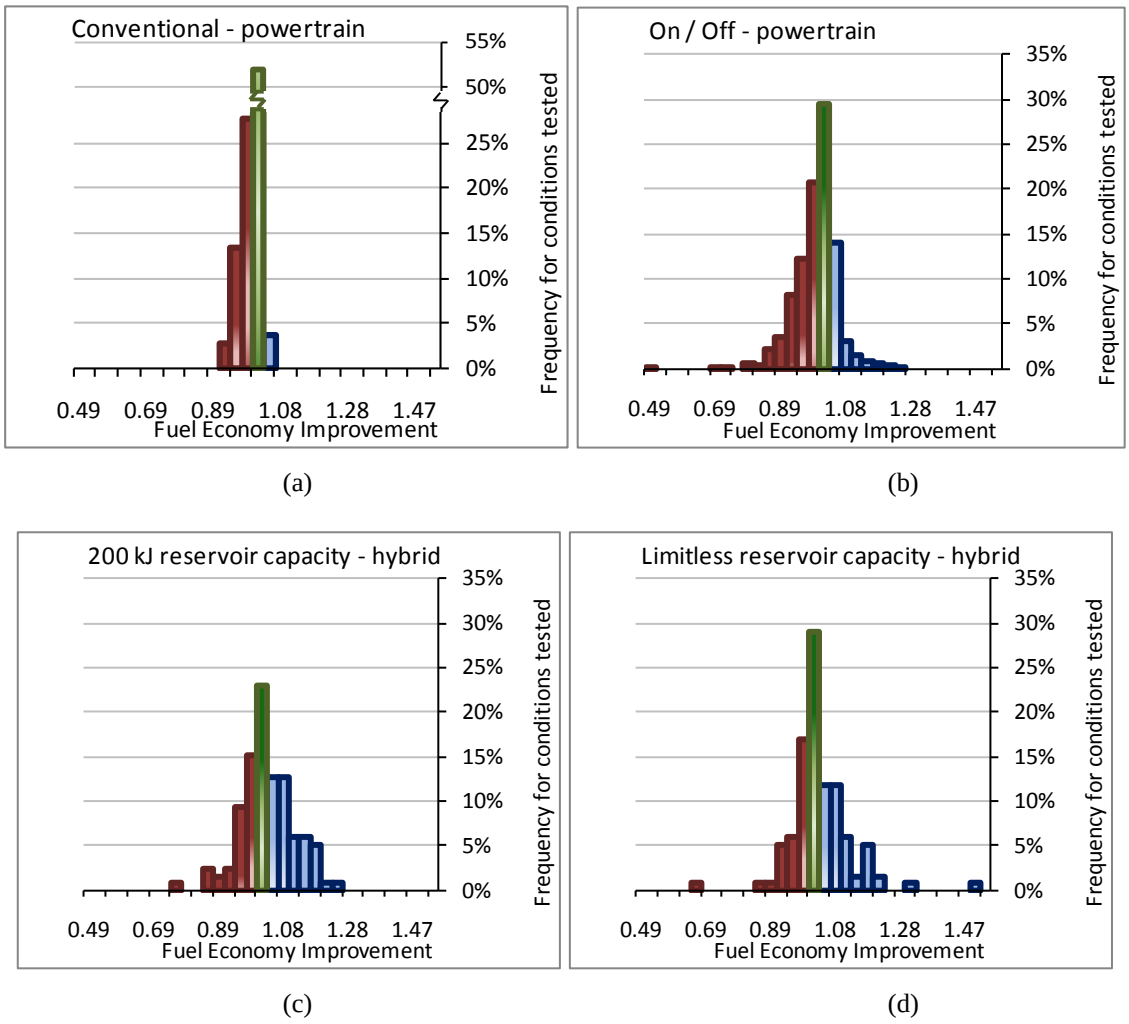

Figure 5.12 Frequency distribution plots of fuel economy improvement (measured as the improvement in fuel economy for each case over its performance in a flat road) for all gradients tested for the *Random Gradients* study-set. The red green and blue columns represent the frequency of cases exhibiting a worse, equal (or insignificant) or better fuel economy than the zero-gradients case respectively.

It is important to note for the *Sinusoidal Gradients* and the *Random Gradients* study-sets a road with gradients is being superimposed over a road originally designed intended for a flat road. In reality, the driver should be expected to respond and react according to the road gradients encountered. However, the unbiased application of the driving schedule on varying road gradient conditions, provides both advantageous and disadvantageous scenarios giving considerable confidence to the results.

5.2.3. Road gradients study conclusions

The simulations carried out have shown that roads with high gradients have a negative effect on the fuel economy for conventional powertrains, but that conversely hybrid vehicles with regenerative-braking capabilities and enough capacity in its energy reservoir can exploit the gains in potential energy to its advantage and improve their fuel economy considerably.

As mentioned earlier, current fuel economy and emissions assessment standards either disregard the effect of road gradients completely or its effect is considered low. Although convenient, these assumptions are comparing one of the best case scenarios for the conventional powertrain against one of the worst case scenarios of the regenerative-braking powertrain. This suggests that the benefits of hybrid vehicles might be underestimated under certain conditions. This may not be significant with the current hybrid vehicles available on the market as they have limited regenerative braking capabilities. However, as hybrid vehicles with more efficient regenerative braking capabilities are introduced, it might be necessary to reassess tests procedures to correctly account for the benefits of these vehicles. This will benefit manufacturers, policy makers and consumers in matching technologies with locations to maximise the effectiveness of hybrid vehicles in mitigating emissions and improving fuel economy.

5.3. Factors Determining the Fuel Economy of Hybrid Vehicles

Part of the objectives of the research of this PhD is the identification of vehicles parameters that affect the effectiveness of hybrid vehicles in improving fuel economy. The vast amount of simulations carried out for the studies presented in the last section provided a good starting point from which to carry out this analysis. The charts presented hereafter correspond to the simulations for all the study-sets combined.

It is well recognised that internal combustion engines exhibit a varying thermal efficiency depending on the torque and speed demanded. In fact, the engine management strategy for some hybrid vehicles includes the use of a CVT transmission at the engine's output that allows for the operation of the ICE along its best specific fuel consumption (bsfc) line. This is the case for example of the Toyota's Prius which uses a planetary gear set and an electric motor as a CVT transmission to operate the ICE in this manner.

An adequate shifting strategy can also help to constraint the use of the ICE to certain areas of higher efficiencies, as in the case of the 5-speed gearbox employed in CAPTAIN. This can be appreciated in Figure 5.13, which shows all the possible operating points with their corresponding efficiencies for the ICE shown in Figure 4.3 (page 111). In Figure 5.13, the smaller region marked with red dots, corresponds to the possible operating points as constrained by the shifting strategy (which is the area delimited by the red and green lines in Figure 4.3). The operating points for an ideal operation (bsfc line) are also shown in the figure. It is important to note that higher power demands correspond to areas of higher ICE efficiency especially with an appropriate shifting strategy.

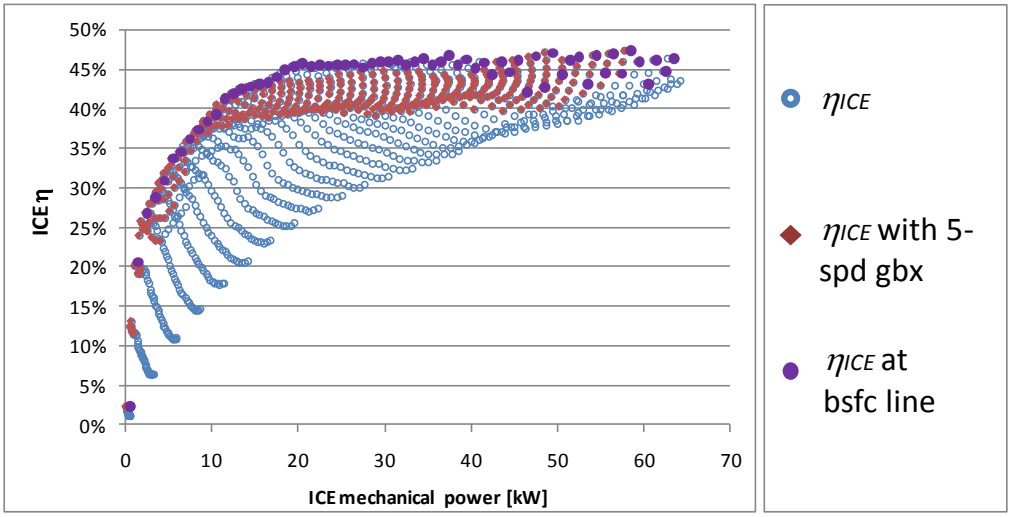

Figure 5.13 Thermal efficiency versus developed mechanical power for the ICE presented in Figure 4.3. The blue markers represent the possible operating area of the ICE, the red markers represent the area of operation when applying a shifting strategy with a 5-speed gearbox, and the purple markers represent the line of bsfc achievable with a CVT transmission.

Referring back to the vehicle effectiveness equation 5.1, it is worth noting that the minimum energy required to drive the vehicle (numerator) is not affected by road topology as long as the net gain in potential energy for the whole cycle is zero (as is the case for the road topologies used in this study). The denominator in equation 5.1 is a measure of the energy developed by the ICE and of the efficiency by which it is produced, and it can be expressed as

$$Energy\ content\ of\ used\ fuel = \frac{\bar{P}_{ICE} * \%ON_{ICE} * duration\ of\ cycle}{\bar{\eta}_{ICE}} \tag{5.2}$$

where $\bar{P}_{ICE}$ is the average mechanical power developed by the engine and given by

$$\bar{P}_{ICE} = \frac{Total\ Energy\ develoed\ by\ ICE}{Total\ time\ the\ ICE\ is\ ON}$$

and where $\bar{\eta}_{ICE}$ is the average thermal efficiency of the ICE for the whole drive cycle, and $\%ON_{ICE}$ is the percentage of time that the engine is ON for the duration of the cycle.

We can then use these elements to generate a factor related to vehicle effectiveness and fuel consumption:

$$f = \frac{\bar{\eta}_{ICE}}{\bar{P}_{ICE} * \%ON_{ICE}} \tag{5.3}$$

Plotting this factor against vehicle effectiveness for all the *ideal-parallel-hybrid vehicle* cases simulated in section 5.2 results in a linear relationship for each drive cycle as shown in Figure 5.14.

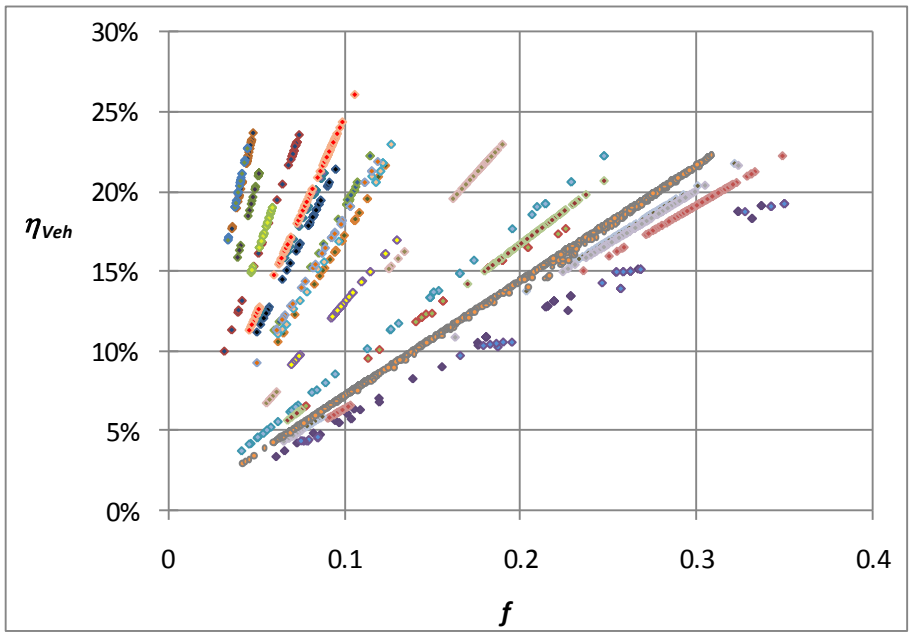

Figure 5.14 Plot showing the linear relationship between the factor defined in equation (5.3) and vehicle effectiveness. Each line corresponds to a different drive cycle, and the slope is the minimum average power required to drive the vehicle.

In Figure 5.14, each line represents a different drive cycle, where the slope can be shown to be equal to the ratio of the minimum energy required to drive the vehicle over the duration of the cycle (or the average power that the car would require if it was driven by an ideal powertrain).

Although this positive and linear relationship is expected, it sheds light on the elements that might be necessary on control strategies to improve vehicle effectiveness. The relationship that each of these elements holds with factor *f* will now be presented. Plots (a) through (d) in Figure 5.15 show these relationships for the *ideal-parallel-hybrid vehicle* with a limitless energy reservoir capacity. Plot (a) demonstrates an inverse relationship between vehicle effectiveness and the percentage of periods that the ICE is on. This is expected as a less frequent use of the engine is associated with less fuel usage. Plot (b) shows a positive relationship between vehicle and ICE efficiency which is expected as well. Plot (c) requires further explanation as the relationship, clearly positive, might be counterintuitive. This plot shows how the effectiveness of the vehicle increases with higher average power developed by the ICE. Clearly higher ICE power goes in hand with higher fuel usage, however it is being

developed at higher ICE efficiencies, This was shown in Figure 5.13, and is confirmed with plot (d) in Figure 5.15, which shows the average engine efficiency against the average power developed by the ICE (for each of the cases simulated and over the whole cycle).

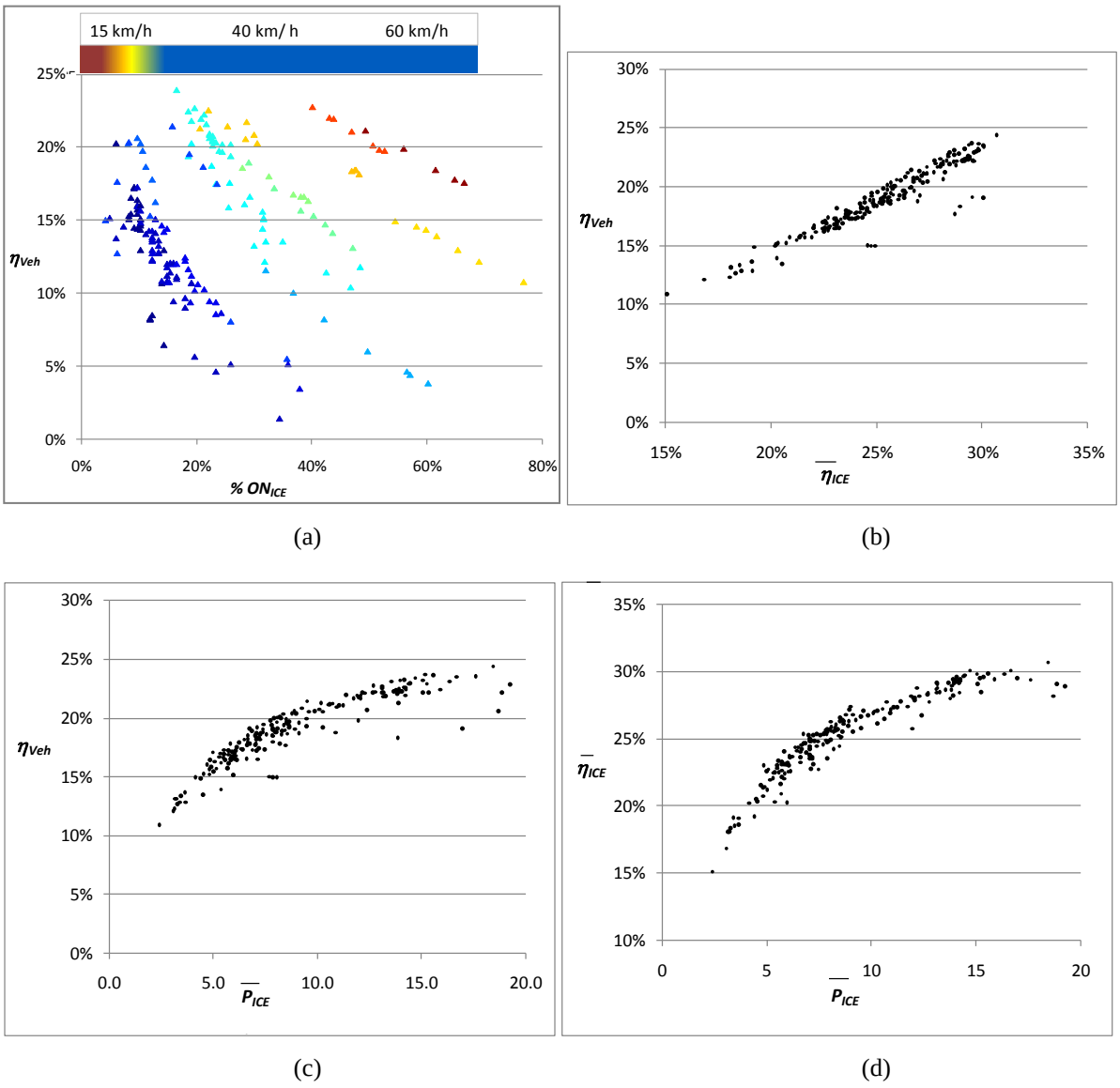

Figure 5.15 The plots in this figure correspond to the simulations of the *ideal-parallel-hybrid vehicle* with a limitless energy reservoir capacity for all the study-sets. Plot (a) shows an inverse relationship between vehicle effectiveness and the percentage of periods the ICE is on. The colour scale shows the relationship that the average velocity for the cycle holds. Plot (b) shows an expected positive relationship between vehicle effectiveness and average efficiency of the ICE for the whole cycle. In plot (c) vehicle effectiveness exhibits a positive relationship with average power developed by the ICE which is explained by a higher engine efficiency at these conditions which can be appreciated in plot (d).

The strong correlation between these variables and vehicle effectiveness decreases as the energy capacity of the energy reservoir is decreased (this is shown in Figure 5.16). However, the relationship between factor f and vehicle effectiveness is maintained, as is the

relationship between mechanical power produced by the ICE and its efficiency (plot (d) in Figure 5.16).

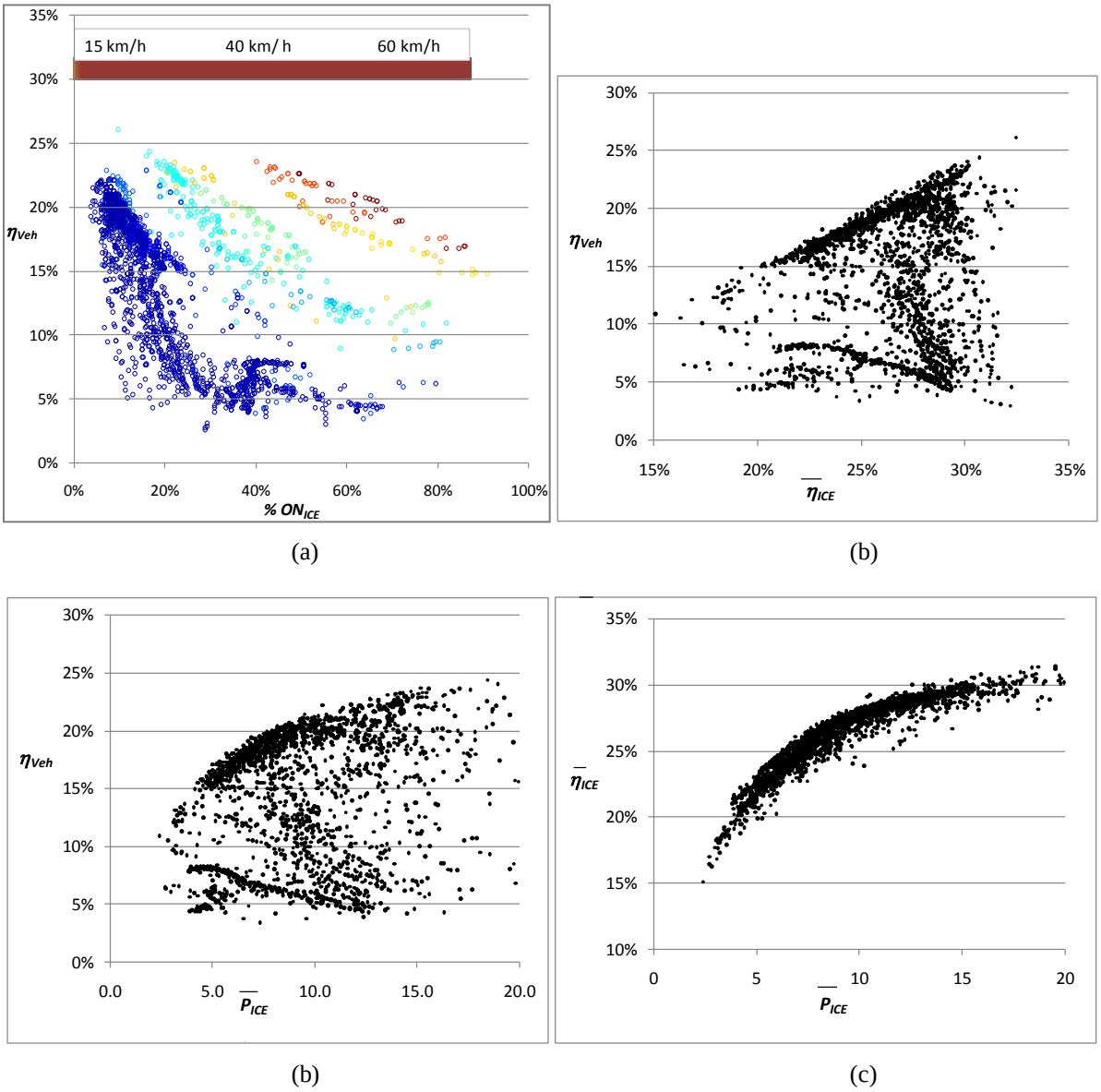

Figure 5.16 The plots in this figure correspond to the simulations of the *ideal-parallel-hybrid vehicle* including all energy reservoir capacities for all the study-sets. Referring back to the plots shown in Figure 5.15, the inverse relationship between vehicle effectiveness and the percentage of periods the ICE is on is maintained (plot (a) above), but the relationships shown in plots (b) and (c) are lost. The relationship between ICE efficiency and average power produced is independent of the hybrid powertrain and is thus maintained for all the cases (plot (d)).

Therefore, the interpretation that can be given to factor f is that higher powertrain efficiencies (and thus higher fuel economy) are best accomplished by a hybrid strategy demanding higher power from the ICE but less frequently. A control strategy developed on a qualitative assessment of factor f is presented in the next section.

5.4. Anticipatory control strategy

Section 4.6.3 briefly touched on the possibility of the development of control strategies for hybrid vehicles that exploit knowledge of future road and traffic conditions. Such control strategies could use its predictions of conditions ahead to choose how and when to use the energy stored in the hybrid's energy reservoir with the aim of increasing the powertrain's effectiveness in delivering either higher power of fuel economy.

A practical implementation of such a control strategy has limitations, but it is far from inconceivable. Advances in telemetry have allowed for the commercialisation of systems that give drivers real-time knowledge of the traffic ahead based on information gathered from portable devices (i.e. mobile phones and GPS devices) [95]. This technology along with route planning can reliably predict the traffic and road topology conditions that the driver is likely to encounter. Furthermore an intelligent control system capable of learning the driving habits of the vehicle's chauffeur could use this information to further adjust its control strategy.

To demonstrate this potential, a control strategy was implemented in CAPTAIN. This strategy was termed *anticipatory control strategy* and its aim is to discriminate when to deliver power from the energy reservoir with the specific aim of improving fuel economy.

The algorithm works by 'looking ahead' into the next consecutive time steps with vehicle power demand (accelerating or cruising episodes) and ranking the time steps from the ones with the lowest to the highest energy demand. The algorithm then maximises the amount of time that the ICE is turned off by allocating the available energy in the reservoir to the time steps with the lowest energy demand until all the energy available in the reservoir has been allocated.

This strategy has two effects linked with the factor f discussed in the previous section. First the ICE is turned off for longer periods, and when it is used it is done at higher power demands where the efficiency of the ICE is higher.

The effect of such a control strategy can be explained with a brief example that uses the same *ideal-parallel-hybrid vehicle* as before, but with two different control strategies: the *blind control strategy* used in the previous analyses (and explained in section 4.6.3), and the *anticipatory control strategy*, and where the energy reservoir starts completely depleted.

Plots (a) and (b) in Figure 5.17 compare how each strategy allocates the energy available in the reservoir. Plot (a) corresponds to the *blind control strategy* and plot (b) to the *anticipatory control strategy*. Each plot shows a segment of the UDC cycle (Figure 4.2 (a) on page 106) corresponding to the periods between seconds 118 to 156. The energy required by the vehicle for each one second time step is shown in blue columns, the energy delivered by the reservoir during the time step is shown in red columns, and the energy available in the reservoir is shown with a green line. The energy available at $t = 118$ sec is the almost the same for both cases (49 kJ and 50 kJ for the *blind* and *anticipatory* control strategies respectively). In the *blind control strategy* shown in plot (a), this energy is used continuously until the reservoir is depleted, which it does in 14 consecutive seconds for the 6 periods that follow second 125, in order to deliver it to the 12 periods that follow second 144.

The effect of the *anticipatory control strategy* is reflected in the fuel economy of the hybrid vehicle which shows an improvement of 15% compared to the one achieved with the *blind control strategy*.

It is important to note that this particular cycle is well suited for this implementation of the *anticipatory control strategy* in CAPTAIN as the algorithm used 'looks ahead' only for consecutive periods of positive vehicle power demand. Thus a drive cycle with a higher frequency of accelerating and braking events has less time steps from which to discriminate against. For example the same analysis on the UDDS cycle which shows a more aggressive driving pattern (Figure 4.2 (b) on page 106), produces a lower (but still significant) fuel economy improvement of 4%.

Although the analysis of this control strategy was performed on the *ideal-parallel-hybrid vehicle*, real hybrid vehicles could also find substantial advantages from the application of an anticipatory control strategy.

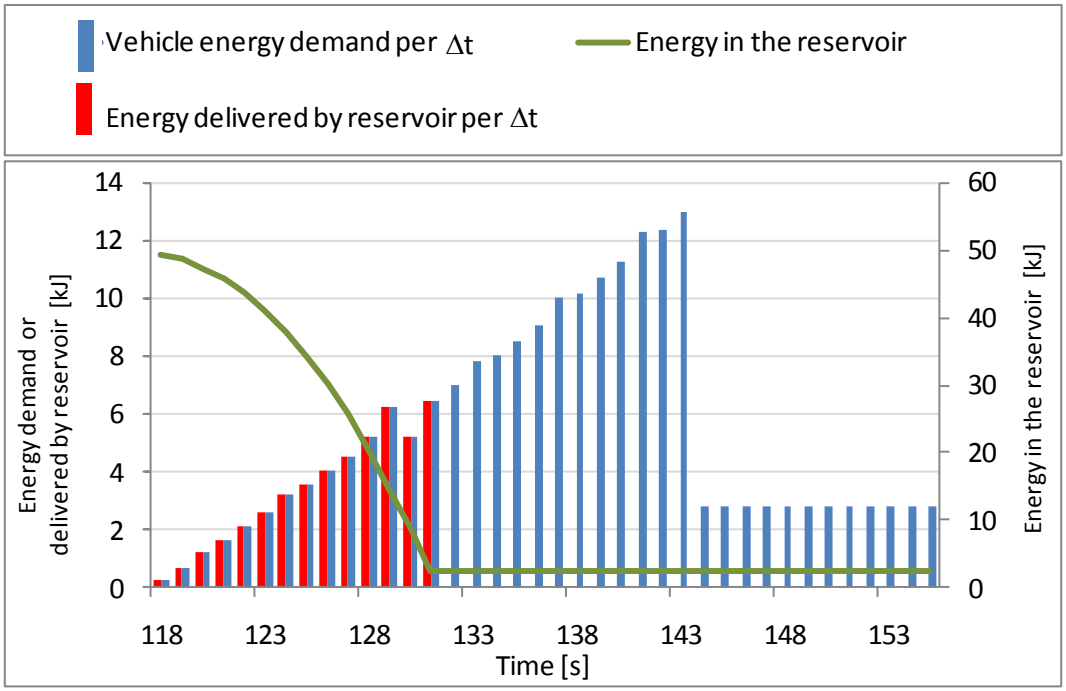

(a)

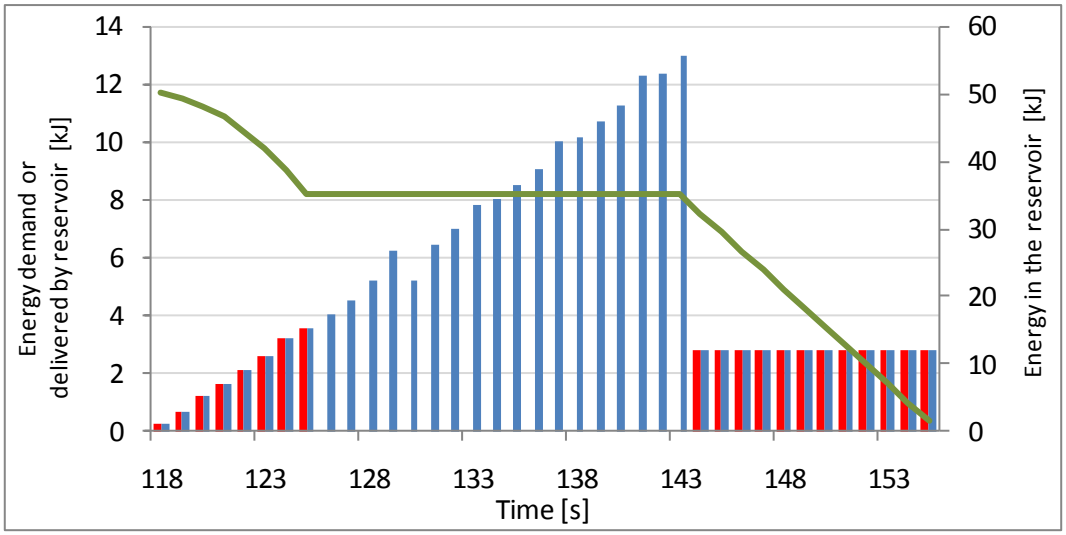

(b)

Figure 5.17 The plots above correspond to a section of the UDC cycle that exhibits a period of constant acceleration followed by a cruising period. The blue columns represent the energy demanded by the vehicle for each time step, the red columns are the energy delivered by the energy reservoir and the green line is the energy stored in the reservoir. Plot (a) corresponds to the application of the *blind control strategy* and plot (b) to the application of the *anticipatory control strategy*. A comparison of the plots shows that the reservoir is used for six more periods with the application of the *anticipatory control strategy* allowing the ICE to be turned off for longer.

5.5. Fuel Economy Potential for Hybrid Vehicles Summary

This chapter has presented thorough analyses on factors that affect vehicle effectiveness. Avoiding the use of the ICE has been identified as a key strategy in improving fuel economy and the potential benefits of an "anticipatory" control strategy that minimises its use have also been demonstrated. The different effect that road topology has on conventional and hybrid vehicles has been shown, and the importance of the energy capacity of the hybrid reservoir has been shown.

The main findings presented in this chapter can best be summarised by reviewing the first two figures presented in this chapter which show how energy is spent in the *conventional vehicle* as it follows the UDC cycle. The examination of these figures established that vehicle effectiveness was only 5.7% which was the result of operating the ICE continuously and at a low efficiency (16%).

A similar analysis for the *ideal-parallel-hybrid vehicle* using the *anticipatory control strategy* over the same driving conditions produces a stark contrast (see Figure 5.18). The energy spent in accelerating the vehicle is reused, which saves a considerable amount of energy (177 kJ). However the highest energy savings come from minimising the use of the ICE having the final effect of reducing the fuel needed by the *ideal-parallel-hybrid vehicle* to only a quarter of what is needed for the *conventional vehicle*. This results in a much higher vehicle effectiveness for the *ideal-parallel-hybrid vehicle* of 22% with an average ICE efficiency of 26%.

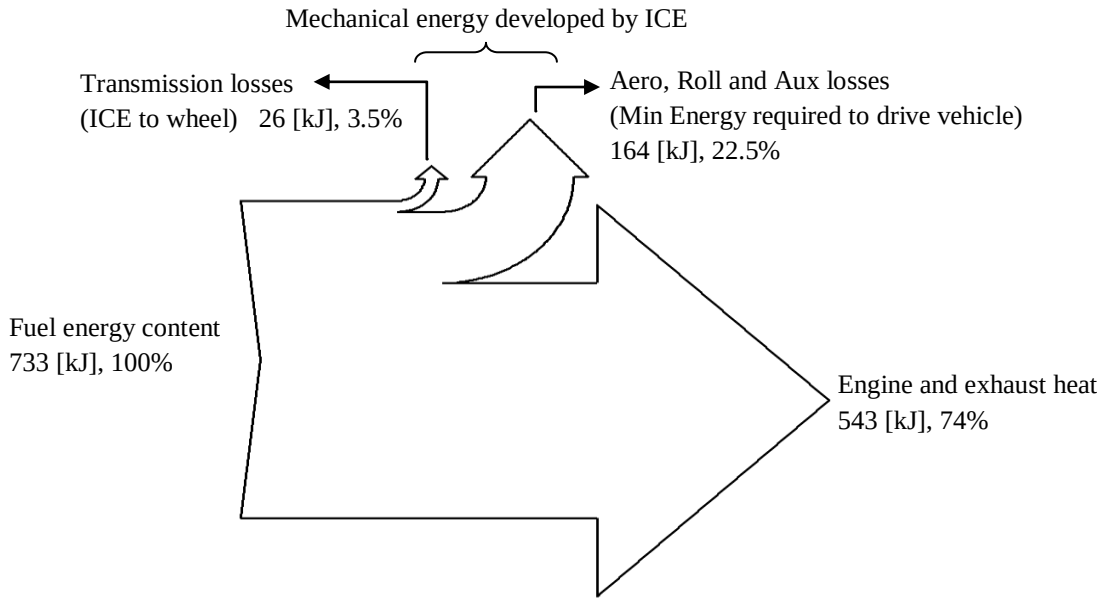

Figure 5.18 Energy flow through the *ideal-parallel-hybrid vehicle* from fuel to wheels, for the same conditions as the conventional vehicle presented in section 4.3, The contrast with Figure 5.1 and Figure 5.2 is quite interesting as it can be appreciated that the largest energy saving comes from a substantial decrease in fuel usage, which is possible by the powering of the vehicle through the reutilisation of the inertial energy of the vehicle.

6. ANALYSIS OF CONTINUOUSLY VARIABLE TRANSMISSIONS INCORPORATING FLYWHEELS

This chapter will present a series of analyses studying the use of CVT transmissions in hybrid vehicles incorporating flywheels.

Given the wide variability of transmissions and flywheels found in the literature survey (section 2.1.2), the analysis presented in section 6.2 will describe the effect that changing the inertia of the flywheel will have on the kinematics and performance of the transmission.

Section 6.3 of the present chapter will use the methodology on power split transmissions presented in section 3.4 to dimension a number of transmissions delivering different speed ratios with some of these operating with no power recirculation and some with positive power recirculation in the variator branch. In section 3.4, a discussion of the trade-offs involved in changing this power split ratio has already been discussed. The analysis presented in section 6.3 will study how these trade-offs will operate in a transmission incorporating a flywheel.

The discussion up to section 6.4 should have established a basic understanding of how CVT transmissions and in particular power split transmission can be used in hybrid vehicles incorporating flywheels. Section 6.4 will present a brief discussion on how the ratio coverage and performance of a hybrid vehicle may be increased with the introduction of transmissions permitting more than one regime and a simple analysis using a variator-only CVT transmission with a two-speed gearbox in series will be used to illustrate this point.

In section 6.5 a table comparing the performance of the CVT powertrains discussed throughout this thesis is presented. It does not provide a definite comparison between powertrains but it is offered as a general guide on the relative performance that could be expected with these specific transmission designs.

6.1. Common nomenclature for the analyses of this chapter

Figure 6.1 presents a schematic diagram for the hybrid-vehicle powertrain. It is important to draw a distinction between the two clearly marked areas, where the *CVT transmission* can consist of any of the transmissions discussed in Chapter 3 (Variator, PGS or power split transmission), and where the *Hybrid transmission* includes the *CVT transmission* as well as all the fixed gears between the flywheel and the wheel of the vehicle as shown in the figure.

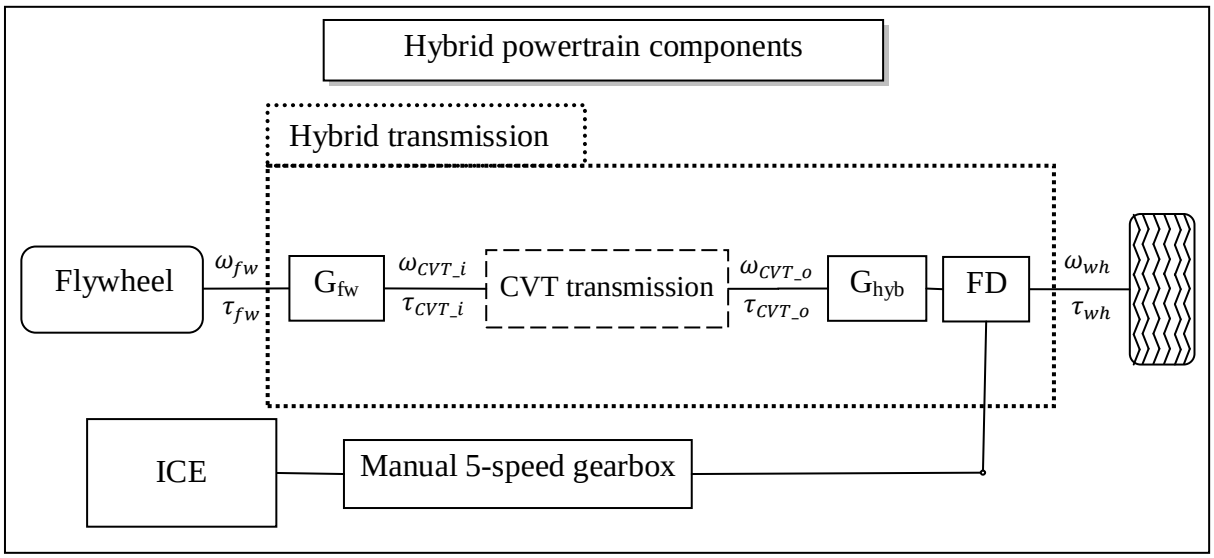

Figure 6.1 Schematic diagram showing the components common to all hybrid powertrains along with the relevant nomenclature.

With reference to

Figure 6.1 and using equation (3.1), a *hybrid transmission ratio* can be written as

$$r_h = \frac{\omega_{wh}}{\omega_{fw}} \tag{6.1}$$

and a *CVT transmission ratio* as

$$r_{CVT} = \frac{\omega_{CVT\_o}}{\omega_{CVT\_i}} \tag{6.2}$$

Using equation (3.5) first introduced in section 3.4.2, the *hybrid transmission normalised ratio coverage* can be written as

$$C_{h\_r} = \frac{r_{h(V_{\max})} - r_{h(V_{\min})}}{r_{h(V_{\max})}} \tag{6.3}$$

As the speed variability in the hybrid transmission is given by the CVT section, the ratio coverage of the hybrid transmission and CVT section is the same, namely $C_{h\_r} = C_{CVT\_r}$. It is important to remember (as discussed in section 3.4.2) that the ratio coverage for the CVT transmission (C_{CVT_r}) may be different to that of the variator (C_{Var}, equation (3.10)) and should not be confused.

The simulations presented in this chapter use the vehicle parameters presented in Table 4.2 and unless otherwise specified the UDC drive cycle presented in section 4.2.1 is used. Different hybrid powertrains are used, but the same control strategy (4.6.3) and engine management (4.6.4) is employed for all powertrains. Variator power ratings may vary, but the same ratio limits are used $0.4 \leq V \leq 2.5$ giving a normalised ratio coverage $C_{Var} = 0.84$. The PGS power rating is also allowed to vary, but its ratio is kept constant at $R_p = 0.78$. This value was chosen as it can be accomplished by a single stage PGS. Nevertheless, the ratio of the PGS is irrelevant for the studies of PS-CVT presented in this chapter as any equivalent kinematic design of these transmissions can be accomplished for any ratio as proven in section 3.4.

For all the analyses, simulations are repeated adjusting the initial state of charge of the energy reservoir until the initial and final values are the same in order to get a real potential fuel economy.

It is also worth remembering (from section 3.2) that the modes of operation are referred to as RB for regenerative braking, FA for flywheel assisted acceleration, and N for neutral operation (when the hybrid system is neither in RB nor FA mode).

6.2. Effect of flywheel size on the kinematics and performance of Flywheel-hybrid powertrains

In section 2.4.3 the effect that changing the inertia of the flywheel would have on its acceleration and torque for a given input power was discussed. It was shown that for two different flywheels with inertias I_{fw_1} and I_{fw_2}, the ratio of their torques followed the relationship $\tau_{fw\_2}/\tau_{fw\_1} = \sqrt{I_{fw\_2}/I_{fw\_1}}$ (equation (2.9)) and that the ratio of their angular acceleration was given by $\alpha_{fw\_2}/\alpha_{fw\_1} = \sqrt{I_{fw\_1}/I_{fw\_2}}$ (equation (2.8)). This latter relationship can also be applied to flywheel speed,

$$\frac{\omega_{fw\_2}}{\omega_{fw\_1}} = \sqrt{\frac{I_{fw\_1}}{I_{fw\_2}}} \tag{6.4}$$

The effect that this relationship may have on the transmission becomes evident on inspection of equations (6.1) and (6.4), where it can be seen that for the same vehicle speed (same ω_{wh}), the hybrid transmission ratio must change with changes in the flywheel's inertia. This rate of change can be written by combining these equations as

$$\frac{r_{h_2}}{r_{h_1}} = \sqrt{\frac{I_{fw_2}}{I_{fw_1}}} \tag{6.5}$$

This behaviour was corroborated by using CAPTAIN to test the performance of a f*lywheel-hybrid powertrain* under various inertias and transmission ratios designs. A defined powertrain design was used to provide a simulation with a base vehicle performance (measured in fuel economy), and a sweep of simulations with varying flywheel inertias was carried out in discrete steps with the aim of achieving the same vehicle performance regardless of the torques and speeds of the hybrid transmission components.

The base simulation consisted of a hybrid vehicle following the UDC cycle with a PS-CVT powertrain with normalised ratio coverage $C_{h\_r} = 0.78$ and a flywheel with inertia $I_{fw} = 0.014$ kg m^2. Under these conditions the transmission operates with a power split with no recirculation as the normalised ratio coverage of the transmission is less than that of the variator.

The simulation sweep was carried considering ten different flywheel inertias with range $0.014 \leq I_{fw} \leq 0.635$ [kg m^2], where its dimensional ratio (radius over length) are chosen to provide the lightest flywheel with the lowest angular momentum as described in section 2.4.7, this means that the flywheel's mass will increase linearly with the increase in inertia. The minimum design transmission ratio $r_{h(V_{\min})}$ for each simulation was calculated by using equation (6.5) and the original values used for the base case. The maximum design transmission ratio $r_{h(V_{\max})}$ was adjusted to always provide the same C_{h_r} value. The gearing of the PS-CVT transmission was sized according to the methodology presented in 3.4.3 assuming a PGS ratio $R_p = 0.78$. Performance of the powertrain depends in part on the efficiency of the components and the weight they add to the vehicle. To correct for these factors, the system was initially modelled ignoring the efficiencies of the variator and PGS as well as the losses of the flywheel and the weight of all components.

The predicted fuel economy for all the cases of the simulation sweep was the same as for the base case (32 km/l) as was the average power received (4.88 kW) and delivered (2.52 kW) by the flywheel as shown in Figure 6.2. These averages are calculated over the periods when the flywheel is either receiving or delivering energy. Although the same amount of energy is received and delivered for the whole cycle, the average power is different as the system is more frequently used during RB mode than FA mode.

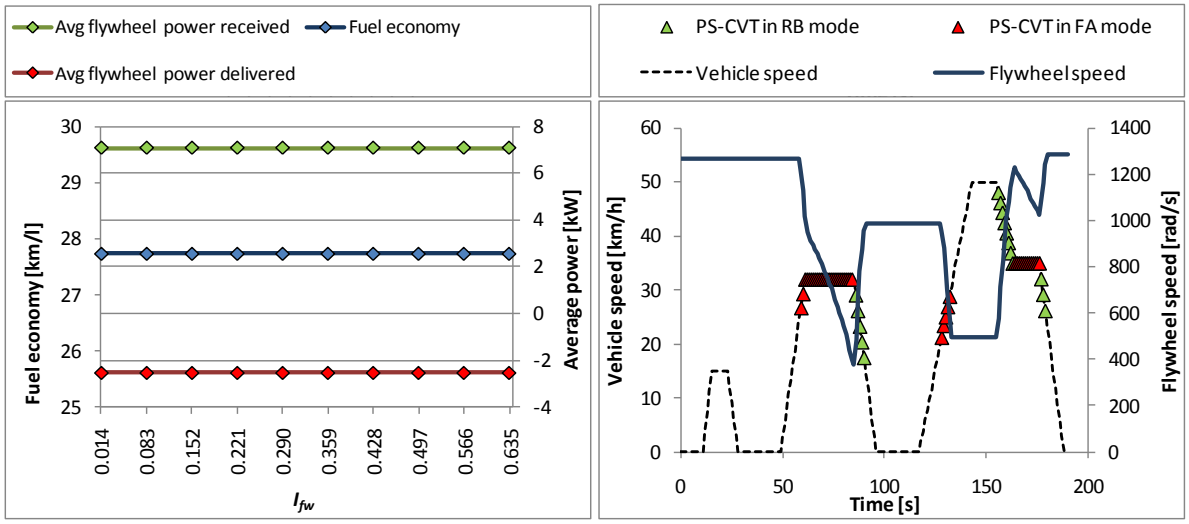

(a) (b)

Figure 6.2 Plot (a) shows the fuel economy achieved by the hybrid vehicle for all flywheel inertias for a lossless hybrid transmission. Average power received and delivered by the vehicle also remains constant.
Plot (b) shows the first 200 seconds of the UDC cycle for the simulation with inertia $I_{fw} = 0.083$. This plot illustrates the operation of the PS-CVT transmission and is the same for all the inertias investigated.

As expected, the average speed and torque of the flywheel change with its inertia. Plot (a) in Figure 6.3 shows the average torque and angular speeds experienced by the flywheel for the ten simulations as well as the predicted values obtained by using equations (2.9) and (6.4), showing excellent agreement. Plot (b) in the same figure shows the corresponding average torque and angular speed for the variator along with the predicted values which were obtained using the same method as for the flywheel.

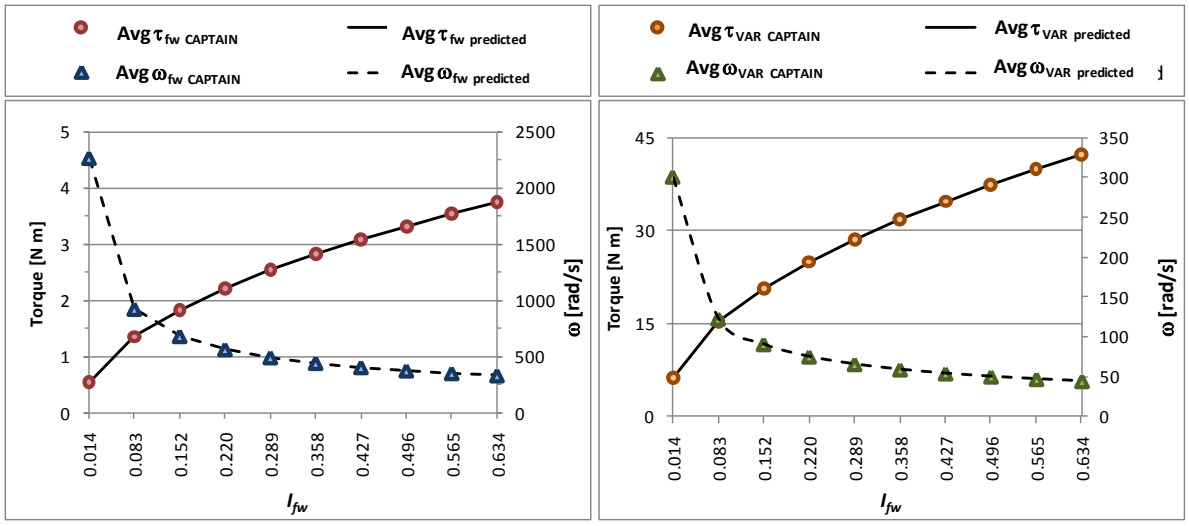

(a) (b)

Figure 6.3 With the system neglecting the efficiencies and weight of the components, plot (a) shows the average torques and angular speeds achieved by the flywheel in the simulations as the inertia of the flywheel changes, as well as the predicted values obtained using equations (2.9) and (6.4). Plot (b) shows the corresponding average torques and angular speeds of the variator and its predicted values obtained using the same relationships as for the flywheel.

The significance of these relationships is that they show that kinematically equivalent transmissions can be designed with different flywheel inertias as long as the design transmission ratios are adjusted accordingly. In the design methodology used in this example, the transmission ratio limits were defined for the whole hybrid transmission (as shown in Figure 6.1) and its components were sized in order to accomplish them. This means that the values of the fixed ratios G_{fw}, G_{hyb} or FD can be adjusted to provide any combination of torque and speed desired in the components of the CVT transmission (including the variator and PGS) regardless of the hybrid transmission kinematic design and the torques and speed values of the flywheel.

When the efficiencies and weight of the components are taken into account, then the fuel economy predicted by the simulations as well as the operation of the system start to change as well, although the effect in the simulations is almost negligible as appreciated in the magnitudes shown in Figure 6.4. There are a few reasons for this. First, the efficiency maps used for the variator and PGS as shown in section 0 are scaled with the torque and speed rating of the transmission and therefore their efficiency is very similar for all the simulations. Second, flywheel losses are assumed at 3% regardless of flywheel size, and are therefore independent of changes in flywheel area or in drag coefficients brought about by changes in the flywheel's size and speed. Finally, only the added weight of the flywheel's material is taken into account and thus the extra mass of a higher torque transmission is not taken into account, which underestimates total weight.

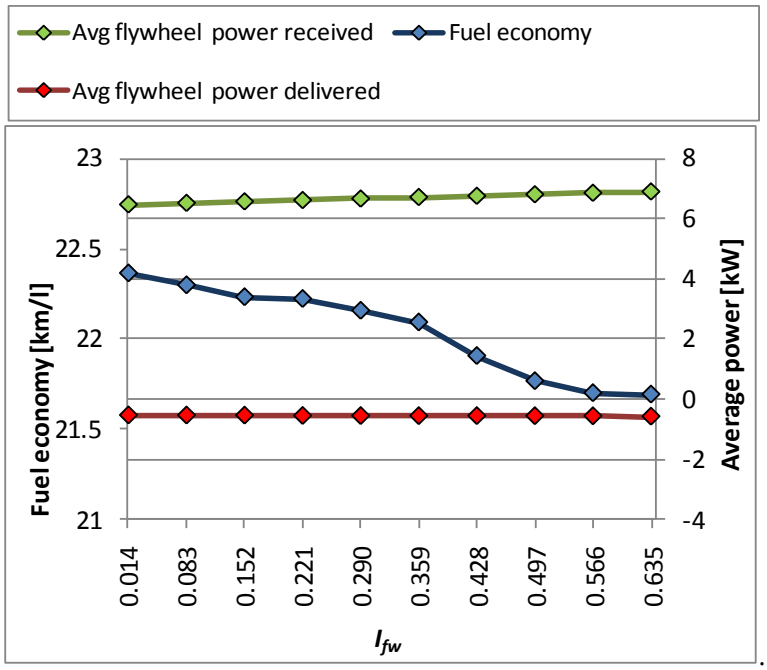

Figure 6.4 Shows the fuel economy achieved by the hybrid vehicle for all flywheel inertias when considering the efficiencies and weight of the components. Average power received and delivered by the vehicle remains fairly constant.

Nevertheless, the operation of the system and the trends for torque and angular speeds will be similar than for the lossless simulations. Plots (a) and (b) in Figure 6.5 still show good agreement between the average torques and speed values obtained from the simulations and the predicted values. The use of more accurate estimations on flywheel losses, added weight and efficiencies of components may cause more deviation between simulated and predicted values, but a reasonable agreement with the scaling equations should be maintained.

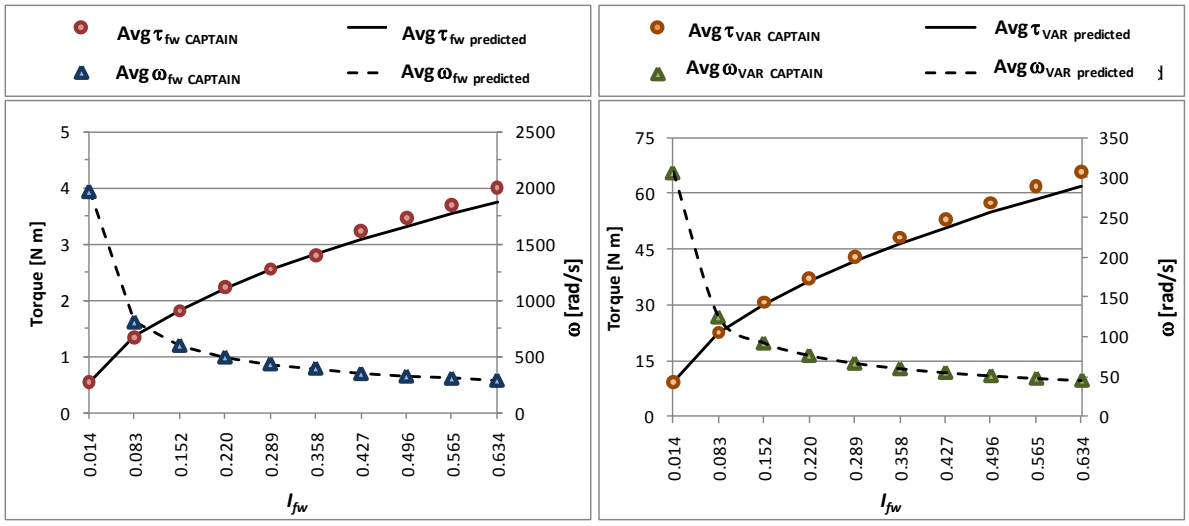

(a) (b)

Figure 6.5 Taking into account the efficiencies and weights of the components, plot (a) shows the average torques and angular speeds achieved by the flywheel in the simulations as the inertia of the flywheel changes with predicted values shown as well. Plot (b) shows the corresponding average torque and angular speed of the variator along with their predicted values.

Therefore the relationships presented in this section can be used as a first approach in setting the size of components, particularly the flywheel. This might be especially useful when the kinematic characteristics and power rating of the flywheel is very different to that of other components of the powertrain. The size of variators and PGS may be expected to be within specific ranges, but a quick glance at the flywheels used in the various research projects presented in section 2.1.2 shows that for flywheels there is a wide array of variability in speeds, torque rating and probably efficiency achieved by these flywheels with no clear design proving indisputable advantage.

6.3. Analysis of a Power-split transmission in a Flywheel-hybrid powertrain

In section 3.4 an extended analysis of PS-CVTs was presented in which the trade-offs involved in the operation of transmissions with varying power splits were identified and discussed. In Table 3.4 the different possible operating modes for the power split were presented according to the design ratio coverage of the transmission and its relation to the ratio coverage of the variator.

Two modes of operation were identified for their potential in achieving the design objectives presented in section 3.1. Operating under no power recirculation suffers from decreased ratio coverage than using a variator directly but offers increased efficiency as only a fraction of the power goes though the variator. Conversely, operating with positive power recirculation offers increased ratio coverage but lower efficiency than the sole use of a variator.

These operating modes as they apply to a hybrid transmission incorporating a flywheel and an ICE are investigated in this section. For this, a sweep of simulations was carried out using CAPTAIN with components as described in section 6.1. The analyses presented in the previous section showed that for a lossless powertrain, the choice of flywheel inertia will have no effect on the kinematic performance of the hybrid powertrain or on the fuel economy achieved by the hybrid vehicle, and that these effects would be small for a powertrain where these losses are considered. Thus the choice of flywheel inertia for the analyses of this section will bear no effect on the performance of the powertrain. Nevertheless, a flywheel inertia must be assumed, and in this case a value $I_{fw} = 0.028$ kg m^2 was chosen as it provides a relatively small sized flywheel which is easier for packing, while maintaining reasonable flywheel maximum speeds of around 20,000 rpm.

The normalised ratio coverage of the transmission was changed in ten discrete steps. Five of them operate with a power split with no power recirculation and their normalised transmission range is $0.66 \leq C_{h\_r} \leq 0.804$. One simulation covers the operation of a variator-only transmission with no power split which occurs when $C_{h\_r} = C_{Var} = 0.84$. The remaining four simulations cover the positive power recirculation operating mode and have a range $0.876 \leq C_{h\_r} \leq 0.984$.

Two sets of sweeps were carried out, one ignoring the efficiencies of the PS-CVT transmission and a second one considering them.

Results when ignoring efficiencies are shown in Figure 6.6Figure 6.6. Plot (a) shows the power split ranges experienced by the transmission as the normalised transmission ratio increases. Power though the variator branch becomes higher than the transmission's input power when the normalised ratio coverage of the PS-CVT exceeds that of the variator at $C_{h\_r} = 0.84$. Plot (b) shows the fuel economy predicted, fraction of vehicle velocity covered by the PS-CVT and the frequency of operation of the PS-CVT. The close relationships that these variables hold is clearly appreciated in the plot. As the normalised ratio coverage of the PS-CVT increases, it is capable of covering a larger portion of the vehicle velocity and as a result it is able to operate more frequently resulting in higher fuel economy. At the highest values of normalised ratio coverage, the PS-CVT is capable of covering almost all the vehicle velocities which results in a stagnation of fuel economy gains. In this first analysis, the highest fuel economy, which occurs at $C_{h\_r} = 0.912$, is 34 km/l which is 10% higher than the fuel economy of the variator only case ($C_{h\_r} = 0.84$) and 73% higher than that of the lowest ratio coverage analysed ($C_{h\_r} = 0.66$). Plot (a) also shows the maximum torque through the variator which augments with increasing levels of power transmitted through it.

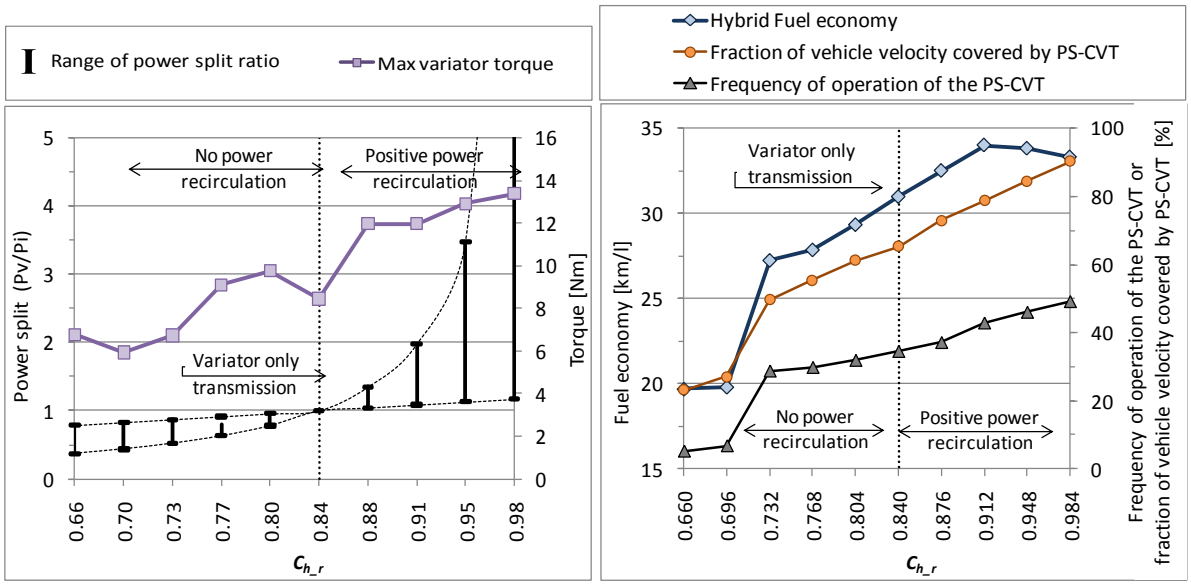

(a) (b)

Figure 6.6 Plot (a) shows the range of power split (i.e. power through the variator) as the normalised ratio coverage is increased. Power split is less than one (i.e. no power recirculation) when the ratio coverage of the transmission is less than that of the variator, and conversely it is greater than one when it is greater. The maximum torque through the variator is also shown.
Plot(b) shows the fuel economy of the hybrid vehicle, frequency of operation of the PS-CVT and fraction of vehicle velocity covered by PS-CVT.

When accounting for the efficiencies of the PGS and variator the PS-CVT exhibits a similar response to the lossless case. This can be appreciated in Figure 6.7. Plot(a) shows that as the

normalised ratio coverage of the PS-CVT increases, the power through its variator branch also increases resulting in higher variator losses and in a higher maximum variator torque. As in the lossless case, as the normalised ratio coverage of the transmission increases so does the fraction of vehicle velocity covered and the frequency of operation of the PS-CVT, although for the latter parameter it does so at a lower rate, as shown in plot (b). The increase in the frequency of utilisation of the PS-CVT results in higher fuel economy, although the gains are more modest than for the lossless case. The highest fuel economy is achieved under conditions of positive power recirculation (occurring at $C_{h\_r} = 0.876$ and $C_{h\_r} = 0.984$) where a gain of 6% is achieved compared to the variator only case and a gain of 26% compared to the lowest ratio coverage analysed ($C_{h\_r} = 0.66$).

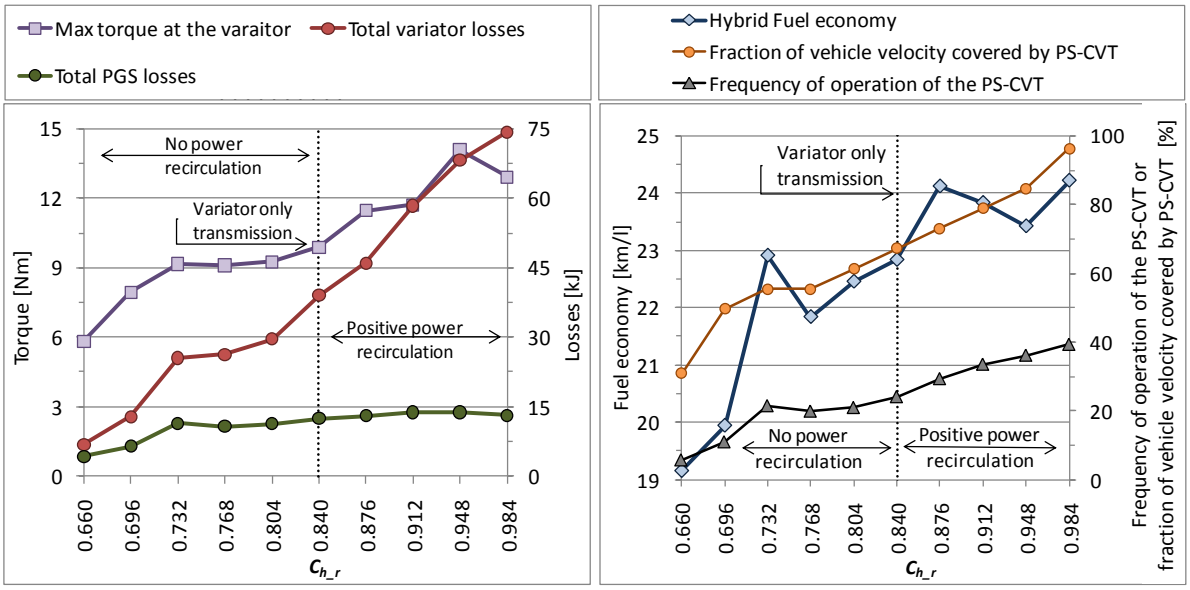

(a) (b)

Figure 6.7 Plot (a) shows the losses of the variator unit and the PGS as the ratio coverage and power split of the transmission increases, showing a detrimental effect on fuel economy. The maximum torque through the variator is also shown,
Plot(b) shows the fuel economy of the hybrid vehicle, frequency of operation of the PS-CVT and fraction of vehicle velocity covered by PS-CVT.

Further results with the UDDS cycle for both scenarios are shown in Appendix F, where the same trends as exhibited for these analyses are found

It is important to note, that the choice of normalised ratio coverage is not enough to fully dimension the PS-CVT. From equation (3.5) it can be seen that its values depend on the maximum and minimum ratio coverage of the transmission ($r_{(V_{\max})}$ and $r_{(V_{\min})}$ repectively). For the simulations presented here, the values for $r_{(V_{\max})}$ and $r_{(V_{\min})}$ selected provide the best fuel economy achievable for each of the normalised ratio coverage studied.

It has been shown that the increase in ratio coverage results in an increase in the fraction of vehicle velocity that the PS-CVT is able to cover. This is better visualised with the plots depicted in Figure 6.8.

These plots show the operation of the PS-CVT during a segment of an urban driving cycle. Plot (c) for instance shows three periods in which the flywheel is used to propel the vehicle (segments 57-63 sec, 127-130 sec and 164-176 sec which are marked with red triangles) and three periods in which the flywheel's energy is regenerated following vehicle braking events (segments 86-90 sec, 156-162 sec and 177-180 sec which are marked with green triangles). In every case, the PS-CVT transmission can only transmit power when the ratio of flywheel speed to vehicle velocity falls within the range that the PS-CVT can cover. Thus in plot (c), even though the flywheel starts charged it can only deliver power once the vehicle reaches a certain speed, which it does in second 57. At this stage, a syncromesh is used to engage a dog cutch and the PS-CVT starts operating, transferring energy from the flywheel to the vehicle. The PS-CVT continues to operate for 6 seconds, lowering the flywheel speed and accelerating the vehicle until the speed ratio between the vehicle and flywheel falls out of the range covered by the PS-CVT and the dog clutch is disengaged. Once the vehicle starts braking with its conventional brakes and the vehicle starts to slow down, the speed ratio between the vehicle and flywheel will again be within the permissible range of the PS-CVT, allowing for the dog clutch to engage and for the PS-CVT to operate transferring energy from the vehicle to the flywheel which slows the vehicle (segment 86-90 sec).

Thus, the plots depicted in Figure 6.8 show an increase in the frequency of operation of the PS-CVT as the normalised normalised ratio coverage of the transmission is increased. It can be seen from plot (f) that further increasing the ratio coverage is unlikely to increase the frequency of utilisation of the PS-CVT as most of the vehicle velocity can be covered with this value of normalised ratio coverage and thus no more significant fuel economy gains can be expected.

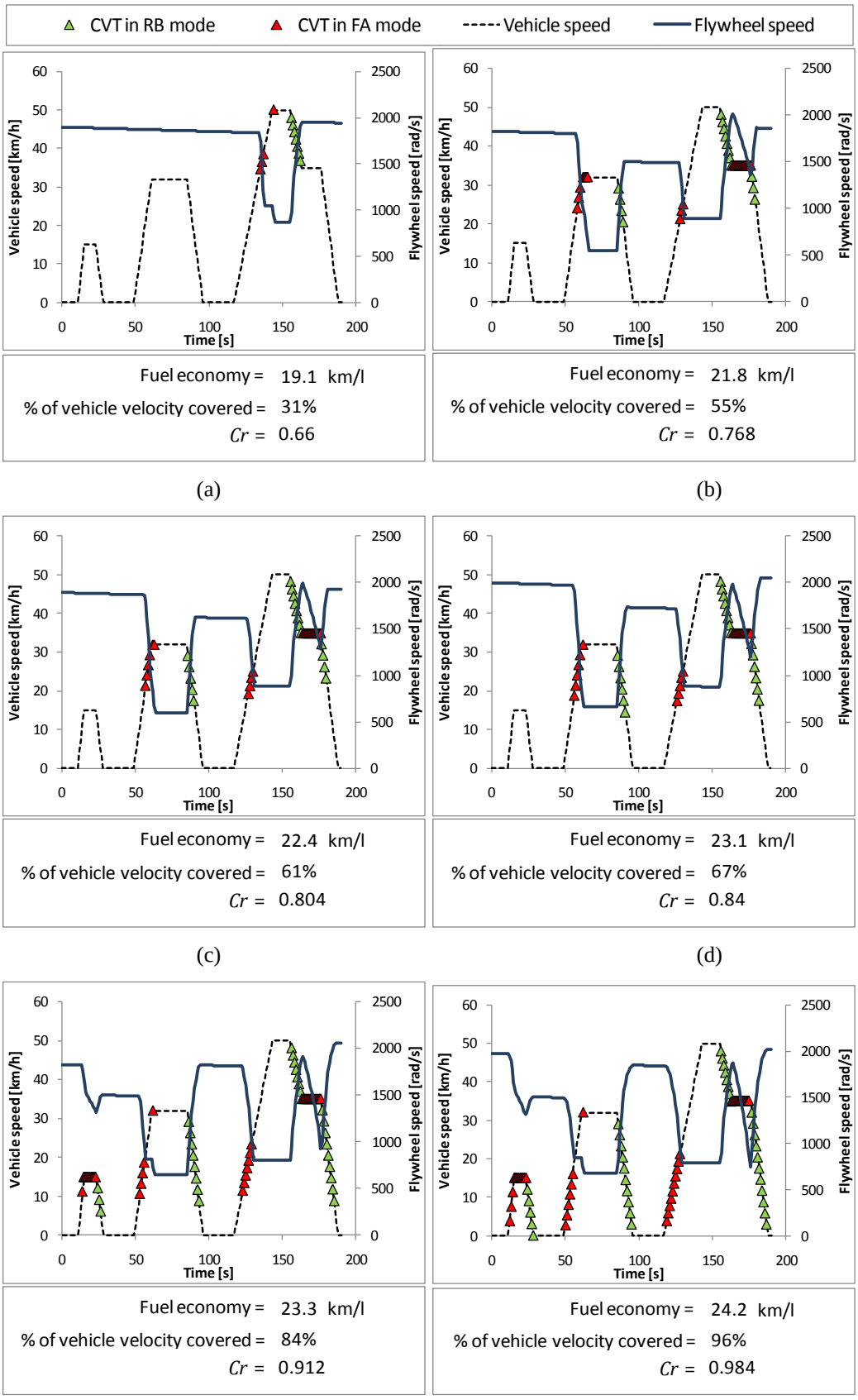

Figure 6.8 Plots (as) through (f) show the operation of the PS-CVT transmission under increasing values of normalised ratio coverage. The values for $r_{(V_{\max})}$ and $r_{(V_{\min})}$ are adjusted to provide the highest fuel economy for a given transmission coverage. The fraction of vehicle velocity covered increases with C_{h_r}.

The analyses of this section have shown that an increase in the normalised transmission ratio coverage increases the fraction of vehicle velocity that can be covered by the transmission resulting in a higher frequency of utilisation of the PS-CVT. The increase in ratio coverage comes at the expense of higher power through the variator reducing the efficiency of the PS-CVT and stagnating fuel economy gains.

The PS-CVT exhibits the highest fuel economy under positive recirculation, but this commands a higher maximum torque through the variator and a transmission design operating under these conditions would require a larger and potentially more expensive variator. With the parameters used in these analyses the use of a variator-only transmission seems the most attractive option as the increase in fuel economy from operating with positive power recirculation with a PS-CVT do not seem to justify the increase in complexity from using a power split transmission.

6.4. Extending the transmission range of a CVT transmission with a discrete gearbox

In the previous section, the extension of the transmission spread of a PS-CVT by increasing power recirculation was analysed. It was found that the increase in power through the variator branch generated losses large enough to offset any increase in the frequency of operation of the hybrid transmission. Another option for extending this range is to use a discrete gearbox in series with a variator. The use of such a transmission was briefly discussed in section 3.3, and has been previously proposed by the University of Wisconsin Group [31].

A discrete gearbox could also be used with other CVT transmissions, such as the PS-CVT transmissions previously discussed, but the packaging of such a transmission is likely to be more challenging. For simplicity, the analysis of this section will only consider the use of a variator. Figure 6.9 shows a schematic diagram of such a transmission, where the *CVT transmission* corresponds to the area marked as such in Figure 6.1

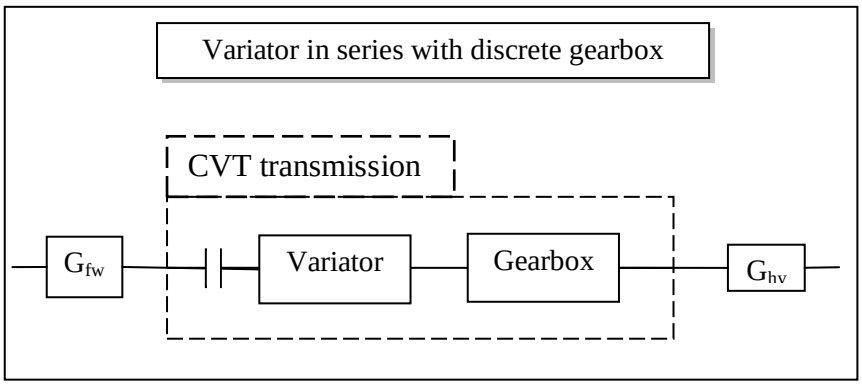

Figure 6.9 Schematic diagram of a CVT transmission consisting of a variator and a two-speed gearbox.

In this transmission, the maximum and minimum *hybrid transmission ratios* attainable, which occur at the speed-ratio limits of the variator V_{max} and V_{min} are given respectively by

$$r_{h(V_{\max})} = FD * G_{hyb} * G_{fw} * G_{gbx\_max} * V_{max} \tag{6.6}$$

and

$$r_{h(V_{\min})} = FD * G_{hyb} * G_{fw} * G_{gbx\_min} * V_{min} \tag{6.7}$$

where FD, G_{hyb},and G_{fw} are gears with fixed speed ratios as shown in Figure 6.1, and where G_{gbx_min} and G_{gbx_min} are the maximum and minimum speed ratios available in the gearbox.

The ratio spread of the transmission as defined by equation (3.4) is given by

$$r_{ht} = \frac{r_{h(V_{\max})}}{r_{h(V_{\min})}} \tag{6.8}$$

For a case with only the variator and no gearbox $r_{ht} = r_{Var}$.

Gear ratios in the gearbox can be sized to provide a continuous ratio for the transmission without overlapping

$$G_{gbx(N)} = G_{gbx(1)} \left(\frac{V_{max}}{V_{min}}\right)^{N-1}$$

where $G_{gbx(N)}$ is the speed gear ratio for the Nth gear. Sizing the gears with this method causes the transmission spread to increase exponentially with the number of gears: $r_{ht} = V_t^N$.

To study the effect of the addition of a gearbox on the performance of a hybrid vehicle, CAPTAIN was used to simulate two different CVT transmissions. One consisting of a variator with no gearbox and another one with an additional two-speed gearbox in series with the variator. This particular setup would not provide a synchronous gear shift, which would be desirable, but is not dissimilar to gear shifting in a conventional gearbox.

Considering first the case with no gearbox, simulations were run with varying minimum *hybrid transmission ratios* $r_{h(V_{\min})}$, which caused the CVT transmission to operate at different vehicle speed ranges. As the transmission spread remains constant ($r_{ht} = r_{Var} = 6.25$), the maximum *hybrid transmission ratio* is obtained with equation (6.8).

Plots (a) though (d) in Figure 6.10 show the operation of the hybrid powertrain for four different minimum *hybrid transmission ratios*. The limited ratio spread of the transmission with no gearbox only allows the transmission to operate within a constrained range of vehicle speeds. As this *hybrid transmission ratio* increases, the vehicle speeds at which the hybrid system operates increase as well. Therefore the operation of such a transmission will be highly dependent on the fixed gears chosen (G_{hyb} and G_{fw}) and on the vehicle velocities of the drive cycle used.

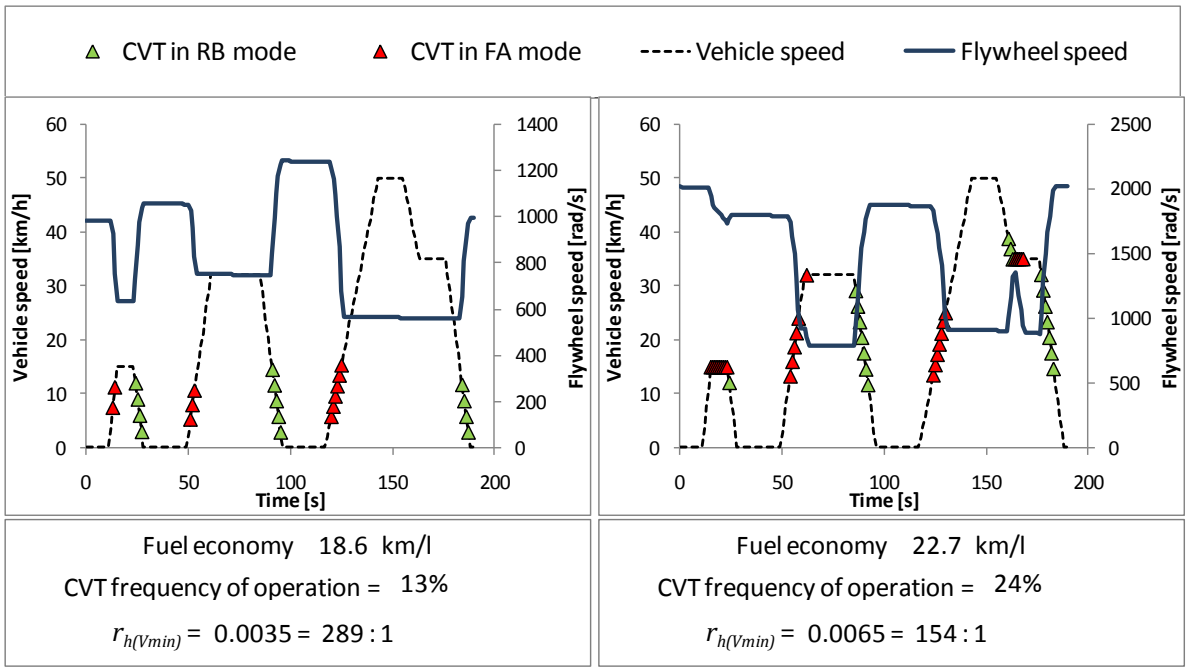

(a) (b)

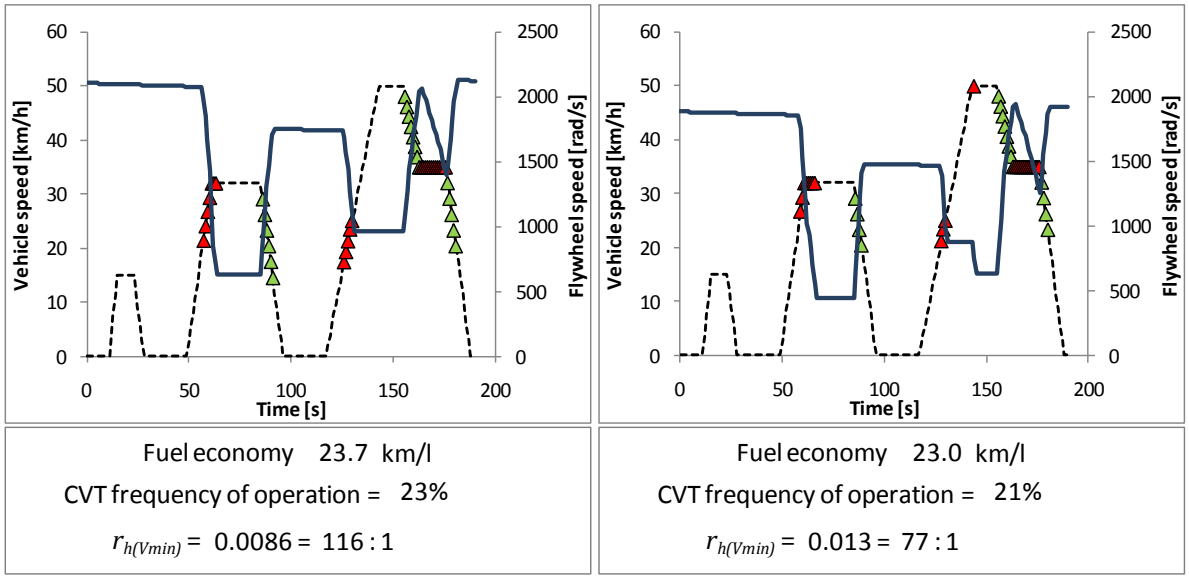

(c) (d)

Figure 6.10 Plots (as) through (d) show the operation of the variator-only transmission with no gearbox for different minimum *hybrid transmission ratios*. The transmission spread is the same for all transmissions, but the minimum and maximum ratios which can be adjusted by varying G_{hyb} and G_{fw}, cause the hybrid system to operate at different vehicle speeds. The limited ratio coverage of the transmission makes it highly sensitive to the choice of fixed gears and drive cycle.

For the case with the two-speed gearbox, the ratio spread will be the square of that of the variator with no gearbox, which for the values used in this analysis becomes $r_{ht} = 39$. Two different minimum *hybrid transmission ratios* were considered for this analysis.

Plot (a) in Figure 6.11, shows a remarkable increase in the range of vehicle velocities over which the CVT transmission is able to operate. This case exhibits an increase in frequency of operation of the CVT transmission of 15% over the powertrain with no gearbox, but the increase in fuel economy is more modest at just under 9%. However, it can be seen that the careful choice of gears G_{hyb} and G_{fw} which determine this minimum ratio, allow the system to operate over a wide range of vehicle speeds that should make this powertrain more effective over a wider range of driving conditions. At the speed ranges shown in plot(a), the CVT transmission could be engaged with the use of a slipping clutch, which is not modelled in this analysis.

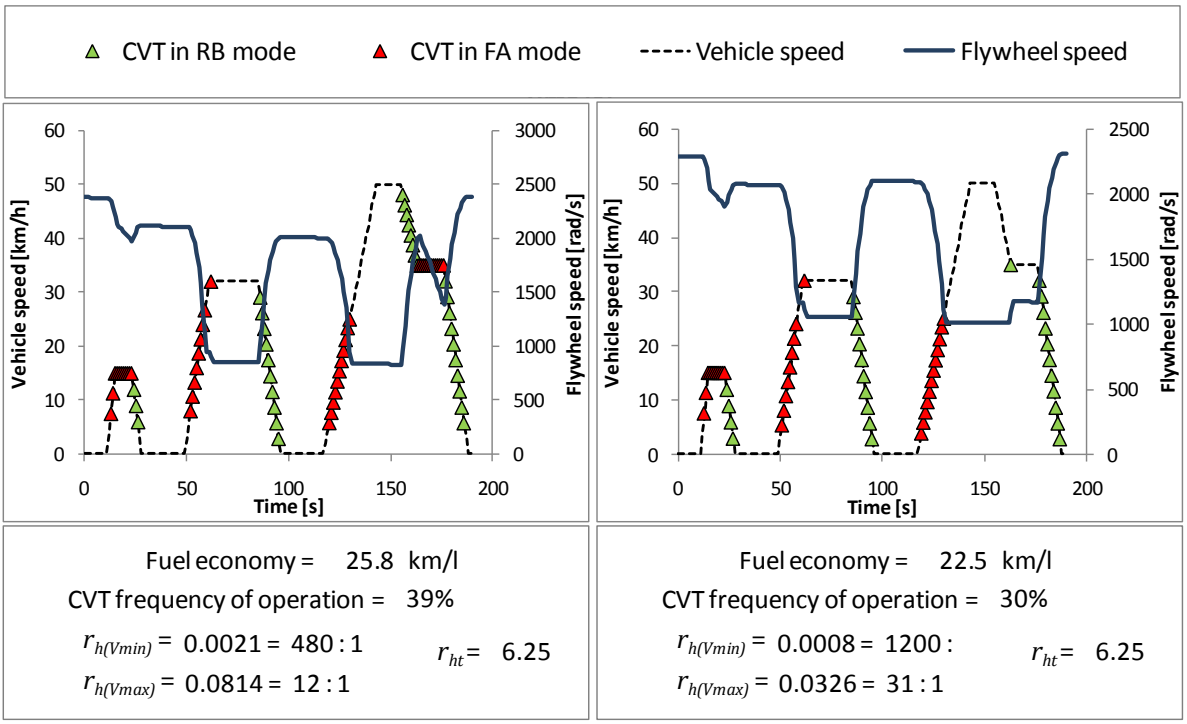

(a) (b)

Figure 6.11 Plots (a) and (b) show the operation of the variator transmission in series with a two-speed gearbox for two different minimum *hybrid transmission ratios*. Plot (a) shows that a careful choice of gear ratios G_{hyb} and G_{fw} (which determine this minimum ratio) results in a system that is able to operate over a wide range of vehicle speeds. Further decreasing the transmission ratio greatly limits the use of the system at higher speeds as seen in plot (b).

Increasing the number of gears available in the gearbox will extend the ratio spread of the CVT transmission even further, however the fuel economy gains will be marginal as the ratio spread of the two-speed gearbox CVT is already capable of covering the vehicle velocities typically encountered in urban driving conditions for the variator used in this analysis.

6.5. Comparison of various CVT transmission using various drive cycles

Several powertrains have been discussed and analysed throughout this thesis. The comparison between these powertrains is not always straightforward. As shown in the previous section, the introduction of regimes give rise to different ratio coverage affecting the effectiveness of these powertrain in delivering better fuel economy, and many multi-regime powertrains that have been proposed for conventional vehicles (some briefly discussed in section 3.6) may be applied in powertrains incorporating flywheels.

Nevertheless, some of the powertrains studied throughout this thesis have shown their potential in reducing fuel consumption and a general comparison is useful. This is presented in the form of a table at the end of this section where the predicted fuel economy and effectiveness (as defined in section 5.1) of several powertrains are presented.

The three *flywheel-hybrid powertrains* simulated are:

A. A PS-CVT with no power recirculation (described and analysed in sections 3.4, 4.6.2 and 6.3).

B. A variator in series with a two-speed gearbox (described and analysed in sections 3.3, 4.6.2 and 6.4).

C. A PGS transmission with brake control (described in sections 3.5 and 4.6.2 and in article [50]).

In addition, three more vehicles were simulated as well to serve as basis over which to compare the performance of the *flywheel-hybrid powertrains*. These are:

D. A conventional vehicle with no hybrid capabilities. (model described in section 4.3).

E. The *Ideal-parallel hybrid vehicle* described in section 4.6.1, which provides the maximum fuel economy attainable for a parallel hybrid vehicle with a lossless hybrid-transmission, limitless capacity of its energy reservoir and the control strategy employed by the *flywheel-hybrid powertrains*. As this model considers a blind control strategy, it does not provide an absolute performance ceiling for a hybrid vehicle, but it does for a hybrid vehicle with the control strategy and engine management used by the *flywheel-hybrid powertrains* of this thesis.

F. An *Ideal-parallel-series hybrid vehicle* with the same lossless, weightlessness and control system as the *Ideal-parallel hybrid vehicle* except that the ICE is operated along its best specific fuel consumption line. This powertrain mimics the behaviour of the Prius that allows the engine to operate at its optimum speed for a given torque demand, and that stores the extra energy in a reservoir for future use (what would be the bank of batteries in the case of the Prius).

G. The *ON/OFF vehicle* described in section 4.4. This vehicle determines the fuel economy arising from simply turning off the engine during idling and braking events. It does not model a start-stop system in detail, but it does serves a guideline for the ideal fuel economy of a vehicle with such an engine management strategy but with no regenerative braking capabilities.

Finally, published data for Toyota´s Prius 2009 third-generation model [96] are presented as well for comparison. However caution is advised when comparing this vehicle, as values for mass, aerodynamic and rolling losses are different to those of the Ford Focus used in the simulations, and as the Prius is a Petrol-hybrid as opposed to the Diesel-hybrid used throughout this thesis. For the Prius, a Diesel equivalent fuel consumption based on the energy developed by the Petrol-Prius is also presented.

The same vehicle (including final drive gear), control strategy and engine management as used throughout the analyses of this thesis are used for all vehicles (all are described in detail in Chapter 4). In addition, the *flywheel-hybrid powertrains* use the same flywheel with $I_{fw} = 0.028$ kg m^2. The components specific to the *flywheel-hybrid powertrains* are shown in Table 6.1.

Table 6.1 Parameter values specific for the *flywheel-hybrid powertrain* components.

Powertrain	C_{hr}	C_{Var}	$r_{h(V_{min})}$	$r_{h(V_{max})}$	r_{ht}	R_p	Gears specific to the powertrain
Brake-only PGS	-(1)	-	-(1)	-(1)	-(1)	0.965	$G_{hyb} = 1:1$ $G_{fw} = 1:1$
PS-CVT	0.72	0.84	0.014 (71:1)	0.051 (20:1)	3.57	0.78	$G_{hyb} = 2.5:1$ $G_{fw} = 2.5:1$ $G_V = 1.9:1$ $G_M - 1.3:1$
Variator with gearbox	0.97	0.84	0.0021 (480:1)	0.0814 (12:1)	39.06	-	$G_{hyb} = 2.5:1$ $G_{fw} = 2.5:1$ $G_{gbx(1)} = 8:1$ $G_{gbx(12} = 1.3:1$

(1) The Brake-only PGS transmission has different transmission spreads for RB and FA modes as described in section 3.5 and cannot be compared directly with the other powertrains.

As in previous analyses, in order to get a more accurate fuel economy prediction, simulations were repeated with the energy reservoir initially charged until there was no net difference between the initial and final SOC of the reservoir. Results for the simulations are shown in Table 6.2 on the next page.

Table 6.2 Fuel economy and vehicle effectiveness for various powertrains over the UDC, EUDC and NEDC cycles.

Powertrain		UDC (City)				EUDC (Highway)				NEDC (Combined)			
		FE [km/l]	η_{veh}	ΔFE over Conv	ΔFE over On/Off	FE [km/l]	η_{veh}	ΔFE over Conv	ΔFE over On/Off	FE [km/l]	η_{veh}	ΔFE over Conv	ΔFE over On/Off
Conventional		13.1	6%	-	-	17.4	15.9%	-	-	16.6	12.4%	-	-
ON/OFF		18.4	8.4%	40%	-	19	17.3%	9%	-	19.6	14.6%	18%	-
Flywheel hybrid powertrains	Brake-only PGS	20.3	9.6%	55%	10%	19.3	17.8%	11%	2%	20.5	15.6%	23%	5%
	PS-CVT	23.3	11%	78%	27%	19.5	18.1%	12%	3%	21.2	16.1%	28%	8%
	Variator with gearbox	25.8	12.2%	97%	40%	21	19.4%	21%	11%	23.4	17.8%	41%	19%
Prius (2009 model) [96]		25.6	-	-	-	27	-	-	-	25.6	-	-	-
Prius (diesel equivalent)		29.7	-	-	-	31.3	-	-	-	29.7	-	-	-
Ideal-parallel-hybrid		43.3	19.8%	231%	135%	24.6	22.4%	41%	29%	30	22.4%	81%	53%
Ideal-parallel-series-hybrid		69.5	31.9%	432%	278%	36.5	33.2%	109%	92%	45.3	33.8%	172%	131%

Looking at the results of the previous table, it is important to take notice on the impressive fuel savings from the ON/OFF vehicle. The importance of having an engine management strategy that avoids the use of the ICE as much as possible has already been demonstrated in the analyses of Chapter 5, and its effect particularly for city driving can be appreciated in the fuel economy achieved by the ON/OFF vehicle.

The *flywheel-hybrid powertrains* employ this engine management strategy and therefore as a minimum, the savings of the ON/OFF vehicle can be expected for these powertrains. The Brake-only PGS powertrain is able to achieve a 10% improvement in fuel economy compared to the ON/OFF vehicle in city driving conditions, however in highway mode its limited ratio coverage limits reduced this improvement to 2%. This powertrain also has an imbalance between its speed ratios covered for RB and FA modes as was shown previously in section 3.5.2, which limits its usage.

Both the PS-CVT and Variator with gearbox powertrains, have better ratio coverage than the Brake-only PGS, and do not suffer from an imbalance in their ratio coverage for RB and FA modes. Their fuel economy improvement over the ON/OFF vehicle for city driving is impressive for both with 27% and 40% respectively. However, the increased ratio coverage of the Variator with gearbox transmission makes a big difference under highway conditions where it is able to operate at higher vehicle speeds, achieving a further 19% fuel economy improvement over the ON/OFF vehicle.

The fuel economy achieved by *the ideal-parallel-hybrid powertrain* demonstrates that there are still many gains to make from improved hybrid powertrains capable of making full use of regenerative braking to further improve the effectiveness of the vehicle, particularly for city driving.

It is interesting to note, that the Prius achieves a higher fuel economy than the *ideal-parallel-hybrid powertrain* for the EUDC cycle, which is a cycle with little opportunities for regeneration and long periods of high velocity. However, the *ideal-parallel-series-hybrid* which optimises the use of the engine, still performs better than the Prius under these conditions.

Finally, remembering the analysis presented in section 5.4, the use of an *anticipatory control strategy* that anticipates future vehicle power demand may further improve the effectiveness of all these vehicles in improving fuel economy and reducing emissions.

6.6. Summary

This chapter presented a number of analyses that used the simulation model presented in Chapter 4 to study the behaviour of various powertrains incorporating flywheels.

In section 6.2 the torque, speed and ratio coverage scaling of the transmission as the flywheel inertia was changed and studied. It was shown that kinematic equivalent transmissions could be designed for flywheels of different inertias, as long as the design ratio coverage of the transmission was scaled accordingly.

Section 6.3 used the methodology presented in section 3.4 on the design of power split transmissions to study a number of powertrains with varying degrees of power splits, including CVTs with and without power recirculation. It was shown that the benefits that could be expected from increased ratio coverage of the transmission were offset by the increase in variator losses as the power through it increased. The PS-CVT with no power recirculation and the variator only transmission were identified as powertrains with a high potential to deliver better fuel economy.

The use of multiple regimes to further increase the ratio coverage of the CVT was finally analysed in section 6.4, where a transmission consisting of a variator in series with a gearbox was simulated. That analysis showed that the increase in ratio coverage substantially increased the frequency of operation of the hybrid powertrain resulting in improved fuel economy. The advantage of this two-regime powertrain was finally demonstrated with the simulations presented in Table 6.2.

7. SUMMARY AND CONCLUSIONS

7.1. Summary of research and contributions

This thesis has presented several analyses on the integration of high-speed flywheels in hybrid vehicles. In Chapter 2 the general characteristics of flywheels were discussed and in particular the challenge of mechanically linking the flywheel with a conventional powertrain was recognised. The use of a continuously variable transmission was identified as essential for this purpose. The application of CVT transmissions in powertrains incorporating flywheels is particularly challenging as the flywheel speed varies with its state of charge. Therefore the ratio spread required for a powertrain incorporating a flywheel is higher than that of a conventional powertrain for which CVT transmissions are better characterised.

It follows that the performance of a vehicle incorporating a flywheel is highly dependent on its transmission. Therefore, an appropriate appraisal of the use of a flywheel as an alternative energy storage device for hybrid vehicles must take into account the transmission. The literature review presented in Chapter 2 revealed many projects, prototypes and ideas, but little fundamental analyses that could be used directly by a designer to make an informed judgment on the choice and sizing of a flywheel and its transmission. Therefore, the characterisation of the performance of some fundamental CVTs and their dependence on flywheel inertia became a main objective of this research.

The variator, planetary gear set, and their combined use in a power split transmission were identified as three fundamental designs that could be used as CVT transmissions in flywheel-powertrains. The analysis on the kinematic behaviour of these components was the objective of Chapter 3. As the fundamental analyses presented are independent on the specific choice of variator technology, the specific actuation mechanisms for specific variators as well as its sources of power losses were not studied.

In Chapter 3, special effort was devoted to the development of a simple and complete methodology that could be used to study and assess the kinematic behaviour of PGS and PS-CVT transmissions.

The analyses of PS-CVTs require special attention, especially when all the possible ways in which a PGS can be connected within the transmission are considered. In the kinematic

analyses of PGS, a planetary ratio is defined according to the relative speed of its gears to aid in the characterisation of the transmission. The treatment of this ratio can be have a significant impact in the complexity of the analysis of transmissions incorporating PGSs. An example of this can be seen in references [73,74], which correspond to two articles from the same institution (Southwest Research Institute) and presented in the same conference. Both articles present derivations of the transmission ratio of PS-CVTs, but their treatment of the planetary ratio leads to the development of twelve different but equivalent expressions, one for each of the possible arrangement of a PGS within a PS-CVT. Furthermore, since a different planetary ratio is chosen in each article, the equations of each article are equivalent but different. If then the torque and speeds of the components are to be analysed, it is easy to see that this approach requires the derivation of a large number of formulas that make it tedious and prone to errors. In [72] White recognised that not assigning branches of the PGS to the kinematic equation describing its transmission (equation (2.16)) leads to a set of equations that can be applied to any PGS configuration within the PS-CVT. The analysis by White can be further developed by using a PS-CVT transmission like the one propose by the Southwest Research Institute articles which can be used to design a transmission with any speed ratio coverage desired (within the practical constraints imposed by gear sizes).

An important contribution of this thesis is the application of White's treatment of the planetary ratio, to the general transmission case proposed by Pohl, Fussner and Singh in [73,74], resulting in a simple methodology (presented in section 3.4) that can be easily applied to design a transmission that can provide any transmission ratio coverage and for which power split, torques and speed of components can be easily predicted for any configuration of PGS branch assignment. Evidence for the simplicity of this approach is found in the analyses of maximum torque and speed through the variator for two different power split designs as shown in section 3.4.5. This methodology was also used in sizing the PS-CVTs that made the simulations incorporating flywheels and presented in sections 6.2 and 6.3 possible.

White's treatment of the planetary ratio was also applied to the PGS-only transmission presented in section 3.5. This approach allowed the analysis of this transmission to be generalised for different PGS branch arrangements, allowing for the identification of transmission limits and PGS configurations over which the PGS-only transmission can

operate. The results of experimental work carried out by the author with Diego-Ayala and reported in [50] were used in section 3.5.3 to confirm the transmission limits predicted.

The fuel economy potential for hybrid vehicles was analysed in Chapter 5. In general, the analyses presented in sections 5.2 and 5.3 confirm the common perception that hybrid vehicles have the most advantage over conventional vehicles in low speed driving conditions and with frequent stops where there is ample opportunity for regenerate braking events to take place. Critically the role that regenerative braking plays in displacing ICE usage was identified as the main source of energy savings for hybrid vehicles. This led to the proposal and analysis of an *anticipatory control strategy* that based on the prediction of future vehicle power demand adjusts the delivery of available energy in the hybrid reservoir to maximise fuel economy. With the implementation of the *anticipatory control strategy* in the *ideal-parallel-hybrid* vehicle, there was an estimated improvement of 15% in fuel economy achieved for an urban drive cycle.

Chapter 5 also presented an analysis comparing the different effect that road gradients have on hybrid and conventional vehicles. The analyses showed as expected, that the fuel economy of conventional vehicles decreases under the presence of road gradients. Interestingly, the analyses also showed that the fuel economy of hybrid vehicles tended to increase under the presence of road gradients, and that this increase was more pronounced as the energy capacity of the energy reservoir was increased. Table 8.4 in Appendix E shows a summary of the performance of both vehicles for the three study cases analysed, where an impressive 85%, 40% and 61% of cases with road gradients presented an improvement in the fuel economy of the *ideal-parallel-hybrid vehicle* over a base case of a road with zero gradients.

In section 3.4 the possibility of designing a power split transmission that allowed for power recirculation to increase its speed ratio coverage was identified. Several PS-CVT transmissions with increasing levels of power recirculation were studied and simulated in section 6.3. The analysis showed that as the power through the variator branch increases, the losses of the whole transmission increased, but also the speed ratio coverage that the transmission can cover. It was found that the increase in ratio coverage tended to compensate the increase in transmission losses even under power recirculation. With the urban drive cycle used and vehicle parameters used in the analysis of section 6.3, the highest fuel economy achieved occurred under conditions of positive power recirculation (both at $C_{h\_r} = 0.876$ and

$C_{h\_r} = 0.984$) where a gain of 6% over the variator only case and a of 26% over a power split transmission with no recirculation ($C_{h\_r} = 0.66$) were estimated.

The analysis of section 6.4 showed however, that a more effective way of increasing the fuel economy of a hybrid vehicle with a CVT transmission is to introduce a multi-regime operation. Such a transmission was accomplished with the use of a two-speed gearbox in series with a variator. The system used the same variator spread as the one used previously in the PS-CVT studies presented in chapter 6.3. Using this two-regime operation, a fuel economy of 25.8 km/l was estimated, which is 6.6% higher than the highest one accomplished with power recirculation. Furthermore, the power going through the variator is lower and thus the required size of the variator is also lower.

A final examination of Table 6.2, in section 6.5 confirms that from the powertrains analysed in Chapter 6, the variator with gearbox transmission is the most effective powertrain in increasing the ratio coverage and fuel economy of the hybrid vehicle. Under urban driving conditions this powertrain shows a similar performance to the 2009 Prius model, but under highway driving conditions where the vehicle operates for longer at steady speeds, the superior steady state engine management of the Prius allows it to achieve a better fuel economy than even the *ideal-parallel-hybrid*. In this last case, a better benchmark is the *ideal-parallel-series-hybrid* which also uses the engine intermittently as little as possible, but crucially as well, it operates the engine along its best specific fuel consumption line. For the UDC (city), EUDC (highway) and NEDC (combined) cycles the fuel economy estimates for the *ideal-parallel-series-hybrid* were 69.5 km/l, 36.5 km/l and 45.3 km/l respectively.

7.2. Recommendation for future work

This thesis has analysed the performance of various fundamental combinations of components giving rise to continuously variable transmissions. However it was recognised that the introduction of more regimes of operation is likely to be the most effective way in which to increase the speed ratio coverage of flywheel-powertrians. Future research could focus on the development of different multi-regime transmissions or on the study of existing multi-regime proposals as they would apply to flywheel-powertrains, with an emphasis on their practicality and the ease by which the shift between different regimes takes place (using synchronous shifting for example).

Investigation of possible transmissions can be concurrent to the research of practical flywheel designs. However, it is the opinion of the author that the building of a detailed transmission and any experimental validation should be avoided until a practical and effective combination of flywheel and transmission is identified.

In the analyses presented in this thesis, the use of petrol fuels as primary energy source for vehicles has been assumed. In these types of vehicles, the largest fuel economy benefits from the use of a flywheel arise from the same source as for hybrid electric vehicles, which is from using (or reusing) energy to displace the use of the ICE particularly when its efficiency is lowest.

There is an important potential use of flywheels in electric vehicles as well though, and although it could function on the same principles of charging through regenerative braking and assisting in acceleration, its most important benefits would not be reflected in its energy savings but in the cost of the system. Under these conditions the flywheel would serve as a power buffer limiting the charging and discharging current and cycles of the batteries, which are highly determinant of their service life. Considering the great fraction of the cost that batteries have in electric vehicles (as discussed in section 2.3.1), the use of a flywheel could have an important impact in lowering the cost of electric vehicles.

The study of such an alternative is thus recommended for future research. A main focus should be a proper estimation of the increase in service life that could be expected of batteries as the commercial success of such a hybrid would be highly dependent on its reduced cost. Electrical flywheels could be also be considered for this application, but the mechanical flywheel is likely to have a lower cost.

BIBLIOGRAPHY

[1] "Joint science academies' statement on growth and responsibility: sustainability, energy efficiency and climate protection" Available: http://www.royalsoc.ac.uk. Accessed: 24 August 2007

[2] *Technical Summary. In: Climate Change 2007: The Physical Science Basis. Contribution of Working Group I to the Fourth Assessment Report of the Intergovernmental Panel on Climate Change.*, Cambridge University Press, Cambridge, United Kingdom and New York, NY, USA, .

[3] "World Resources Institute" Available: http://www.wri.org/ Accessed: 12 Novemeber 2007.

[4] "Kyoto Protocol" Available: http://unfccc.int/kyoto_protocol. Accessed: 24 August 2007

[5] Environmental Protection Agency, *Endangerment and Cause or Contribute Findings for Greenhouse Gases Under Section 202(a) of the Clean Air Act*, Environmental Protection Agency, 2009.

[6] "Carbon Dioxide Information Analysis Center" Available: http://cdiac.ornl.gov/.

[7] European Commission: Directorate-General for Energy and Transport, *Energy & Transport in Figures 2006. Part 2 : Energy*, European Commission: Directorate-General for Energy and Transport, 2006.

[8] World Business Council for Sustainable Development., *Mobility 2030 : meeting the challenges to sustainability.*, [Conches-Geneva Switzerland]: World Business Council for Sustainable Development, 2004.

[9] European Parliament and Council, "Directive 2005/55/EC of the European Parliament and of the Council," *Official Journal of the European Union L 350*, 2005, pp. 1-163.

[10] Commission of the European Communities, *Results of the review of the Community Strategy to reduce CO2 emissions from passenger cars and light-commercial vehicles: Communication from the Commission to the Council and the European Parliament. COM (2007)19 final*, 2007.

[11] European Automobile Manufacturers Association, "European automobile manufacturers demand cost-effective policy to cut carbon emissions from cars | ACEA."

[12] C.W. Jones, S. Friedman, M. Andre, R.D. Mesiti, M. Audinet, and A. Kunzer, "HYZEM: a joint approach towards understanding hybrid vehicle introduction into Europe," *IMechE Conference on Combustion Engines and Hybrid Vehicles*, Technical paper C529/015: IMechE, 1998.

[13] P.J. Crutzen, A.R. Mosier, K.A. Smith, and W. Winiwarter, "N2O release from agro-biofuel production negates global warming reduction by replacing fossil fuels," *Atmospheric Chemistry & Physics Discussions*, vol. 7, Aug. 2007, pp. 11191-11205.

[14] J. Tuckman, "Tortilla Turmoil," *The Guardian*, Aug. 2007.

[15] J. Ziegler, *Report of the Special Rapporteur on the right to food to the General Assembly*, United Nations, 2007.

[16] P. INVESTIRE NETWORK, *Investigation on Storage Technologies for Intermittent Renewable Energies: Evaluation and recommended R&D strategy. ST6: Flywheel*, Uk: Investire Network, 2003.

[17] B. Knight, "Better Mileage Now," *Scientific American*, vol. 302, 2010, pp. 50-55.

[18] J. King, *The King Review: Index*, London: UK HM Treasury, 2007.

[19] Department of Transportation. National Highway Traffic Safety Administration, *Average Fuel Economy Standards. Passenger Cars and Light Trucks. Model Years 2011-2015. Notice of Proposed Rulemaking.*, Department of Transportation. National Highway Traffic Safety Administration, .
[20] B. Berman, "HybridCars.com - History of Hybrid Vehicles" Available: http://www.hybridcars.com/history/history-of-hybrid-vehicles.html. Accessed: 27 August 2007
[21] M. Bellis, "History of Electric Vehicles," *About.com* Available: http://inventors.about.com/library/weekly/aacarselectric2a.htm. Accessed: 27 August 2007
[22] B. Berman, "HybridCars.com - 2006 US Sales" Available: Accessed: 27 August 2007 http://www.hybridcars.com/market-dashboard/dec06-us-sales.html.
[23] V. Rao and J. Saini, "Green Car Congress: Hybrid Electric Vehicles Slowly But Surely Gain Market Share in Europe" Available: http://www.greencarcongress.com/2007/03/hybrid_electric.html#more. Accessed: 28 August 2007
[24] Vehicle Certification Agency, "Vehicle Certification Agency" Available: http://www.vcacarfueldata.org.uk. Accessed: 24 August 2007
[25] R.F. Post, "A new look at an old idea - The electromechanical battery," *Science and Technology Review ; PBD: Apr 1996*, 1996, pp. pp. 12-20 ; PL:
[26] FIA, *2009 Formula One Technical Regulations*.
[27] R.C. Clerk, "The utilization of flywheel energy," *SAE Proceedings 1964*.
[28] K.L. McLallin, R.H. Jansen, J. Fausz, and R.D. Bauer, "Aerospace Flywheel Technology Development for IPACS Applications," Savannah, GA, United States: National Aeronautics and Space Administration, 2001.
[29] R. Cardenas, R. Pena, M. Perez, J. Clare, G. Asher, and P. Wheeler, "Power smoothing using a flywheel driven by a switched reluctance machine," *Ieee Transactions on Industrial Electronics*, vol. 53, 2006, pp. 1086-1093.
[30] N.H. Beachley, C. Anscomb, and C.R. Burrows, "Evaluation of split-path extended range continuously-variable transmissions for automotive applications," *Journal of the Franklin Institute*, vol. 317, Apr. 1984, pp. 235-262.
[31] N.H. Beachley, A.A. Frank, F.S. Jamzadeh, M. Nohr, and T. Volz, "Continuously-variable transmission designs for flywheel-hybrid automobiles," *Proc. Int. Symp. Gearing Power Transmissions*, Tokyo: 1981, pp. 393–398.
[32] A.A. Frank, N.H. Beachley, T.C. Hausenbauer, and P. Ting, "The fuel efficiency potential of a flywheel hybrid vehicle for urban driving," 1976, pp. 17-24.
[33] N.A. Schilke, A.O. DeHart, L.O. Hewko, C.C. Matthews, D.J. Pozniak, and S.M. Rohde, "The design of an engine-flywheel hybrid drive system for a passenger car," *ARCHIVE: Proceedings of the Institution of Mechanical Engineers, Part D: Transport Engineering 1984-1988 (vols 198-202)*, vol. 200, 1986, pp. 231-248.
[34] P. Dietrich, M.K. Eberle, and H.U. Hörler, "Results of the ETH-Hybrid III-vehicle project and outlook," *International Congress and Exposition*, SAE paper 1999-01-0920: SAE, 1999.
[35] S.W. Shen and F.E. Veldpaus, "Analysis and control of a flywheel hybrid vehicular powertrain," *IEEE Transactions on Control Systems Technology*, vol. 12, 2004, pp. 645-660.
[36] M.M. Flynn, J.J. Zierer, and R.C. Thompson, "Performance testing of a vehicular flywheel energy system," *SAE transactions*, vol. 114, 2005, pp. 840–847.

[37] R.J. Hayes, D. Weeks, M. Flynn, J.H. Beno, A. Guenin, and J. Zierer, "Design and Performance Testing of An Advanced Integrated Power System With Flywheel Energy Storage," 2003.
[38] B. Murphy, D. Bresie, and J. Beno, "Bearing Loads in a Vehicular Flywheel Battery," *SAE Special Publications*, Detroit, Mi, US: SAE, 1997.
[39] J. Miller, L.B. Sibley, and J. Wohlgemuth, *Investigation of Synergy Between Electrochemical Capacitors, Flywheels, and Batteries in Hybrid Energy Storage for PV Systems*, Sandia National Laboratories (SNL), Albuquerque, NM, and Livermore, CA, 1999.
[40] *Flywheel Energy Storage - Federal Technology Alert*, Washington, DC., USA: Federal Energy Management Program, 2003.
[41] "NASA P&PO: Aerospace Flywheel Development" Available: http://space-power.grc.nasa.gov/ppo/projects/flywheel/. Accessed: 17 October 2007
[42] "Williams Hybrid Power" Available: http://www.williamshybridpower.com/. Accessed: 30 April 2010
[43] C. Brockbank and D. Cross, "Mechanical Hybrid System Comprising a Flywheel and CVT for Motorsport & Mainstream Automotive Applications," *SAE 2009 World Congress & Exhibition*, Detroit, MI, USA: 2009.
[44] C. Brockbank and C. Greenwood, "Fuel Economy Benefits of a Flywheel & CVT Based Mechanical Hybrid for City Bus and Commercial Vehicle Applications," *SAE 2009 Commercial Vehicle Engineering Congress & Exhibition*, Rosemont, IL, US: Soc, 2009.
[45] D. Cross and J. Hilton, "High Speed Flywheel Based Hybrid Systems for Low Carbon Vehicles Flybrid Systems LLP," *Hybrid and Eco-Friendly Vehicle Conference, 2008. IET HEVC 2008*, Warwick University, UK: The Institution of Engineering and Technology, 2008.
[46] S. Shah, "The Design and Development of a High Speed Composite Flywheel for Hybrid Vehicles," Imperial College, Department of Mechanical Engineering, 2006.
[47] U. Diego-Ayala, "An investigation into hybrid power trains for vehicles with regenerative braking," Imperial College, Department of Mechanical Engineering, 2007.
[48] U. Diego-Ayala, P. Martinez-Gonzalez, and K.R. Pullen, "A Simple Mechanical Transmission System for Hybrid Vehicles Incorporating a Flywheel," *Hybrid and Eco-Friendly Vehicle Conference, 2008. IET HEVC 2008*, Warwick University, UK: The Institution of Engineering and Technology, 2008.
[49] S. Shah, U. Diego-Ayala, and K.R. Pullen, "Mechanical Energy Storage Hybrid Vehicle – Simulation and Life Cycle Costs," *European ELE- Drive Transportation Conference and Exhibition*, Estoril, Portugal: 2004.
[50] U. Diego-Ayala, P. Martinez-Gonzalez, N. McGlashan, and K.R. Pullen, "The mechanical hybrid vehicle: an investigation of a flywheel-based vehicular regenerative energy capture system," *Proceedings of the Institution of Mechanical Engineers, Part D: Journal of Automobile Engineering*, vol. 222, Nov. 2008, pp. 1903-1917.
[51] M. Millikin, "Green Car Congress" Available: http://www.greencarcongress.com/2004/08/a_short_field_g.html. Accessed: 28 September 2007
[52] "Hybrid vehicle drivetrain - Wikipedia, the free encyclopedia" Available: http://en.wikipedia.org/wiki/Hybrid_vehicle_drivetrain. Accessed: 29 September 2007
[53] M. Anderman, "The challenge to fulfill electrical power requirements of advanced vehicles," *Journal of Power Sources*, vol. 127, Mar. 2004, pp. 2-7.
[54] K.T. Chau and Y.S. Wong, "Hybridization of energy sources in electric vehicles," *Energy Conversion and Management*, vol. 42, 2001, pp. 1059-1069.

[55] E. Karden, P. Shinn, P. Bostock, J. Cunningham, E. Schoultz, and D. Kok, "Requirements for future automotive batteries - a snapshot," *Journal of Power Sources*, vol. 144, Jun. 2005, pp. 505-512.
[56] E. Karden, S. Ploumen, B. Fricke, T. Miller, and K. Snyder, "Energy storage devices for future hybrid electric vehicles," *Journal of Power Sources*, vol. 168, May. 2007, pp. 2-11.
[57] M. Soria, F. Trinidad, J. Lacadena, J. Valenciano, and G. Arce, "Spiral wound valve-regulated lead-acid batteries for hybrid vehicles," *Journal of Power Sources*, vol. In Press, Corrected Proof, 2007.
[58] "GoodCleanTech" Available: http://www.goodcleantech.com/2007/09/mercedes_beats_competition_in.php. Accessed: 29 September 2007
[59] I. Buchmann, "Battery University" Available: http://www.batteryuniversity.com. Accessed: 26 September 2007
[60] J. Alson, B. Ellies, and D. Ganss, *Interim Report: New Powertrain Technologies and Their Projected Costs*, U.S. Environmental Protection Agency, 2005.
[61] "Official Honda Web Site" Available: http://automobiles.honda.com. Accessed: 22 July 2009
[62] "Lexus RX 400h - Wikipedia, the free encyclopedia" Available: http://en.wikipedia.org/wiki/Lexus_RX_400h. Accessed: 29 September 2007
[63] "Toyota Highlander - Wikipedia, the free encyclopedia" Available: http://en.wikipedia.org/wiki/Toyota_Kluger. Accessed: 29 September 2007
[64] "VAG - The smart move. - The Company" Available: http://en.vag.de/?pid=102. Accessed: 9 October 2007
[65] L. Pan, "Advanced electric buses on trial in Shanghai" Available: http://www.gov.cn/english/2007-06/11/content_644057.htm. Accessed: 9 October 2007
[66] G. Genta, *Kinetic Energy Storage: Theory and Practice of Advanced Flywheel Systems*, London: Butterworths, 1985.
[67] J.J. Zierer, J.H. Beno, R.J. Hayes, J.L. Strubhar, R.C. Thompson, and T. Pak, "Design and Proof Testing of a Composite Containment System for Mobile Applications," *2004 SAE World Congress*, Detroit, Mi, US: 2004.
[68] "Flybrid Systems - Containment" Available: http://www.flybridsystems.com/containment.html. Accessed: 10 May 2010
[69] A.T. McDonald, "Simplified Gyrodynamics of Road Vehicles with High-Energy Flywheels," *Flywheel Technology Symposium*, Scottsdale, Arizona: Lawrence Livermore National Laboratories, 1980, pp. 240-258.
[70] K.R. Pullen and C.W. Ellis, "Kinetic energy storage for vehicles," *Hybrid Vehicle Conference, IET The Institution of Engineering and Technology, 2006*, 2006, pp. 91 - 108.
[71] D. Hofmann, "Gearing for high speed motors," *IEE Seminar Digests*, vol. 1997, Jan. 1997, p. 3.
[72] G. White, "Properties of Differential Transmissions," *The Engineer*, vol. 224, 1967, pp. 105–111.
[73] B. Pohl, "Cvt Split Power Transmissions, a Configuration Versus Performance Study With An Emphasis on the Hydromechanical Type," *Transmission and Driveline Systems Symposium 2002*, Detroit, Mi, US: 2002.
[74] D. Fussner and Y. Singh, "Development of Single Stage Input Coupled Split Power Transmission Arrangements and Their Characteristics," *Transmission and Driveline Systems Symposium 2002*, Detroit, Mi, US: 2002.
[75] M. Fischetti, "No More Gears," *Scientific American*, vol. 294, Jan. 2006, pp. 92-93.

[76] “HowStuffWorks "Pulley-based CVTs"” Available: http://auto.howstuffworks.com/cvt2.htm. Accessed: 11 May 2010
[77] S. Akehurst, N.D. Vaughan, D.A. Parker, and D. Simner, “Modelling of loss mechanisms in a pushing metal V-belt continuously variable transmission. Part 1: torque losses due to band friction,” *Proceedings of the Institution of Mechanical Engineers, Part D: Journal of Automobile Engineering*, vol. 218, 2004, pp. 1269-1281.
[78] “Bosch” Available: http://www.cvt.bosch.com/. Accessed: 11 May 2010
[79] S. Akehurst, N.D. Vaughan, D.A. Parker, and D. Simner, “Modelling of loss mechanisms in a pushing metal V-belt continuously variable transmission. Part 2: pulley deflection losses and total torque loss validation,” *Proceedings of the Institution of Mechanical Engineers, Part D: Journal of Automobile Engineering*, vol. 218, 2004, pp. 1295-1306.
[80] S. Akehurst, N.D. Vaughan, D.A. Parker, and D. Simner, “Modelling of loss mechanisms in a pushing metal V-belt continuously variable transmission. Part 3: belt slip losses,” *Proceedings of the Institution of Mechanical Engineers, Part D: Journal of Automobile Engineering*, vol. 218, 2004, pp. 1283-1293.
[81] R. Fuchs, Y. Hasuda, and I. James, “Full Toroidal Ivt Variator Dynamics,” *Transmission and Driveline Systems Symposium 2002*, Detroit, Mi, US: 2002.
[82] S. Akehurst, C.J. Brace, N.D. Vaughan, and P.J. Milner, “Performance Investigations of a Novel Rolling Traction Cvt,” *Transmission & Driveline Systems Symposium*, Detroit, Mi, US: 2001.
[83] “Imperial College -Tribology Research” Available: http://www3.imperial.ac.uk/tribology. Accessed: 11 May 2010
[84] G. Mantriota, “Power split continuously variable transmission systems with high efficiency,” *Proceedings of the Institution of Mechanical Engineers, Part D: Journal of Automobile Engineering*, vol. 215, Jan. 2001, pp. 357-358.
[85] G. Mantriota, “Theoretical and experimental study of a power split continuously variable transmission system Part 1,” *Proceedings of the Institution of Mechanical Engineers, Part D: Journal of Automobile Engineering*, vol. 215, Jan. 2001, pp. 837-850.
[86] C. Brockbank, “Multi regime full-toroidal IVT for high torque and commercial vehicle applications” Available: http://www.torotrak.com/. Accessed: 9 April 2010
[87] K. Wipke, M. Cuddy, and S. Burch, “ADVISOR 2.1: a user-friendly advanced powertrain simulation using a combined backward/forward approach,” *IEEE Trans. Veh. Technol.*, vol. 48, 1999, pp. 1751-1761.
[88] R.D. Senger, M.A. Merkle, and D.J. Nelson, “Validation of ADVISOR as a simulation tool for a series hybrid electric vehicle, SAE technical paper number 981133,” *International Congress and Exposition*, Detroit, Michigan: SAE, 1998.
[89] R.J. North, R.B. Noland, W.Y. Ochieng, and J.W. Polak, “Modelling of particulate matter mass emissions from a light-duty diesel vehicle,” *Transportation Research Part D: Transport and Environment*, vol. 11, Sep. 2006, pp. 344-357.
[90] P. Soltic and L. Guzzella, “Performance simulations of engine-gearbox combinations for lightweight passenger cars,” *Proc. Inst. Mech. Eng., Part D J. Automob. Eng.*, vol. 215, 2001, pp. 259-271.
[91] Secretaria de Comunicaciones y Transportes de México, *Normas de Servicios Técnicos, Proyecto Geométrico*, México, 1991, pp 23.
[92] U.S. Environmental Protection Agency, *Fuel Economy Labeling of Motor Vehicles. Revisions to Improve Calculation of Fuel Economy Estimates*, U.S. Environmental Protection Agency, 2006.
[93] M. Andre, “Driving cycles development: characterization of the methods,” *International*

Fuels & Lubricants Meeting & Exposition, Dearborn, Mi, US: SAE, 1996.
[94] "Garmin Connect" Available: http://connect.garmin.com/. Accessed: 16 November 2009
[95] *Travel Time Measurements using GSM and GPS Probe Data*, TomTom, . Available: http:/www.tomtom.com/. Accessed: 20 May 2010
[96] Vehicle Certification Agency, "Vehicle Certification Agency" Available: http://www.vcacarfueldata.org.uk. Accessed: 24 May 2010
[97] V.H. Johnson, "Battery performance models in ADVISOR," *Journal of Power Sources*, vol. 110, 2002, pp. 321-329.

8. APPENDICES

A. APPENDIX – ANALYSIS OF DYNAMIC EFFECTS OF A FLYWHEEL ON A MOVING VEHICLE (FROM SECTION 2.4.7)

The magnitudes and effects of the induced gyroscopic torques can be illustrated by using an example using the methodology proposed in [69]:

A conventional vehicle with a mass of 1200 kg, length between its front and back axles L = 2.4 m, a track dimension (side wheel distance) T = 1.7 m and height of its centre of gravity of 0.6 m will be used.

A yaw movement of the vehicle (as defined by Figure 2.9) is the most common manoeuvre the vehicle will experience as it corresponds to going around a curve. The rate of precession depends on how fast the curve is taken, which is limited by the lateral acceleration of the vehicle. A lateral acceleration of 0.6 g is about the maximum that a driver will willingly tolerate. For such a manoeuvre, a precession rate of about 0.7 rad/sec can be expected.

The highest pitch movement of the vehicle under non-emergency situations would probably involve hitting a speed bump at high speed. For a vehicle travelling at about 100 km/h, a precession rate of up to 4.7 rad/sec could be experienced. Similarly, a vehicle could conceivably step over a highway's embankment inducing a precession rate of about 1.3 rad/sec.

The size of the flywheel can be chosen according to different criteria, but it can be assumed that the capacity desired is equivalent to the energy available during a regenerative braking event from 100 km /h. This would require a flywheel of just less than 500 kJ of energy capacity. Figure 2.10 shows the possible flywheel maximum speed, mass and angular momentum for a solid carbon fibre flywheel of this capacity. In this example, a flywheel design with a radius to length ratio close to one will be used, which will minimise angular

momentum to H=185 Nms while keeping the mass of the flywheel within acceptable limits. Now, assuming that the vehicle carries out the manoeuvre when the flywheel is fully charged, equation (2.14) can be used to find the maximum magnitude of the reaction torque for all possible flywheel orientations and vehicle manoeuvres. These are shown in the first column of Table 8.1. The corresponding reactions, found by dividing the induced torque over the dimension of the vehicle over which it acts (i.e. a pitching torque acts over the length of the vehicle), are found in the second column of Table 8.1. Finally to put these reactions in perspective, the resulting reactions can be divided by the vehicle's weight per axis (for a pitching reaction), weight per side (for rolling reactions) or by the maximum sliding friction (for yawing reactions). These resulting ratios are summarised in the last column of Table 8.1.

Table 8.1 (a) Resultant gyroscopic torques; (b) corresponding vertical or sliding reactions; and (c) ratio of reaction to vehicle weight or maximum lateral sliding friction according to flywheel orientation and normal vehicle manoeuvre.

	Normal Operation								
	(a) Sense and resultant reaction torque $\tau_{gyro} = \Omega \cdot H$ [Nm]			(b) Veritcal reaction R_V per vehicle axle or lateral reaction R_L per side [N]			(c) Reaction / Vehicle weight or Maximum lateral sliding friction per axle or side		
Orientation of flywheel	Direction of precession Ω			Direction of precession Ω			Direction of precession Ω		
	+ Yaw	+ Roll	+ Pitch	+ Yaw	+ Roll	+ Pitch	+ Yaw	+ Roll	+ Pitch
+ Vertical	-	- Pitch 235	+ Roll 869	-	$R_{V,Front\ axle}$ 98	$R_{V,Right\ side}$ 511	-	2%	9%
+ Longitudinal	+ Pitch 132	-	- Yaw 869	$R_{V,Rear\ axle}$ 55	-	$R_{L,Rear\ axle}$ 362	1%	-	7%
+ Lateral	-Roll* 132	+ Yaw 235	-	$R_{V,Right\ side}$* -77	$R_{L,Front\ axle}$ 98	-	-1%*	2%	-

A similar analysis can be repeated for emergency operation of the vehicle in which precession rates under extreme circumstances could briefly reach just over 2 rev/min. This assumes accidental conditions and a fully charged flywheel to represent the worst case scenario. The induced gyroscopic torques and corresponding reactions are presented in Table 8.2.

Table 8.2(a) Resultant gyroscopic torques; (b) corresponding vertical or sliding reactions; and (c) ratio of reaction to vehicle weight or maximum lateral sliding friction according to flywheel orientation and emergency vehicle manoeuvre.

	Emergency Operation								
	(a) Sense and resultant reaction torque $\tau_{gyro} = \Omega \cdot H$ [Nm]			(b) Veritcal reaction R_V per vehicle axle or lateral reaction R_L per side [N]			(c) Reaction / Vehicle weight or Maximum lateral sliding friction per axle or side		
Orientation of flywheel	Direction of precession Ω			Direction of precession Ω			Direction of precession Ω		
	+ Yaw	+ Roll	+ Pitch	+ Yaw	+ Roll	+ Pitch	+ Yaw	+ Roll	+ Pitch
+ Vertical	-	- Pitch 3107	+ Roll 2743	-	$R_{V,Front\ axle}$ 1295	$R_{V,Right\ side}$ 1614	-	22%	27%
+ Longitudinal	+ Pitch 2590	-	- Yaw 2743	$R_{V,Rear\ axle}$ 1079	-	$R_{L,Rear\ axle}$ 1143	18%	-	22%
+ Lateral	-Roll* 2590	+ Yaw 3107	-	$R_{V,Right\ side}$ 1523	$R_{L,Front\ axle}$ 1295	-	26%	25%	-

The induced gyroscopic forces on the vehicle for normal operation of the vehicle are not significant, particularly if the flywheel is installed with a lateral orientation. Even for the extremes conditions considered for the emergency operation analysis, the induced torques are relatively small.

Although the magnitudes of the induced gyroscopic torques can be expected to increase for flywheels with a higher angular momentum, these magnitudes will in general by of little significance. For exceptional cases where large flywheels are needed these induced gyroscopic torques can be avoided by applying any of the techniques described in the latter part of section 2.4.7.

Finally it is worth mentioning that if when installing a flywheel on a positive lateral orientation, the generated gyroscopic torques generated during a yawing manoeuvre would oppose the forces generated by the centripetal acceleration that tend to cause vehicle rollovers. However, precisely because as shown the magnitude of the gyroscopic torques are small, the contribution towards decreasing vehicle rollovers is small as well.

B. APPENDIX – OPERATION OF THE BRAKE-ONLY PGS TRANSMISSION (FROM SECTION 3.5)

The operation of the brake-only PGS transmission described in [50] is briefly described here.

In this system, the flywheel is connected to the sun branch, the vehicle to the carrier branch, and a brake is installed at the ring branch which is used to control power flow.

The wide speed ratios necessary for connecting the flywheel with the vehicle's drive axle without the use of a variator make it more convenient to use a double-stage PGS such as the one shown in Figure 8.1. The equations describing the kinematic and torque behaviour of the double stage PGS are the same as for a single stage PGS except that the dimensional ratio R_p is calculated depending on how the different stages are connected, which for a double-stage PGS connected as in Figure 8.1

$$R_4 = \frac{D_R(D_{S1} + D_{S2} + D_R)}{(D_{S1} + D_R)(D_{S2} + D_R)}$$

where D_R, is the pitch diameter of the ring gear, and D_{S1} and D_{S2} are the pitch diameters of the sun gears for the first and second stages of the PGS.

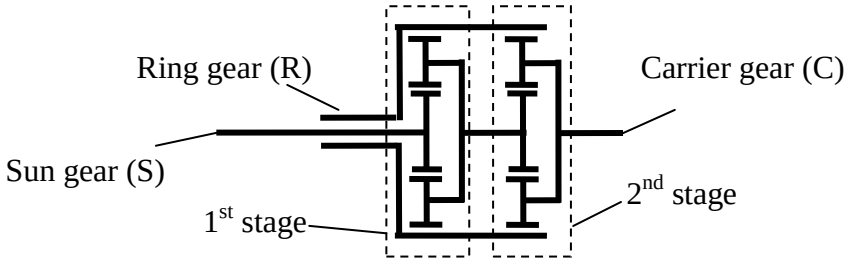

Figure 8.1 A double stage planetary gear set (PGS).

Figure 8.2 shows an example of a RB and FA modes. During RB mode (a), all the branches of the PGS rotate in the same direction. In this state, a torque opposite to the speed is applied at the ring so that it decelerates. Equation (2.20) can be used to find the sense of the torques at the sun and carrier branches. The combination of speed and torque senses show that in this operating mode power flows from the carrier branch (vehicle) to the ring (friction brake) and

sun branches (flywheel). As the only means of control is decelerating the ring, regenerative braking is only possible up until the ring branch reaches zero speed, which will occur before the vehicle is fully stopped. Therefore not all the braking energy is available can be captured for storage.

Figure 8.2 (b) shows the operation of the FA mode. Again, the brake is used to decelerate the ring. This mode of operation is only possible for the initial stages of vehicle acceleration, when the carrier speed is low enough so that with a charged flywheel, the ring speed will be negative. Applying the ring brake at this condition, forces a power transfer from the sun branch to the ring and carrier branches, launching the vehicle forward.

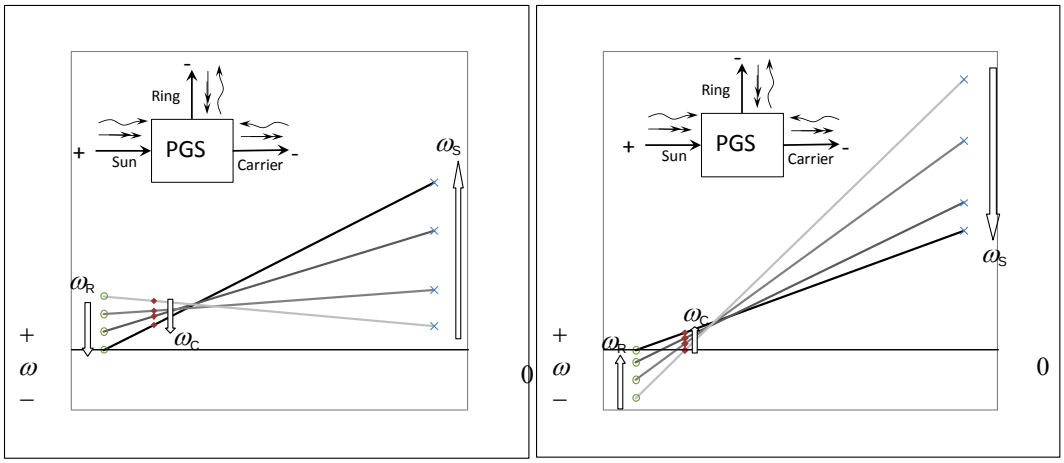

Figure 8.2 Nomogram showing (a) a regenerative braking event and (b) an acceleration event using a flywheel. The speed, torque and power senses for both conditions are also shown.

C. APPENDIX – ELECTRIC VEHICLE MODEL (FROM CHAPTER 4)

The electric vehicle model is very similar to the conventional vehicle model, but it replaces the ICE with an electric motor and a bank of batteries. The manual 5-gear transmission is replaced with a simple 2-gear transmission and weight adjustments are made based on the components replaced. The conventional and electric vehicles have otherwise the same characteristics. Efficiency maps for the electric motor/generator were taken from ADVISOR. An efficiency map for a 75 kW induction motor is shown in Figure 8.5

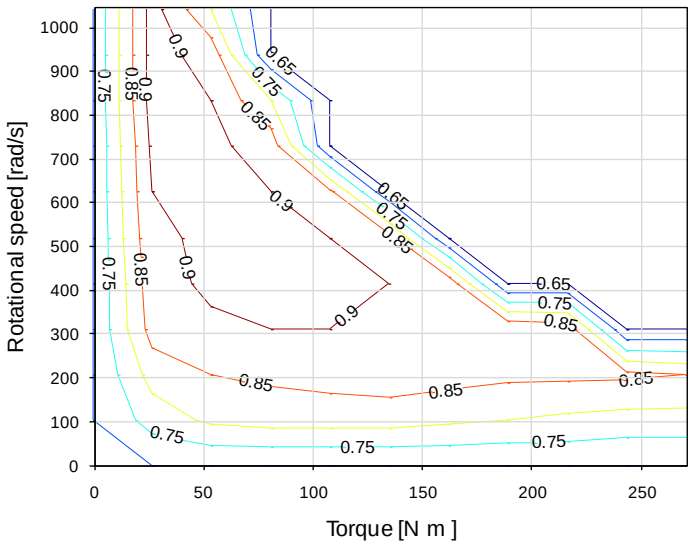

Figure 8.3 Efficiency map for a 75 kW AC Induction motor.

The modelling of the battery pack is the most complex, as the performance of batteries depends on a variety of environmental and usage factors such as temperature, state of charge and voltage (and as discussed in section 2.3.1). The model used here is the RC model used in ADVISOR (shown in Figure 8.6), which models the battery in two parts, a *body* section of the battery which holds the most energy content and that has the highest internal resistance, and a *surface-area* section of the battery that simulates the most immediately available but much smaller energy capacity.

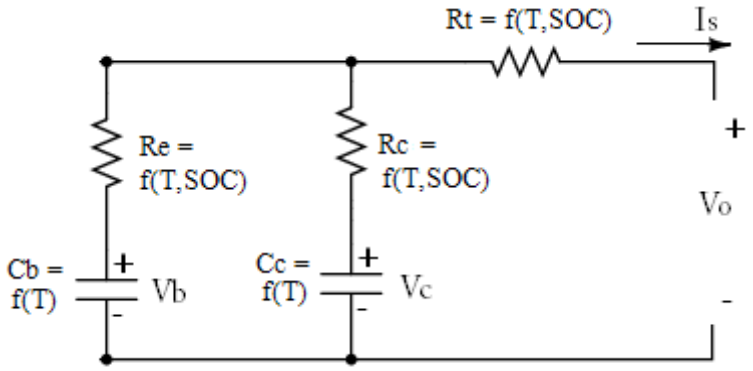

Figure 8.4 ADVISOR RC model.

The voltage balance equations at the battery are obtained using Kirchhoff's second law:

$$V_o = \begin{bmatrix} \frac{R_c}{R_c + R_e} & \frac{R_e}{R_c + R_e} \end{bmatrix} \begin{bmatrix} V_b \\ V_c \end{bmatrix} + \left[-R_t - \frac{R_c R_e}{R_c + R_e} \right] [I_s]$$

and the rate of discharge of the capacitors C_b and C_c.

$$\frac{dV_b}{dt} = V_b \left[\frac{-1}{C_b(R_e + R_c)} \right] + V_c \left[\frac{1}{C_b(R_e + R_c)} \right] + I_s \left[\frac{-R_c}{C_b(R_e + R_c)} \right]$$

$$\frac{dV_c}{dt} = V_b \left[\frac{1}{C_c(R_e + R_c)} \right] - V_c \left[\frac{1}{C_c(R_e + R_c)} \right] + I_s \left[\frac{-R_e}{C_c(R_e + R_c)} \right]$$

For each time step, the model updates the capacitances and internal resistances depending on the operating temperature and SOC of the battery, and these values are then fed to the above equations to solve for voltage at the terminals V_o, line current I_s and the new SOC.

Comparisons between experimental data and simulations using the RC-model are presented by Johnson from the US National Renewable Energy Laboratory [97] and have been shown to be on average within 1% of voltage estimations, providing an excellent agreement between predicted SOC and experimental measurements.

D. APPENDIX –DRIVE CYCLES FOR THE REAL GRADIENTS STUDY-SET (FROM SECTION 5.2)

Table 8.3 Summary of drive cycles sections used for the real gradients study-set. These drive cycles were adapted from data posted in [94]

Activity number in Garmin website	Location	Date data was posted	Duration	Δt per period [sec]	Max Vel [km/h]	Avg Vel [km/h]	Avg road gradient [m/100m]	Δaltitude (final – initial) [m]	Δt vel (final – initial) [km/h]
4497299	Kuala Lumpur	01/03/08	24 min 52 sec	3.4	71	45	2.2	0	38.12
4543430	Lagos	22/04/09	26 min 27 sec	5.2	110	50	1.3	0	-9.65
5326544	Mexico City	05/08/07	22 min 15 sec	3.9	85	44	3	1	25.85
5467238	Mexico City	04/08/07	39 min 23 sec	4.3	112	60	1.6	2	-66.74
5467290	Mexico City	05/08/07	9 min 30 sec	3.9	92	52	4	0	-2.97
5467296	Mexico City	04/08/07	11 min 22 sec	5.5	77	39	3	1	-16.80
6944394	London	22/03/06	3 min 17 sec	3.5	43	20	1.3	1	-4.03
11712914	Copenhagen	22/08/09	7 min 41 sec	4.0	51	27	9	2	-11.70
11926506	Singapore	26/08/09	30 min 3 sec	5.5	70	38	4.3	0	-7.12
12309983	Guangzhou	22/08/09	24 min 2 sec	5.5	92	67	2.6	0	-20.65
12379198	Vancouver	01/09/09	19 min 44 sec	4.5	64	26	7.3	0	19.93
13872718	Mexico City	30/11/06	11 min 21 sec	6.0	92	50	0.73	0	22.82
13975510	Santiago	29/10/06	20 min 0 sec	9.0	54	32	2.5	0	35.42
14056265	Los Angeles	22/05/06	7 min 24 sec	3.2	71	36	2.5	2	58.40
15621988	Cape Town	16/03/07	8 min 34 sec	8.9	74	44	3	0	27.44

E. APPENDIX – FURTHER RESULTS FOR THE ROAD GRADIENTS STUDY (FROM SECTION 5.2)

Figure 8.5 shows the frequency distribution for the fuel economy improvement (over the base case of zero-gradients) of the *ideal-parallel-hybrid vehicle* for all the cases simulated in the *Sinusoidal Gradients* study-set. As the *ideal-parallel-hybrid vehicle* increases the capacity limit of its energy reservoir the frequency of cases performing better than the base case clearly improves. For the purpose of the analysis, an improvement or worsening in fuel economy performance of +/-3% was considered insignificant.

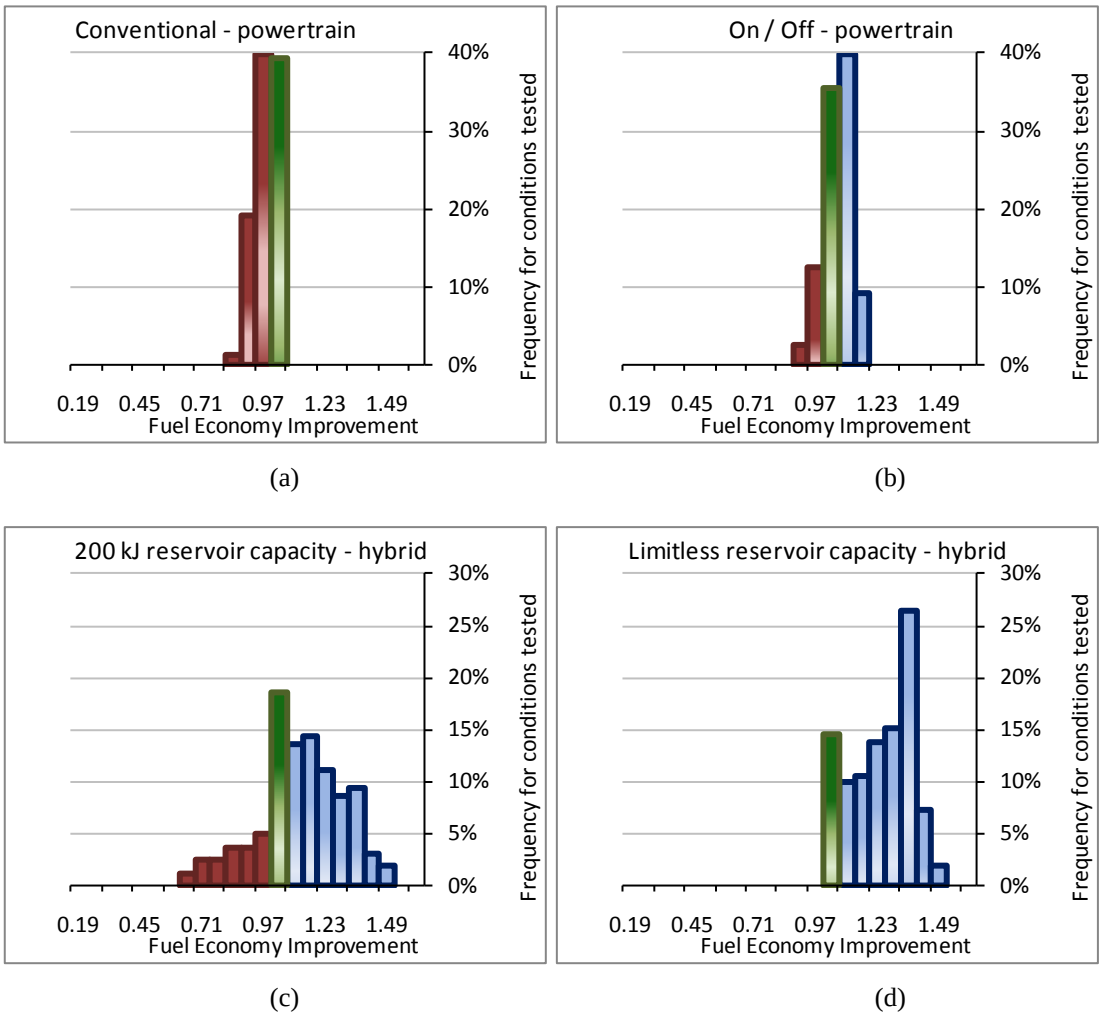

Figure 8.5 Frequency distribution plots of fuel economy improvement (measured as the improvement in fuel economy for each case over its performance in a flat road) for all gradients tested for the *Sinusoidal Gradients* study-set. The red green and blue columns represent the frequency of cases exhibiting a worse, equal (or insignificant) or better fuel economy than the zero-gradients case respectively.

The same response can be seen for the cycles of the *Real Gradients* study-set as seen in Figure 8.6.

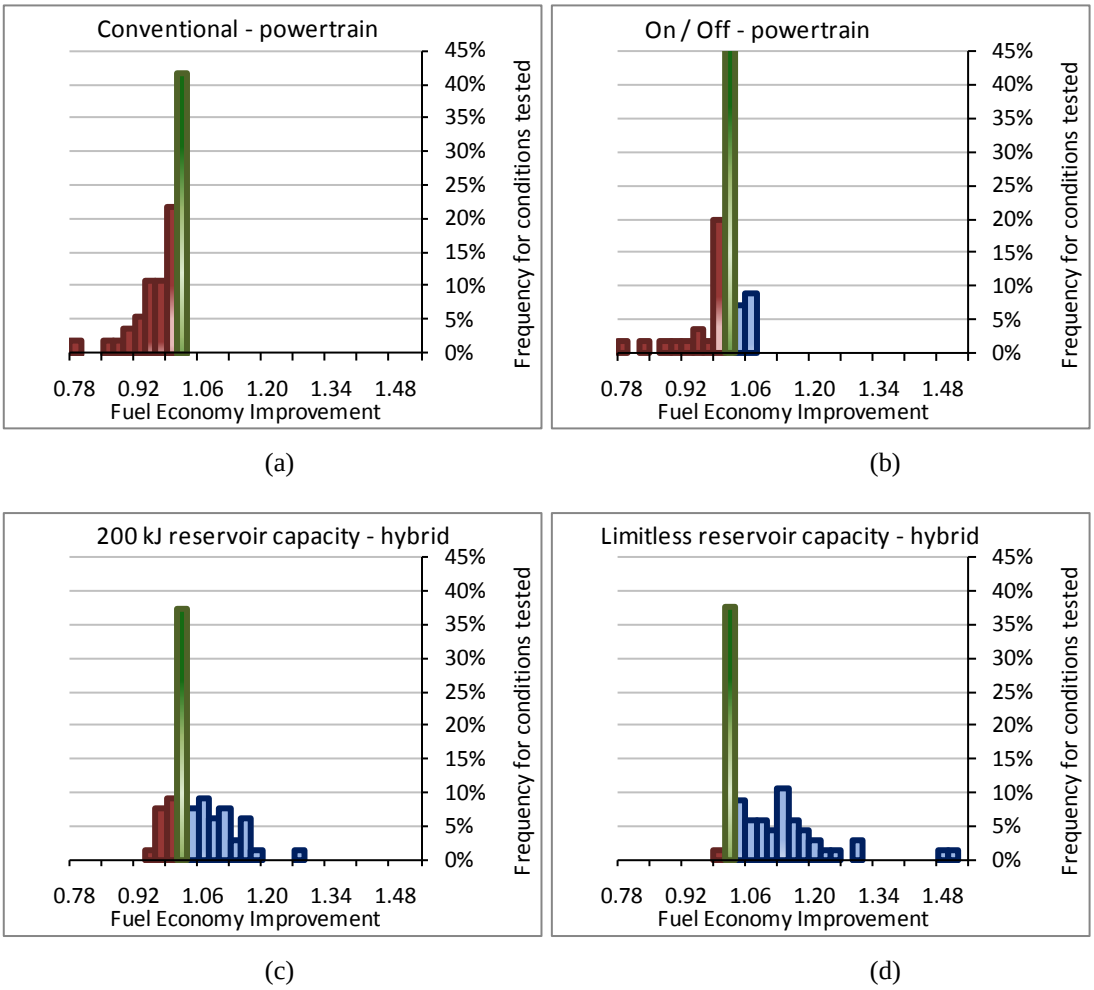

Figure 8.6 Frequency distribution plots of fuel economy improvement (measured as the improvement in fuel economy for each case over its performance in a flat road) for all gradients tested for the *Real Gradients* study-set. The red green and blue columns represent the frequency of cases exhibiting a worse, equal (or insignificant) or better fuel economy than the zero-gradients case respectively.

Table 8.4 Percentage of cases performing better, same or worse than the case with zero-gradients (flat road) for different powertrains and for all case study-sets.

Powertrian	**Sinusoidal gradients**			**Random gradients**			**Real gradients**		
	Worse	Same	Better	Worse	Same	Better	Worse	Same	Better
Conventional	60.6	39.4	0	44.2	51.9	3.8	69.1	30.9	0.0
On / Off	15	35.6	49.4	46.2	31.6	22.2	45.5	34.5	20.0
200 kJ reservoir capacity hybrid	18.8	18.8	62.5	32.5	23.1	44.4	25.0	28.1	46.9
Limitless reservoir capacity hybrid	0	14.6	85.4	30.8	29.1	40.2	1.5	37.9	60.6

.

F. APPENDIX – FURTHER RESULTS FOR THE ANALYSIS OF A POWER SPLIT TRANSMISSION IN A FLYWHEEL HYBRID POWERTRAIN (FROM SECTION 6.3)

This appendix repeats the analyses presented in section 6.3 on the effect of increasing the normalised ratio coverage of a power split transmission on a hybrid powertrain incorporating a flywheel, but using the UDDS driving cycle instead. All the vehicle and transmission parameters are the same as those used for the UDC cycle.

Figure 8.7 shows the results of the simulations considering a hybrid system with a lossless transmission and flywheel. As in the UDC cycle simulations, the fraction of vehicle velocity covered as well as the frequency of utilisation of the PS-CVT increase with increasing normalised ratio coverage, resulting in higher levels of fuel economy as seen in plot (b). The higher power through the variator branch commands a higher torque through it as appreciated in plot (a).

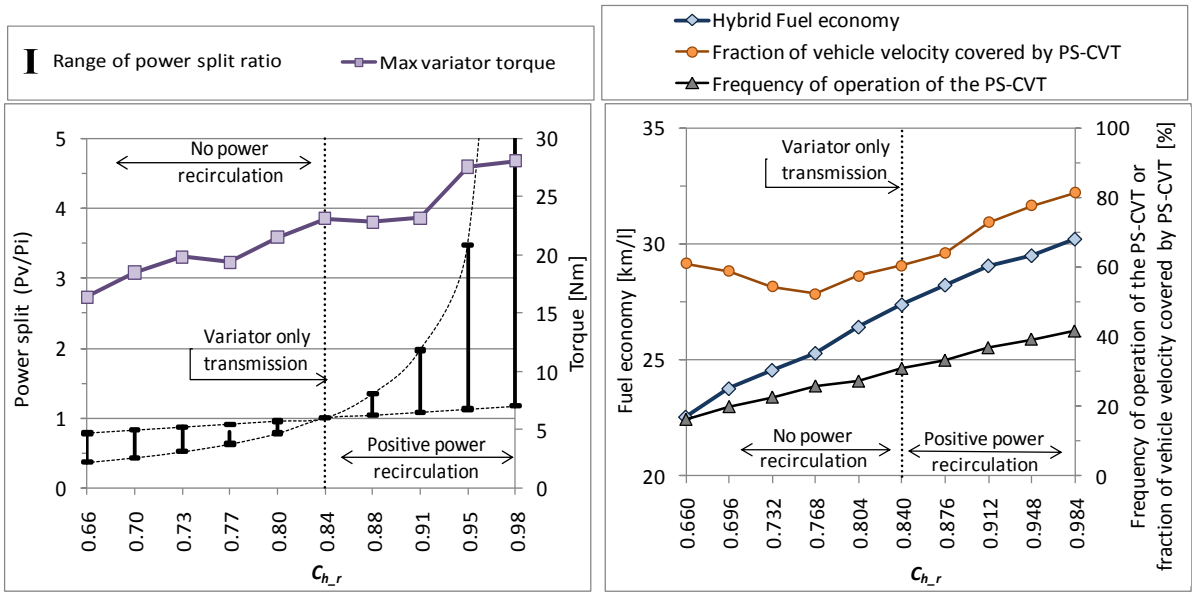

(a) (b)

Figure 8.7 Simulations using the UDDS for a lossless transmission and flywheel.
Plot (a) shows the range of power split (i.e. power through the variator) as the normalised ratio coverage is increased. Power split is less than one (i.e. no power recirculation) when the ratio coverage of the transmission is less than that of the variator, and conversely it is greater than one when it is greater. The maximum torque through the variator is also shown.
Plot(b) shows the fuel economy of the hybrid vehicle, frequency of operation of the PS-CVT and fraction of vehicle velocity covered by PS-CVT.

The corresponding analysis when considering the efficiency of the components of the PS-CVT is presented in Figure 8.8. The results show a similar response as in the simulations following the UDC. In plot (a) a higher torque through the variator can be appreciated as the normalised ratio coverage increases, which results in higher variator losses. Plot (b) shows a tendency of the fraction of vehicle velocity covered to increase with higher levels of normalised ratio coverage. The frequency of operation of the PS-CVT increases with ratio coverage as does the fuel economy achieved by the hybrid vehicle. At the highest levels of transmission ratio coverage which correspond to higher power and losses through the variator branch, the fuel economy predicted stagnates possibly due to an offset from higher variator losses.

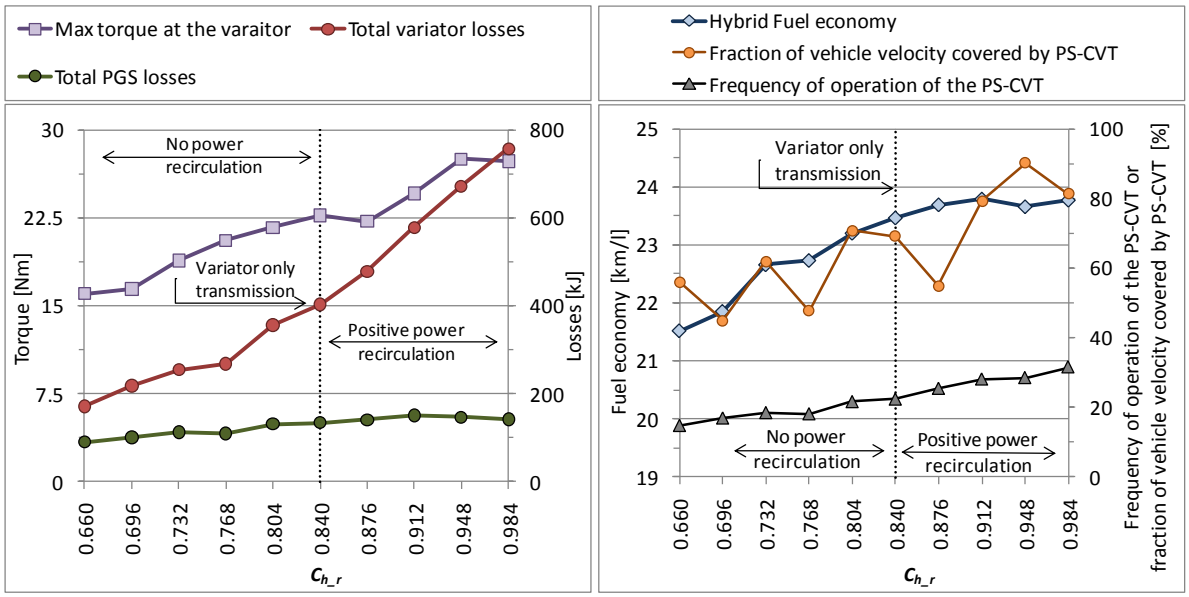

Figure 8.8 Simulations using the UDDS cycle and considering the efficiencies of the components.
Plot (a) shows the losses of the variator unit and the PGS as the ratio coverage and power split of the transmission increases, showing a detrimental effect on fuel economy.
Plot (b) shows how regardless of the frequency of operation of the hybrid transmission, the maximum energy of the flywheel decreases as the losses though the variator increase.